SYNTHESIS, CHARACTERIZATION AND APPLICATION OF DOPED-POLYANILINE (PAni) NANOCOMPOSITES FOR MICROWAVE ABSORPTION

KOH YEN NEE

DISSERTATION SUBMITTED IN FULFILMENT OF THE REQUIREMENT FOR THE DEGREE OF MASTER OF SCIENCE

DEPARTMENT OF CHEMISTRY
FACULTY OF SCIENCE
UNIVERSITY OF MALAYA
KUALA LUMPUR

2014

UNIVERSITI MALAYA

ORIGINAL LITERARY WORK DECLARATION

Name of Candidate: **KOH YEN NEE**

I/C/Passport No: **880917-23-6428**

Regisration/Matric No.: **SGR110071**

Name of Degree: **MASTER OF SCIENCE**

Title of Project Paper/Research Report/Dissertation/Thesis ("this Work"):

"SYNTHESIS, CHARACTERIZATION AND APPLICATION OF DOPED-POLYANILINE (PAni) NANOCOMPOSITES FOR MICROWAVE ABSORPTION"

Field of Study: **POLYMER CHEMISTRY**

I do solemnly and sincerely declare that:

(1) I am the sole author/writer of this Work,
(2) This Work is original,
(3) Any use of any work in which copyright exists was done by way of fair dealing and for permitted purposes and any excerpt or extract from, or reference to or reproduction of any copyright work has been disclosed expressly and sufficiently and the title of the Work and its authorship have been acknowledged in this Work,
(4) I do not have any actual knowledge nor do I ought reasonably to know that the making of this work constitutes an infringement of any copyright work,
(5) I hereby assign all and every rights in the copyright to this Work to the University of Malaya ("UM"), who henceforth shall be owner of the copyright in this Work and that any reproduction or use in any form or by any means whatsoever is prohibited without the written consent of UM having been first had and obtained,
(6) I am fully aware that if in the course of making this Work I have infringed any copyright whether intentionally or otherwise, I may be subject to legal action or any other action as may be determined by UM.

(Candidate Signature) Date:

Subscribed and solemnly declared before,

Witness's Signature Date:

Name **PROFESSOR DR ROSIYAH YAHYA**

Designation

Witness's Signature Date:

Name **DR PHANG SOOK WAI**

Designation

ABSTRACT

Conducting polymer nanocomposites containing aniline (Ani) monomer and hexanoic acid (HA) dopant has been synthesized by template free method. Dielectric (titanium dioxide (TiO_2)) and magnetic (iron (III) oxide (Fe_3O_4), carbon nanotubes (CNT), graphene and etc.) materials have been added to improve the dielectric and magnetization property of the nanocomposites. Fourier Transform Infra Red (FTIR), Ultraviolet-visible (UV-vis), and X-ray diffraction (XRD) analyses have confirmed the chemical structure of the doped-polyaniline (PAni) nanocomposites. Morphology study, thermal behavior, electrical conductivity and magnetic behavior of the nanocomposites have been investigated by Field Emission Scanning Electron Microscope (FESEM), Thermal Gravimetric Analyzer (TGA), resistivity meter and vibrating samples magnetometer (VSM), respectively. Microwave absorption study was carried out by Microwave Vector Network Analyzer (MVNA) from 0.5 to 18 GHz. In this research study, four types of PAni nanocomposites were prepared namely PAni/HA/TiO_2/Fe_3O_4 nanocomposites (with and without chemical treatments), PAni/HA/TiO_2/MWNT nanocomposites (different diameter and length of MWNT), PAni/HA/TiO_2/DWNT nanocomposites (different contents of u-DWNT and c-DWNT) and PAni/HA/TiO_2/GNP nanocomposites (different contents of GNP). In general, high electrical conductivity, dielectric permittivity and magnetic permeability are the few factors that will contribute to a better microwave absorption property of a material. Among all PAni nanocomposites, PAni/HA/TiO_2/MWNT nanocomposites with MWNT (D = 10-20 nm, l = 5-15 μm) possesses the highest reflection loss (RL = -58 dB) at 7 GHz due to the high heterogeneity and high μ_r' and μ_r''. This significantly induces the space charge polarization and eddy current along the PAni backbone. Finally, it indicates the strongest absorption. This material is potentially applied as a good

microwave absorber in computer, which operate at 7 GHz. However, PAni/HA/TiO_2/GNP nanocomposites with 40 % of GNP possesses the poorest microwave absorption with RL of -6.6 dB due to the lower value of μ_r' and μ_r'' and the absent of the nanorods/nanotubes (without heterogeneity). Thus, it significantly impedes the interaction between PAni and GNP, and eventually leads to the weakest microwave absorption.

ABSTRAK

Nanokomposit polimer konduktif mengandungi monomer anilina (Ani) dan dopan asid heksanoik telah disintesis melalui kaedah tanpa templat. Bahan dielektrik (titanium dioksida (TiO_2)) dan magnetik (ferum (III) oksida (Fe_3O_4), nanotiub karbon (CNT), graphene dan lain-lain) telah ditambahkan untuk meningkatkan sifat dielektrik dan magnetik. Analisis Inframerah Transformasi Fourier (FTIR), ultraungu-nampak (UV-vis) dan pembelauan sinar-X (XRD) mengesahkan struktur kimia bagi nanokomposit dop-polianilina (PAni). Kajian morfologi, sifat terma, kekonduksian elektrik dan sifat magnetik bagi nanokomposit telah dikajikan dengan mikroskop pengimas elektron (FESEM), analisis termogravimetrik (TGA), meter perintang dan magnetometer sampel pengetaran (VSM). Kajian penyerapan mikro gelombang telah dijalankan dengan menggunakan pengesan rangkaian vektor mikro gelombang (MVNA) daripada 0.5 hingga 18 GHz. Dalam kajian penyelidikan ini, empat jenis nanokomposit PAni telah disediakan iaitu PAni/HA/TiO_2/Fe_3O_4 (dengan dan tanpa rawatan kimia), nanokomposit PAni/HA/TiO_2/MWNT (MWNT yang berbeza diameter dan panjang), nanokomposit PAni/HA/TiO_2/DWNT (kandungan u-DWNT dan c-DWNT yang berbeza) dan nanokomposit PAni/HA/TiO_2/GNP (kandungan GNP yang berbeza). Secara am, kekonduksian elektrik, ketelusan dielektrik dan ketelapan magnektik adalah beberapa faktor yang menyumbangkan kepada sifat penyerapan mikro gelombang yang baik bagi sesuatu bahan. Antara semua nanokomposit PAni, nanokomposit PAni/HA/TiO_2/MWNT dengan MWNT (D = 10-20 nm, l = 5-15 μm) mempunyai kehilangan pantulan yang tinggi (RL = -58 dB) pada 7 GHz disebabkan oleh heterogeneity dan μ_r' dan μ_r'' yang tinggi. Hal ini akan mendorong polarisasi ruang cas dan arus elektrik eddy di sepanjang “tulang belakang” PAni, akhirnya menunjukkan penyerapan yang paling kuat. Bahan ini berpotensi digunakan sebagai penyerap mikro gelombang yang baik dalam komputer yang beroperasi pada 7 GHz. Walau

bagaimanapun, nanokomposit PAni/HA/TiO_2/GNP dengan 40 % GNP mempunyai penyerapan mikro gelombang yang paling lemah dengan RL sebanyak -6.6 dB disebabkan oleh μ_r' dan μ_r'' yang rendah dan ketidakhadiran nanorods/nanotiub (tanpa heterogeneity). Oleh itu, ini akan menghalang interaksi antara PAni dan GNP, dan akhirnya menghasilkan penyerapan mikro gelombang yang paling lemah.

ACKNOWLEDGEMENT

I would like to thank everyone who had been giving me assistance and support all the way for the completion of this thesis successfully. Appreciation particularly expressed to my supervisor, Dr. Phang Sook Wai and co-supervisor, Prof. Dr. Rosiyah Yahya for their supervision. They have guided me along my study and provided precious suggestions on my research work.

Besides, I would like to express my gratitude to postgraduate student, Mr. Kavirajaa for his kindness in advising my works. My sincere thanks will also go to my dearest family members and lovely friends especially Iris Fan, Yeong Siang, Alice Lee, Ginny Kong, William, Sze Koon and Mok Piew, Kit May and Shin Thung for their kind concern, love, accompanion and encourage all the way in this 2 years period.

Special appreciation expressed to staff of Department of Chemistry, Encik Zul, Encik Hafizie, Kak Nisrin and Encik Hashim for their kind-heartedness to help on my project work and Faculty of Science in completion of this research. Besides, special thanks to Physic garage, Department of Physic for the preparation of pellet and toroid mould. My heart-felt gratitude to Mr. Masato Tadokoro from The Yokohama Rubber Co., Ltd., Japan for the microwave measurement. With his assist, I could test my samples and complete my study in my master degree period. I am really grateful to those who have assisted me directly or indirectly to complete this degree of master in science.

PUBLICATIONS AND PRESENTATIONS

1. **Koh, Yen-Nee**, Sambasevam, Kavirajaa Pandian, Yahya, Rosiyah, & Phang, Sook Wai. (2013). Improvement of microwave absorption for PAni/HA/TiO_2/Fe_3O_4 nanocomposite after chemical treatment. *Polymer Composites, 34*(7), 1186-1194.

2. **Koh, Yen-Nee,** Yahya, Rosiyah & Phang, Sook Wai (2014). Effect of untreated and treated double wall carbon nanotubes on microwave absorption property of polyaniline nanocomposites. *Materials Chemistry and Physics.* (Under review)

3. **Koh, Yen-Nee,** and Phang, Sook Wai (2014). Effect of carbon nanotubes' dimension on microwave absorption property of polyaniline nanocomposites. *Polymer of Advanced Technologies.* (Under review)

4. Microwave Absorption Study of Conducting Polymer Nanocomposites

   Yen Nee Koh, Rosiyah Yahya, Sook Wai Phang. 17th Malaysian Chemical Congress, MCC 2012, October 15 – 17, 2012, PWTC, Kuala Lumpur, Malaysia.

5. Microwave Absorption Study of Conducting Polymer Nanocomposites with Different Types of Carbon Nanotubes

   Yen Nee Koh, Rosiyah Yahya, Sook Wai Phang. 7th International Conference on Materials for Advanced Technologies, ICMAT 2013, June 30 – July 5, 2013, Suntec, Singapore.

TABLE OF CONTENTS

Page

LIST OF FIGURES

Page

LIST OF TABLES

Page

LIST OF SYMBOLS AND ABBREVIATIONS

Ani	Aniline
APS	Ammonium persulphate
c-DWNT	Carboxylic treated double wall carbon nanotubes
CNT	Carbon nanotubes
DWNT	Double wall carbon nanotubes
EB	Emeraldine base
EM	Electromagnetic
EMA	Ethylene methyl acrylate
EMI	Electromagnetic interference
ES	Emeraldine salt
ESD	Electrostatic discharge
FESEM	Field Emission Scanning Electron Microscope
FTIR	Fourier Transform Infra-red
GNP	Graphene nanoplatelets
HA	Hexanoic acid
LE	Leucoemeraldine
MVNA	Microwave vector network analyzer
MWNT	Multiwall carbon nanotubes
OLED	Organic light-emitting diodes
PA	Poly(acetylene)
PAni	Polyaniline
PE	Pernigraline
PEDOT	Poly(3,4-ethlenedioxythiophene)
PP	Poly(propylene)
PPP	Poly(para-phenylene)

PPS	Poly(phenylene sulfide)
PPV	Poly(para-phenylene vinylene)
PPy	Polypyrrole
PTh	Polythiophene
RGO	Reduced graphene oxide
RL	Reflection loss
TGA	Thermogravimetric Analyzer
TPU	Polyurethane
u-DWNT	Untreated double wall carbon nanotubes
UV-vis	Ultraviolet-visible
VSM	Vibrating sample magnetometer
XRD	X-ray diffractometer
A	Absorbance
d	Disntace
D	Diameter
dB	Decibels
Hc	Coercive force
I	Intensity of light
I_0	Initial intensity of light
l	Length
Mr	Remnant magnetization
Ms	Saturated magnetization
S_{11}*	Complex scattering parameters related to reflection
T	Transmittance
tan δ	Loss tangent

T_g	Glass transition temperature
V	Voltage
ε_r'	Real part of dielectric permittivity
ε_r''	Imaginary part of dielectric permittivity
μ_r'	Real part of magnetic permeability
μ_r''	Imaginary part of magnetic permeability
π	Pi
σ	Conductivity

LIST OF APPENDICES

CHAPTER 1

Introduction

1.1 Polymers

Polymers have been studied in chemistry and physic over many decades owing to its fascinating properties. The original model of polymer science is Henri Braconnot's work in the 1830s. Hermann Staudinger was the first to discover that polymers contained long chains of molecules held together by covalent bonds and name these compounds as macromolecules in year 1922 while he received the Nobel Prize in Chemistry in 1953 (Painter & Coleman, 1997).

Polymers are usually the combination large number of monomer linked together in which undergo polymerization and have high molecular weight. The monomers can be jointed through linear chain, branched chain and more complex structure to form macromolecules. Biopolymers (starch, collagen, enzymes, DNA, cotton and etc.) and synthetic polymers (polystyrene, Teflon, polythene, polyamine, polyimide and etc.) are the two examples study of polymer (Peacock & Calhoun, 2006).

Typical polymers have broad applications in various kinds of areas due to their promising chemical and mechanical properties (Hwang, Jeong, & Jung, 1999). Besides, thermal properties like the glass transition temperature, T_g, plays an important role in polymer applications because it is glassy state when the temperature of polymer below T_g while it becomes rubbery state when the temperature of polymer rises above T_g. However in our knowledge, conventional polymers are resistance to electrical conduction and is an insulator where it behaves totally oppositely to metal. Metal is conductive because it possesses free electron cloud to move along the polymer chain.

1.2 Conducting polymers

With the discovery of intrinsically conducting polymer in year 1960 by Alan Heeger, Alan MacDiarmid and Hideki Shirakawa, it has altered the perception that polymer cannot conduct electricity (Z. Zhang & Wan, 2002). Conducting polymer can be defined as organic polymer that manages to conduct electricity and possesses combined mechanical properties of polymer as well as the electronic and optical properties of metals or semi-conductor. Conducting polymers (poly(acetylene) (PA), polyaniline (PAni), poly(3,4-ethlenedioxythiophene) (PEDOT), polypyrrole (PPy), polythiphene (PT) and etc.) in Figure 1.1 are some of the conjugated organic polymers, which contain π-electron backbone responsible for their unusual electronic properties such as electrical conductivity, low energy optical transitions, low ionization potential and high electron affinity (Al-Ibrahim, Ambacher, Sensfuss, & Gobsch, 2005; Fehse, Schwartz, Walzer, & Leo, 2007; Koul, Chandra, & Dhawan, 2000; Yoon, Chang, & Jang, 2007).

In order to make conducting polymer act as a conductor, the main requirement is the conjugated double bonds, which is alternating single and double bonds in the polymer chain. However, it is insufficient for the conducting polymer to be highly conductive. Thus, dopant for the formation of charge carrier in the electric field is required to achieve high conductivity. Dopant, which is either add (n-doping) or remove (p-doping) electron from the polymer chain will create an extra holes (positive charge) or electrons (negative charge) in order for the lonely electron to move easily and thus enhance the electrical conductivity.

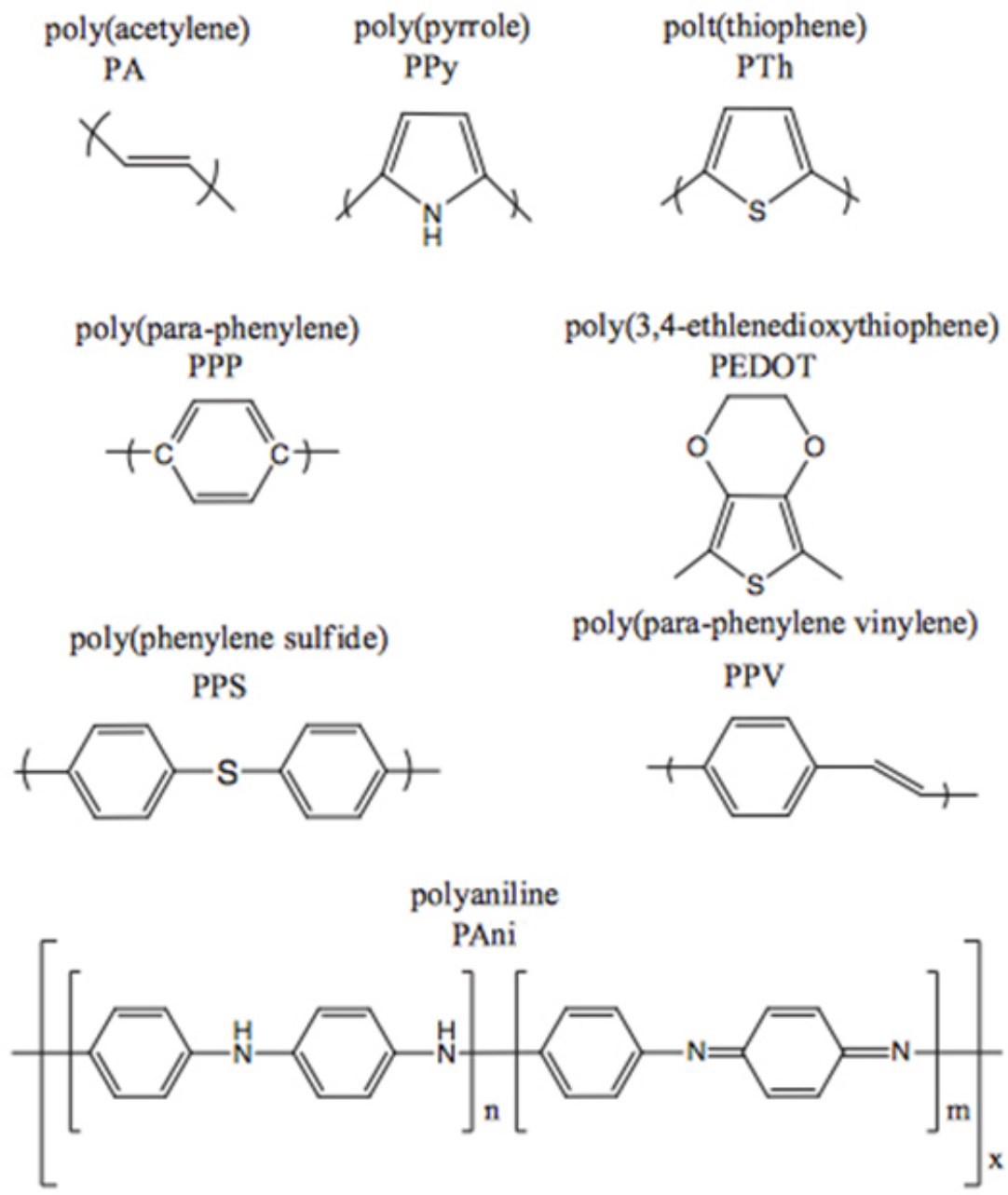

m, n and x = Different repeating units

Figure 1.1 Chemical structures of various types of conducting polymers.

Moreover, p-doping is partial oxidation, while n-doping is partial reduction of the π-backbone of the polymer. Generally, if an electron is removed from one carbon atom, a radical cation (polaron) is acquired and a counter "dopant" ion is added to stabilize the charge on the polymer backbone while a second electron is removed from an oxidized section, a second polaron (bipolaron) is created. Polaron and bipolarons are the foremost charge-carriers in p-doped conducting polymers where commonly conducting polymers can be p-doped or n-doped throughout reaction with either an oxidant or a reductant.

Therefore, a high density and mobility of charge-carriers along the polymer chains are the main factors for doped conjugated polymers act as a good conductors (Heeger, 2001). Various aspects can be manipulated including polaron length, the conjugation length, overall chain length and by the charge transfer to adjacent molecules, which can influence the conductivity of conducting polymers (Abbas, 2007). Basically, all these properties are influenced by synthesis parameter such as different reaction temperature, effect of dopants, different alkyl substituted monomers and etc.

Due to the special properties of conducting polymer as discussed above, it has shown potential application in different areas such as corrosion inhibitors, organic solar cell, electronics, supercapacitors, organic light-emitting diodes (OLED), electrostatic discharge (ESD) protection, electromagnetic interference (EMI) shielding, electromechanical, chemical sensors, interconnection technologies, membrane, biosensors and etc. (Bhadra, Singha, & Khastgir, 2009; Junfeng, Yadong, Yajie, Junsheng, & Jianhua, 2011; Mirmohseni & Oladegaragoze, 2000; Ramya, Sivasubramanian, & Sangaranarayanan, 2013; Xia, Wei, & Wan, 2010).

PA is the first conducting polymer that discovered by Alan Heeger, Alan MacDiarmid and Hideki Shirakawa since 40 years ago but PA exhibits many disadvantages such as chemical instability in doped state and readily reduced in the air (Czekelius et al., 2006). Among the conducting polymers, PAni, PPy and PEDOT have attracted much attentions owing to their high thermal stability when exposed to the air, low cost monomer, can be obtained by bulk synthesis, distinctive chemical and mechanical properties and etc. (Mathew, Praveen Kumar, & John, 2006).

1.3 Polyaniline (PAni)

In the past 50 years, PAni is the most studied conducting polymer due to its unique electrical, chemical and physical properties. Besides, PAni can exist in three oxidation states (leucoemeraldine (LE), emeraldine, pernigraniline (PE)) with different colors that differ from their chemical and physical properties. Commonly, PAni occurs as fully reduced LE where y = 1, half oxidized emeraldine base (EB) where y = 0.5 and fully oxidized PE where y = 0 (Figure 1.2) (Shimano & MacDiarmid, 2001).

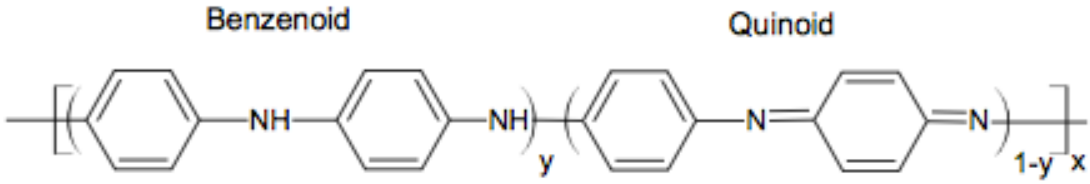

x and y = Different repeating units

Figure 1.2 Three oxidation states of PAni (Leucoemeraldine (LE) (y=1), emeraldine (y=0.5) and pernigraline (PE) (y=0)).

Moreover, highly conductive form of green PAni (emeraldine salt (ES)) can be achieved when PAni doped with acid while a blue, insulating EB form of PAni can be

formed when it dedoped with ammonium hydroxide. This reversible doping process (Figure 1.3) can repeat as many times as required.

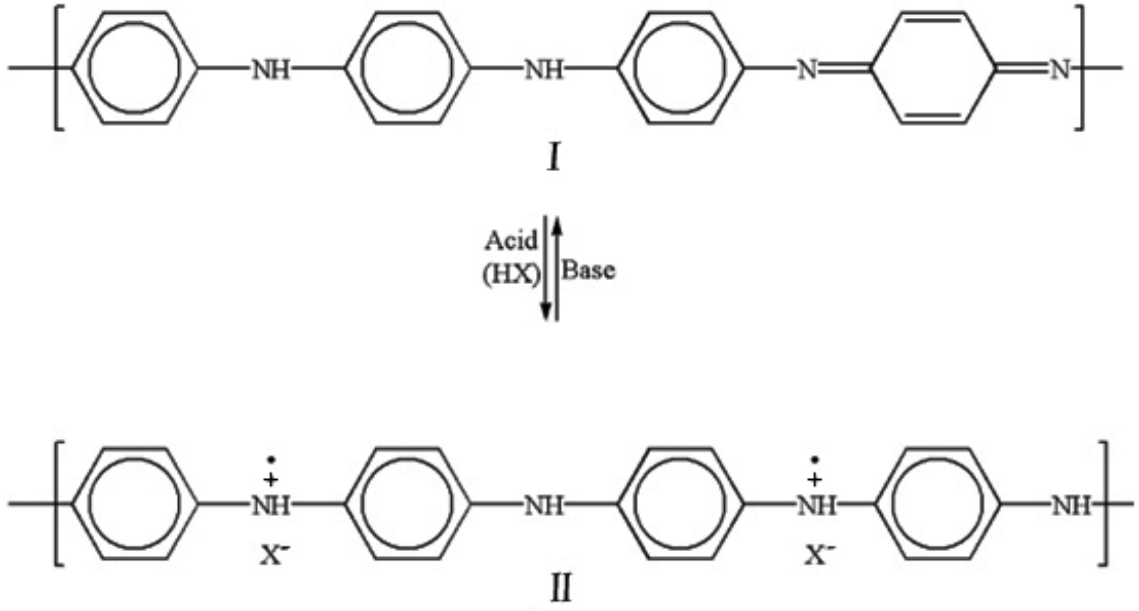

Figure 1.3 Reversible doping mechanism of PAni.

Since early 20th century, various kinds of reports have been published, which was regarding the synthesis, characterization, properties, theory and application of PAni. Usually, highly conductive PAni can be obtained through chemical oxidative or electrochemical polymerization (Deivanayaki, Ponnuswamy, Ashokan, Jayamurugan, & Mariappan, 2013). Bulk synthesis can be obtained through chemical oxidative polymerization while a thin film can be formed on the electrode via electrochemical polymerization in which can be used in sensor application.

The most common PAni based conducting polymer is in green protonated ES form (Figure 1.4), in resulting high conductivity after doped with acid, which in semiconductor level in a range of 10^{-8} to 10^{3} S/cm, higher than usual polymers ($<10^{-9}$ S/cm) but lower than usual metals ($>10^{4}$ S/cm) (Bhadra, Khastgir, Singha, & Lee,

2009). Conductive PAni can apply in different applications like electrostatic dissipation, welding, microcircuits, solar cell, stealth technology and etc.

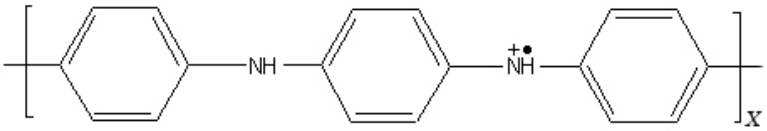

X = Repeating units

Figure 1.4 Chemical structure of green protonated emeraldine.

In general, PAni can convert from one oxidation state to another oxidation state via doping and dedoping process with color changes, in which can apply in electrochromic devices and TV display. Furthermore, it also can be used in chemical or optical sensor due to its reversible doping process where the high recyclability is required. Besides, PAni that possesses various kinds of properties can apply in other applications such as microwave absorber, solar cell, biosensors, chemical sensors, supercapacitors and etc.

1.4 PAni nanocomposites

Few decades ago, composite material has been started by mixing two or more materials that have different properties in order to obtain a composite material with unique properties. Recent year, high expectation has been paid on nanoscale technology owing to its low weight, high surface area and aspect ratio. A nanocomposites is a solid single material that shows the size less than 100 nm in at least one dimension. In general, inorganic materials can improve the unique properties of the nanocomposites such as high surface area in which depend on their specific applications. Inorganic

nanocomposites offer advantages over conventional composites where nanocomposites exhibit not only a combination of high mechanical, electrical and thermal properties but also optical and chemical properties of a nanocomposites. The nanocomposites can be applied in wide applications such as electronic devices, optical sensors, actuators, microwave absorbing materials and etc.

1.5 Microwave absorption materials

Over the past decades, destructive electromagnetic (EM) wave from various kinds of sources, like electronic devices, computer, cellphone, wireless devices and etc. are the crucial cause that initiated the electromagnetic interference (EMI) problem. EM waves are formed when electric field is coupled with magnetic field but there are perpendicular to each other and the direction of wave. The EM wave will continue travel around the space until it is absorbed by a matter (Süsskind, 1988). Thus, microwave absorber is required where the microwave absorber is a kind of well-designed material that able to absorb EM waves efficiently and convert EM energy into thermal energy or make EM waves dissipate by interference in order to prevent the effect that brought by EMI.

Figure 1.5 show an example of commercial radar absorbing material. Generally, traditional microwave absorbing material is heavy and thick but with the discovery of conducting polymer, microwave-absorbing material possesses lightweight, fine thickness and wide-band absorbing range. (Hekmatara, Seifi, & Forooraghi, 2013).

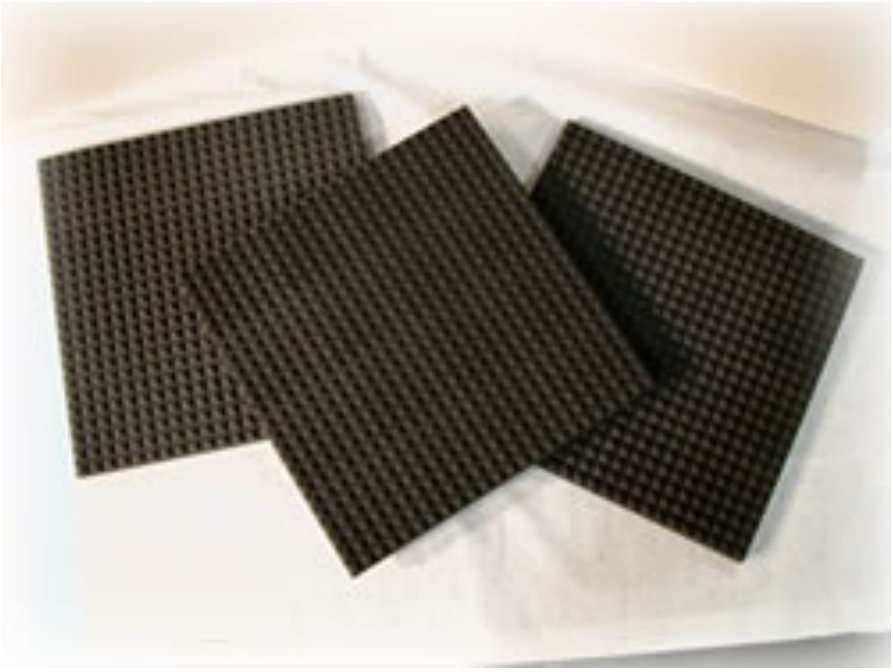

Figure 1.5 An example of commercial radar absorbing material.

1.6 Problem statement

The rapid development of electric and telecommunication industries has brought the problem of EMI. EMI is a disturbance of the electrical circuit among the machine, consumer products and some instruments disturbance, which may interrupt the actual performance, reduce the lifetime of the instrument and affect the welfare operation of electronic devices (Håkansson, Amiet, Nahavandi, & Kaynak, 2007; L. H. Olmedo, P. & Jousse, F, 1997). Hence, all the instruments and electronic devices must be shielded against EM noises or pollution in order to cut down the malfunction that caused by the EMI (M. S. Kim et al., 2002).

In general, traditional microwave absorbing materials such as metal or carbon black only can reflect EM wave. This problem statment restricts the conventional microwave absorber materials in limited application such as electric conductive agent, electronics, radar application and etc. Oppositely, conducting polymer not only can

reflect undesired radiation but also can absorb the EMI radiation at a specific wavelength. The unique property of conducting polymer significantly overcome the problem statement of the conventional material and make it potentially apply as a new and advanced EMI shielding material. Besides, conducting polymer also possesses some advantages such as lightweight, resistance to corrosion, good and easy processability, variability of conductivity, low cost and etc.

The reflection and absorption of the material can be easily altered by the synthesis parameters such as different types of dopants, monomer, synthesis temperature and etc. to achieve the desired application (Faez, Martin, De Paoli, & Rezende, 2001; Fehse et al., 2007). In principal, electrical conductivity, complex dielectric permittivity and complex magnetic permeability are the main factors that contribute to high microwave absorption. Among all the conducting polymers, PAni has received considerable attention due to the excellent electrical and optical properties of semiconductors and metals as well as the high processability and mechanical properties of polymers.

1.7 Research objectives

In this research study, aniline (Ani) acts as the monomer and hexanoic acid (HA) has been added not only to increase the conductivity but also act as template to form the micelles. Besides, dielectric material (titanium dioxide (TiO_2)) and different magnetic materials (ferum oxide (Fe_3O_4), carbonaceous material like carbon nanotubes (multi-walled carbon nanotubes (MWNT) and double-walled carbon nanotubes (DWNT)), graphene nanoplatelets (GNP)) have been added in order to improve the dielectric and magnetic property, respectively. In our knowledge, effect of dielectric

material and different types of magnetic materials on the efficiency of microwave absorption is firstly reported here.

Below are the objectives of this research study:

1. To synthesize some PAni nanocomposites using different synthesis parameters (such as different types of dielectric material, magnetic material, dopants and etc.) through template free method.
2. To characterize the PAni using Fourier Transform Infra-red (FTIR) spectrometer, Ultraviolet-visible (UV-vis) spectrometer, Thermogravimetric Analyzer (TGA), X-ray diffractometer (XRD) and Field Emission Scanning Electron Microscope (FESEM).
3. To investigate the conductivity and magnetic property of PAni nanocomposites by using four point probe and vibrating sample magnetometer (VSM), respectively.
4. To study the microwave absorption property of PAni nanocomposites by using microwave vector network analyzer (MVNA).
5. To investigate the optimum synthesis parameter to synthesize the PAni nanocomposites in order to apply as an adequate and efficient microwave absorber.

CHAPTER 2

Literature Review

2.1 Traditional microwave absorbing material

Recent years, EMI becomes a big issue among the latest technology because the interference between the electronic devices will lead to disruption of usual performance of the instruments and consequently affect our human health. Hence, all the instruments and machines must shield against the EM noise in order to reduce the malfunction that produce by EMI (Huo, Wang, & Yu, 2009).

Metal and carbon black are the conventional microwave absorbing materials due to its promising electrical conductivity and mechanical properties. Recently, there are some studies have been reported by using traditional materials as microwave absorbing materials. In 2013, Kumar and co-workers have reported that metal dispersed nanocomposites-epoxy possesses high value of complex permittivity if compared to pure inorganic material-epoxy nanocomposites. Besides, it also indicates that thin microwave absorbers will give rise to a better reflection loss (RL) (Kumar, Agarwala, & Singh, 2013). Thus, the effectiveness of using metal as microwave absorbing material can be concluded in this study.

However, traditional microwave absorber such as carbon black and metal exhibit some drawbacks like high density, easily corroded, high reflectivity and costly (Schulz, Plantz, & Brush, 1988). Furthermore, metal predominantly only can reflect EM wave but cannot absorb EM wave and the reflection range is very sharp due to their narrow conductivity range (Hsieh, Ho, Huang, Wang, & Chen, 2006).

2.2 Application of PAni nanocomposites as microwave absorber

In order to overcome the disadvantages of traditional microwave absorbing materials, conducting polymer has been introduced owing to the properties like light weight, corrosion resistant, easy processability, controllable conductivity and low cost. Besides, conducting polymer not only reflects undesired radiation but also absorb EMI radiation at particular wavelength. Moreover, conducting polymer also show a broad absorption peak due to their variety of conductivities along the polymer backbone (L. Olmedo, Hourquebie, & Jousse, 1995).

For an effective microwave shielding materials, the shield should retain either mobile charge carrier in the polymer chain or electric and magnetic dipoles that cooperate with incident EM radiation, which consist of electric and magnetic vectors. Figure 2.1 show the interaction between EM waves and shielding material. Complex scattering, S_{11} (or S_{22}) and S_{12} (or S_{21}) are S parameters of the two ports vector microwave vector network analyzer (MVNA) system.

In general, electrical conductivity, dielectric permittivity and magnetic permeability will contribute to a better microwave absorbing material. Previous study show that TiO_2 is a good dielectric material that will increase the dielectric property of a nanocomposites, which will discuss in detail at TiO_2 based compound. For magnetic property part, some magnetic material such as ferrites, carbon nanotubes (CNT) and graphene are the few inorganic materials that give rise to a better magnetic property as proven by the previous study. Among all the carbonaceous material, CNT and graphene not only will increase the magnetic property but also significantly increase the electrical conductivity while for the ferrite based compound, it show a better magnetic property but it will also decrease the electrical conductivity of a material.

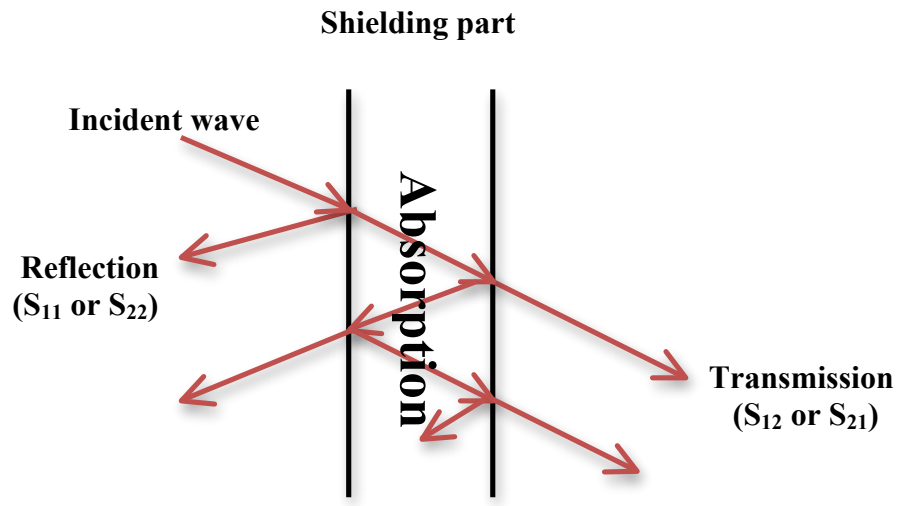

Figure 2.1 Interaction between EM waves with shielding material.

2.2.1 TiO_2 based compound

In the past 20 years, high interest has been shown on TiO_2 owing to its special surface, electronic and photocatalytic properties. Thus, conducting polymer doped TiO_2 has shown a promising electrical and mechanical properties in different field. In year 2008, Mo and co-workers have reported the effect of TiO_2 nanoparticles or TiO_2 colloids to the dielectric properties of PAni/TiO_2 nanocomposites by in-situ polymerization. Based on the morphology results, it has shown that PAni nanocomposites with TiO_2 nanoparticles exhibit uniform distribution if compared to PAni nanocomposites with TiO_2 colloids. Uniform distribution of PAni nanocomposites will contribute to a high dielectric loss and dielectric constant owing to a better charge transfer network along the PAni chain (Mo, Wang, Chen, & Yeh, 2008).

However, increasing the amount of TiO_2 will significantly decrease the electrical conductivity of the composites. Shakoor and co-workers have proposed the relationships between electrical conductivity and amount of TiO_2. In this study, PPy dodecylbenzenesulfonate (DBSA)-TiO_2 nanocomposites were synthesized through

colloidal solution of TiO_2 nanoparticles. Thermal stability of nanocomposites was improved with the addition of TiO_2. Based on the electrical conductivity result, the conductivity reached the percolation threshold at 20 % of TiO_2 due to the insulating behavior of TiO_2 and thus block the conductive pathway of polymer backbone (Shakoor & Rizvi, 2010).

Besides, the microwave absorption performances of PAni nanocomposites containing TiO_2 nanoparticles and HA dopants were studied by Phang and co-workers in year 2008. The morphology results have proved that PAni nanocomposites undergo polymerization through elongation to form nanorods/nanotubes, in which will significantly increase the dielectric permittivity but in the mean time, it will decrease the electrical conductivity of the nanocomposites (Phang, Tadokoro, Watanabe, & Kuramoto, 2008). Thus, it can be concluded that addition of TiO_2 nanoparticles will block the conductive pathway and significantly reduce the electrical conductivity of the nanocomposites.

2.2.2 Ferrites based compound

On the other hand, ferrites also have been added in order to enhance the magnetic property of nanocomposites. The magnetic effect on different weight of $Zn_{0.6}Cu_{0.4}Cr_{0.5}Fe_{1.5}O_4$ doped with PAni was synthesized by in-situ polymerization has been reported by Jiang and co-workers. Magnetic ferrites show high potential in microwave absorption application owing to the EM loss derived from its complex permittivity and permeability. Besides, conducting polymer also possesses the ability to shield EM waves by magnetic material in low frequency. In summary, morphology results has shown that PAni- $Zn_{0.6}Cu_{0.4}Cr_{0.5}Fe_{1.5}O_4$ nanocomposites exhibit core-shell structure where the ferrite material acts as the core and PAni acts as the shell of the

micelle. Magnetic properties like the saturation magnetization and coercivity were significantly affected by the weight of $Zn_{0.6}Cu_{0.4}Cr_{0.5}Fe_{1.5}O_4$ nanoparticles that added into the compound (Jiang, Li, & Zhu, 2008).

In order to achieve high magnetic permeability, Li and co-workers have reported that PPy/Fe_3O_4 will form a core/shell structure through in-situ chemical oxidative polymerization. Fe_3O_4 will react as the core while the PPy will grow on the surface of Fe_3O_4 nanoparticles to form the shell of the core/shell structure. There is a minimum reflection loss (RL) of -22.4 dB (which indicated good absorption) attained at 12.9 GHz due to the existence of PPy/Fe_3O_4 core shell structure in PPy nanocomposites. Moreover, the thickness of the samples will lead to a low frequency absorbing peak where the thin layer of sample will give rise to a microwave absorbing property at lower frequency (Y. Li, Chen, Li, Qiu, & Liu, 2011).

Although the PPy/Fe_3O_4 will give rise to a better RL, addition of Fe_3O_4 will also significantly decrease the electrical conductivity. Deng and co-workers have studied the effect of addition Fe_3O_4 on electrical conductivity and magnetization property. From the electrical properties result, it can observe that decrease in conductivity of PPy/Fe_3O_4 with increasing of Fe_3O_4 content was mostly due to the insulating behavior of Fe_3O_4 and decrease in doping degree. Furthermore, saturated magnetization was also improved with the increasing amount of Fe_3O_4 owing to the ferromagnetic properties of Fe_3O_4 (Deng et al., 2003).

Moreover, the influence of addition ferrites filler and different weight ratio of TiO_2 on microwave absorbing property has been reported by Akman and co-workers. In this study, pyrrole as monomer, Ba-hexaferrite (BaM) nanoparticles as magnetic filler

and different content of TiO_2 was polymerized by sol-gel method. According to the morphology study, nanoparticles with coated PPy show an overlayer of PPy on the surface of nanoparticles and thus increase the particle size. Besides, dielectric loss also has been improved with coated PPy layer and RL has been enhanced with the addition of ferrite filler. The increase in dielectric loss mainly contributed by the conduction mechanism and polarization mechanism of PPy coating (Akman et al., 2013). Hence, high dielectric loss and magnetization were contributed to better RL and thus apply as efficient microwave absorbers.

Although TiO_2 and ferrites based compound possess better magnetic property, it will also significantly reduce the electrical conductivity of a material. Therefore, addition of carbonaceous materials has been suggested in this study.

2.2.3 Carbon nanotubes based compound

In order to overcome the drawback that possesses by the TiO_2 and Fe_3O_4, carbonaceous material such as CNT and graphene are proposed here. In principal, carbonaceous materials (CNT, graphene, graphite and etc.) are magnetic materials not only possesses high magnetic property but also high electrical conductivity. They show high potential as EMI shielding material owing to their high thermal stability, electrical conductivity and mechanical property. Figure 2.2 show some of the carbonaceous materials like graphite, fullerenes, CNT, graphene and etc.

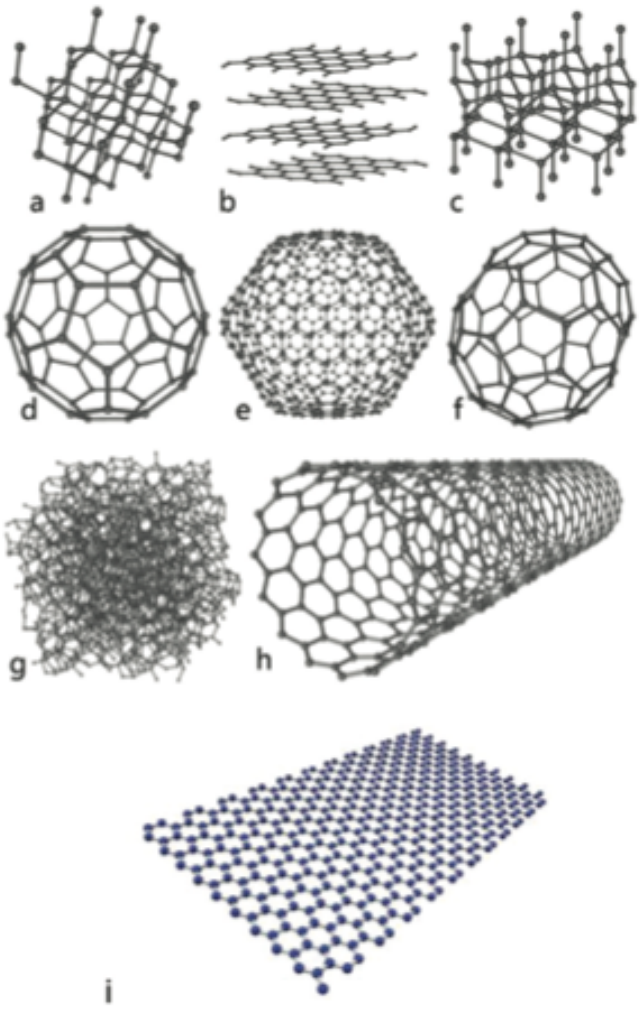

Figure 2.2 Some of the carbonaceous materials: (a) Diamond, (b) Graphite, (c) Lonsdaleite, (d)-(f) Fullerenes (C_{60}, C_{540}, C_{70}), (g) Amourphous carbon, (h) CNT, (i) Graphene

In 1991, the discovery of CNT by Iljima stated that CNT is a hollow, nanometric-sized tubes combined of graphitic carbon (Iijima, 1991). In general, CNT is a rolled up of graphene sheet to form a cylindrical nanostructure with hemisphere of fullerene capped on the ends of CNT, in which having high aspect ratio, tensile strength, conductivity, mechanical properties and etc. (F. Li, Cheng, Bai, Su, & Dresselhaus, 2000). Furthermore, they can be categorized into single wall carbon nanotubes (SWNT), double wall carbon nanotubes (DWNT) and multi wall carbon nanotubes (MWNT) with different morphology and properties while the individual CNT usually held together by Van der Waals forces (Wu & Lin, 2006).

Wu and co-workers have reported the doped PAni composites with chemical functionalized MWNT by using carboxylic acid (c-MWNT) and acylchloride (a-MWNT) groups through in-situ polymerization. Chemical functionalization on MWNT was used to enhance the dispersion in organic solvent and water while increase the interaction between PAni and MWNT. Based on the morphology results, both PAni/c-MWNT and PAni/a-MWNT composites form the core-shell structure where the functionalized MWNT act as core and the Ani monomer polymerized uniformly on the surface of MWNT (as the shell). The electrical conductivity of PAni with functionalized MWNT was 60 – 70 % higher than those MWNT without functionalized (Wu & Lin, 2006).

The interaction between PAni-MWNT composites with different amount of MWNT, its effect on electrical conductivity and RL has been studied by Saint and co-workers in year 2009. FTIR and XRD results show that there is a significantly shifting at characteristic peak of PAni while the morphology result shown that PAni polymerized on the surface of MWNT. Besides, PAni-MWNT composites exhibit high electrical conductivity (19.6 S/cm) owing to the high aspect ratio of MWNT, which lead to significantly interchain transport of charge transfer process between PAni and MWNT. Furthermore, the RL rises from -8 dB to -12 dB when increasing the amount of MWNT in PAni composites made it potentially applied as a good EMI shielding material (Saini, Choudhary, Singh, Mathur, & Dhawan, 2009).

In year 2012, electrical conductivity, dielectric constant and EMI shielding effectiveness properties of the ethylene methyl acrylate (EMA)/MWNT nanocomposites have been reported by Basuli and co-workers. Based on the morphology result, MWNT show a good dispersion in EMA matrix where an interconnected network has been

formed within the nanocomposites. The electrical conductivity and dielectric constant also significantly increase with the increment amount of MWNT. EMI shielding effectiveness also increases with thickness of the samples due to the closely packing conductive network of MWNT loading. Thus, it can conclude that nanocomposites with MWNT possess the ability as effective microwave absorbing material (Basuli, Chattopadhyay, Nah, & Chaki, 2012).

Dubnikova and co-workers have reported the influence of surface modifications and MWNT dimensions on electrical conductivity, mechanical and morphology of poly(propylene) (PP)-based composites through melt mixing process. From the morphology result, long thin nanotubes can be easily entangled due to the high surface area while thick MWNT was distributed well as an isolated non-entangled nanotubes. Moreover, MWNT with high surface area possess the highest electrical conductivity owing to the strong aggregation and entanglement within the thin nanotubes and thus more conductive network can be formed. In conclusion, long large diameter of MWNT possesses the highest dielectric, in which potentially applied as electromagnetic waves shielding material (Dubnikova et al., 2010).

In year 2011, Tishkova and co-workers have stated the distribution of DWNT in polymer matrix by using Raman imaging and compared the result with the electrical conductivity measurements. From the study, conductivity is varying with aspect ratio of CNT, dispersion, polymer type and synthesis method. Based on the Raman imaging, it can conclude that better dispersion of individual DWNT is observed in low concentration but overall dispersion is not homogenous while maximum electrical conductivity is at 10^{-2} S/cm, which is suitable to apply as a good microwave absorbing material (Tishkova et al., 2011).

The comparison of conductivity by using SWNT, DWNT and MWNT has been reported by Li and co-workers. The electronic transport of SWNT is depends on the type of nanotubes while for the MWNT, electron transport can happen throughout the shell of MWNT due to the metallic character that shown by MWNT in conductivity. In summary, DWNT and MWNT exhibit a better conductivity because they have more π conductive than SWNT. Moreover, the length of MWNT play an important role where decreasing in the contact resistance between the CNT will significantly increase the electrical conductivity (Z. Li et al., 2007).

2.2.4 Graphene based compound

Although CNT shows a promising electrical conductivity, magnetic and dielectric properties, graphene has attracted tremendous attention in past few years due to its high aspect ratio (length/diameter) where it possesses much more favorable both magnetic and electrical conductivities. Wallace (Wallace, 1947) was first discussed theory of graphene since 1946. Based on his study, graphene is a two dimensional sp^2 bonded sheet with crystalline form of carbon. It can be described as one layer thick carbon atom and considered as the basic structure of CNT and graphite. Andre Geim and Konstantin Novoselov have won the Nobel Prize in Physics in 2010 for revolutionary experiments concerning the two-dimensional material graphene. Furthermore, graphene also possess high thermal stability, high specific surface area and good electrical conductivity because it exists in a sheet form of hexagonal carbon, in which is adequate to apply as an EMI shielding material (Rao, Biswas, Subrahmanyam, & Govindaraj, 2009).

Chapal and co-workers have studied the microwave absorption ability of graphene and MWNT in polyurethane (TPU) matrix. Based on the FESEM result,

graphene exhibit sheet-like structure whereas MWNT possess a tubular shape. Moreover, the RL of TPU-graphene was -12.56 dB, much more higher than TPU-MWNT (-7.6 dB) at 10 GHz. It has observed that dielectric loss plays a key role in microwave absorption property if compared to magnetic loss of a material. Thus, TPU-graphene that possesses better dielectric loss can be the a new candidate for microwave absorber (Chapal, Pallab, & Swinderjeet, 2012).

High mobile charge carrier and magnetic dipole were needed in order to develop a high efficient EMI shielding material. In year 2013, Singh and co-workers have proposed a three dimensional nanostructured embedded chemical functionalized graphene/Fe_3O_4 with PAni through in-situ emulsion polymerization. Based on the FTIR, Raman spectra and morphology study, the existence of graphene/Fe_3O_4 will lead to the formation of solid-state charge transfer due to the strong polarization. Besides, it also shows a high dielectric loss and magnetic loss, in which will consequently contribute to the RL of -26 dB. Hence, it was concluded that high dielectric and magnetic loss will significantly enhance the absorption properties of a material (Singh et al., 2013).

Most of the previous study was two steps method to synthesize conductive material with graphene but Liu and co-workers have reported three components nanocomposites (PAni-reduced graphene oxide (RGO)-Co_3O_4) by using three steps method. From the morphology study, PAni was distributed uniformly on the surface of RGO while Co_3O_4 was attached on the surface of PAni-RGO. In general, tremendous microwave absorbing properties were the combination of permittivity and permeability whereas a high permittivity will damage the impedance match and reduce the absorption of a compound.

Since PAni-RGO is a typical dielectric loss material, thus addition of magnetic material (Co_3O_4) to form the PAni-RGO-Co_3O_4 can produce the impedance matching between dielectric loss and magnetic loss, thus significantly enhance the EMI shielding property. PAni-RGO shows that maximum RL of -3.1 dB at 11.3 GHz while PAni-RGO-Co_3O_4 possess a higher RL of -32.6 dB at 6.3 GHz. As conclusion, the PAni-RGO-Co_3O_4 nanocomposites show a better microwave absorption property with a broader bandwidth for the three components nanocomposites (Liu, Huang, Wang, & Zhang, 2013).

2.3 Summary of literature review

In general, high electrical conductivity, dielectric permittivity and magnetic permeability are the three significant factors that will contribute to good microwave absorption of a material. Based on the literature review above, previous researches were focused on the microwave absorbing property of the two component composites such as conducting polymer/TiO_2, conducting polymer/CNT, conducting polymer/graphene, conducting polymer/Fe_3O_4 and etc. Based on our knowledge, comparison of microwave absorbing behavior of the three component nanocomposites such as PAni/TiO_2/Fe_3O_4, PAni/TiO_2/CNT, PAni/TiO_2/Graphene and etc. are firstly reported here. Besides, the effect of the inorganic materials such as TiO_2, Fe_3O_4, CNT and graphene on the novel nanocomposites and their synthesis mechanism (morphology) will be discussed in detail in this research study.

CHAPTER 3

Methodology

3.1 Chemicals

Aniline (Ani) as monomer, hexanoic acid (HA) (purity 99 %) as dopant, ammonium persulphate (APS) as oxidant, titanium dioxide (TiO_2) nanoparticles with particle size <30 nm and iron (II) oxide (Fe_3O_4) nanoparticles with particle size <50 nm used in this study were purchased from Sigma Aldrich (USA). Besides, multiwall carbon nanotubes (MWNT) with different diameter and length (D = 60-100 nm, L = 1-2 μm; D = 60-100 nm, L = 5-15 μm; D = 10-20 nm, L = 5-15 μm) were purchased from Shenzhen Nanotech Port Co., Ltd. (China). Untreated double wall carbon nanotubes (u-DWNT) and carboxyl treated double wall carbon nanotubes (c-DWNT) were ordered from Chengdu Organic Chemicals Co., Ltd. (China). Graphene nanoplatelets (GNP) with thickness of 6 – 8 nm and width of 5 microns wide were purchased from Stream Chemicals (USA). Methanol with purity of 99.8 % used for washing purpose was purchased from Systerm. Distilled water used for polymerization was purified by distillation. All others reagents were used without further purification unless noted.

3.2 Apparatus

Apparatus that will be used throughout this study were beaker, dropping funnel, measuring cylinder, petri dish, droppers, test tube, mortal and pestle, micrometer, micropipette, spatula, separation funnel, pellet mould, toroid mould and etc.

3.3 Synthesis of PAni nanocomposites

In this study, Ani will act as the monomer while HA has been added not only to increase the conductivity but also act as template to form the micelles during synthesis of PAni nanocomposites. Furthermore, dielectric material (TiO_2) and different magnetic materials (Fe_3O_4), carbonaceous material like carbon nanotubes (MWNT and DWNT), GNP have been added during polymerization in order to improve the dielectric permittivity and magnetic permeability of the PAni nanocomposites, respectively.

3.3.1 Synthesis of PAni/HA/TiO_2/Fe_3O_4 nanocomposites

HA doped PAni containing TiO_2 and Fe_3O_4 nanoparticles without chemical treatment were synthesized through chemical oxidation (polymerization) by template free method using APS as oxidant. First of all, HA (10 mmol) and H_2O (75 mL) were mixed vigorously in distilled water for 30 mins followed by addition of Ani (10 mmol) and stirred for another 30 mins. After that, dielectric material (TiO_2) (0.10 g, 10 %) and magnetic materials (Fe_3O_4) (0.10 g, 10 %) were added into the solution under ultrasonic action for 1 hour in order to obtain the homogeneous Ani/HA solution containing dielectric and magnetic nanoparticles.

Next, APS aqueous solution (10 mmol) was added dropwise within 2 hours at 0 ^oC to initiate the polymerization. The polymerization was maintaining at 0 ^oC under undisturbed situation. After 24 hours of polymerization, the PAni/HA/TiO_2/Fe_3O_4 nanocomposites were then washed with distilled water followed by methanol three times, respectively by using centrifuge and orbital shaker in order to terminate the reaction and get rid of unreacted monomer. Finally, the nanocomposites were dried in oven at 60 ^oC for 24 hours and grinded to obtain the dried PAni green powder.

For the PAni/HA/TiO_2/Fe_3O_4 nanocomposites with chemical treatment by using iron (III) chloride hexahydrate ($FeCl_3.6H_2O$) (during addition of Fe_3O_4) as reported by Phang and Kuramoto, (Phang & Kuramoto, 2010), Fe_3O_4 nanoparticles were first dispersed well in 3 g of $FeCl_3.6H_2O$ aqueous solution under ultrasonic bath. HA, Ani, and TiO_2 nanoparticles were then added into the solution under ultrasonic for 2 hours in order to get a homogenize mixture. After that, APS was added dropwise for 2 hours and polymerization was continued for 24 hours under undisturbed condition at 0 ^oC.

Same polymerization methods for PAni/HA/TiO_2/Fe_3O_4 nanocomposites with and without chemical treatment by using $FeCl_3.6H_2O$ (during addition of Fe_3O_4) were repeated with 10 % (0.10 g), 20 % (0.20 g) and 40 % (0.40 g) of Fe_3O_4 nanoparticles.

3.3.2 Synthesis of PAni/HA/TiO_2/MWNT nanocomposites

PAni/HA/TiO_2/MWNT nanocomposites were synthesized by chemical oxidation (polymerization) through template free method. Initially, HA (10 mmol) and H_2O (75 mL) were mixed vigorously for 30 mins followed by the addition of Ani (10 mmol) and stirred for another 30 mins. After that, addition of dielectric material (TiO_2) (0.10 g, 10 %) and magnetic material (MWNT) (0.10 g, 10 %) in the solution were stirred vigorously for 24 hours in order to obtain better dispersion of TiO_2 and MWNT in the Ani/HA solution. Subsequently, APS aqueous solution (10 mmol) was added dropwise for 2 hours at 0 ^oC to initiate the polymerization and the polymerization was continued at 0 ^oC under undisturbed situation.

After 24 hours of polymerization, the PAni/HA/TiO_2/MWNT nanocomposites were washed with distilled water followed by methanol three times, respectively by using orbital shaker and centrifuge to separate the PAni precipitate from the unreacted

monomer, oxidant and filler that exist in the liquid layer. Lastly, the nanocomposites were dried in oven at 60 ^{o}C for 24 hours to attain a dried green powder compound. Same polymerization method was repeated with different length and different diameter of MWNT.

3.3.3 Synthesis of PAni/HA/TiO_2/DWNT nanocomposites

Same polymerization method in Part 3.3.2 (synthesis of PAni/HA/TiO_2/MWNT nanocomposites) was repeated for 10 % (0.10 g), 20 % (0.20 g) and 60 % (0.60 g) of u-DWNT and c-DWNT nanoparticles to prepare the PAni/HA/TiO_2/DWNT nanocomposites.

3.3.4 Synthesis of PAni/HA/TiO_2/Graphene nanoplatelets (GNP) nanocomposites

Same polymerization method in Part 3.3.2 (synthesis of PAni/HA/TiO_2/MWNT nanocomposites) was repeated with 10 % (0.10 g), 20 % (0.20 g) and 40 % (0.40 g) of GNP to prepare the PAni/HA/TiO_2/GNP nanocomposites.

3.4 Characterizations of PAni nanocomposites

3.4.1 Fourier Transform Infra-red (FTIR) Spectrometer

FTIR spectroscopy is an useful technique to identify the bonding and chemical structure of a compound in the frequency range of 400-4000 cm^{-1}. A chemical substance will show an IR absorption spectrum that significantly gives rise to close-packed absorption bands. Different characteristic of functional groups and bonds of a compound will show different peaks in the IR spectrum. The peak intensity of a chemical substance is expressed as transmittance (T), in which most of the spectrum has

been plotted as % T versus wavenumber (cm^{-1}). T can be described as the ratio of radiant power transmitted by a sample to the radiant power incident on the sample.

Powder samples of PAni nanocomposites were recorded by Perkin Elmer RX1 model spectrometer. The PAni nanocomposites were grinded into fine powder and dry overnight in oven before FTIR measurement. Small amount of PAni nanocomposites powder was added into the potassium bromide (KBr) powder (PAni: KBr = 1:10) and then was grinded by using mortar and pestle to obtain a homogenous mixed fine powder. The fine powder was distributed well in the mould and pressed to get a transparent, thin and uniform pellet. FTIR measurements of PAni nanocomposites in KBr pressed pellets were analyzed from the wavelength range of 400 to 4000 cm^{-1} at 4 cm^{-1} resolutions at room temperature.

3.4.2 Ultraviolet-visible (UV-vis) Spectrometer

UV-vis absorption spectroscopy is used to study the electronic structure of atomic and molecular species of a compound in the region from 200 nm to 1000 nm. The absorbance of a UV-vis spectrum is the measurement transition from ground state to excited state when the light passing through the sample. The intensity of light passed through a compound was assigned as I while the intensity of light before it passed through the sample was labeled as I_o. The ratio of I/I_o is expressed as transmittance where normally defined as % T. Thus, the absorbance (A) can be calculated using the equation, A = - log (% T / 100 %).

First of all, the instrument needs to be warmed up for approximately half an hour after it is turned on. There are two transmission holes, which are for the samples and blank substrate. Next, the instrument has to be calibrated with two blank substrates

in order for the samples can be run without any recalibration. For the sample preparation, approximately 0.005 g of PAni nanocomposites was dissolved in methanol and put under ultrasonicator for few hours in order to obtain a homogenous solution. The solution was then transferred into cuvette for UV-vis measurement. UV–vis absorption spectra were taken by Shimadzu UV-1650 PC model by using double-beam photometric system, silicon photodiode detector and halogen lamp as light source. The PAni nanocomposites in methanol solutions were then recorded from 300-900 nm with scanning speed of 400 nm/min at room temperature.

3.4.3 X-ray Diffractometer (XRD)

X-ray diffraction is a common technique used to characterize the solid state of chemistry and material sciences while define the size and shape of any crystalline compound. From X-ray diffraction, there are few types of information can be studied such as degree of crystallinity, how the compound packed together, molecule structure and fingerprint characterization of crystalline material. Generally, each crystalline solid compound can be identified easily because it has its own unique X-ray diffraction pattern. However, amorphous phase of a material may result in irregular baseline with noise and pulsed shape while they did not exhibit periodicity and the atoms are randomly distributed in the 3D space. Hence, X-ray crystallography can be applied to identify structure of the compound once the material has been classified.

As to test for the X-ray pattern, PAni nancomposites that have been dried overnight in oven was grinded into fine powder and distributed well in a steel plates sample holder. The XRD pattern was recorded by Siemens D500 model at room temperature and the amorphous behavior of PAni nanocomposites were identified using

Cu Kα (Kα = 1.54056 Å) at 35 kV and the results obtained were in the 2θ range of 0-80^{o} with scanning step of 0.1^{o} in 2θ.

3.4.4 Thermogravimetric Analyzer (TGA)

Thermogravimetric analysis (TGA) is a technique used to determine the weight change in related to the temperature change of a compound and usually used to identify the decomposition point of solvent residue, degradation temperature, the level of organic and inorganic compound in a material and composition of composites. The analyzer generally contains a high-precision balance with a ceramic pan that consists of sample and the weight change has been recorded. Besides, the atmosphere in the instrument must be purged with inert gas such as nitrogen (N_2) gas in order to avoid oxidation or any others undesired reaction happen. The heating temperature can be started from 55 ^{o}C to 1700 ^{o}C (depend on the type of sample's pan) and a percentage of weight loss versus temperature can be plotted. Thus, thermal stability of a compound can be studied through the graph.

For the sample preparations, PAni nanocomposites were grinded into fine powder and dried in oven overnight. Then, approximately 0.005 g of PAni fine powder was trasnferred into the ceramic pan for TGA analysis. Thermograms of PAni nanocomposites were recorded using Perkin Elmer TGA 4000 model with the continuously purge with N_2 gas into the chamber from 50 ^{o}C to 900 ^{o}C with heating rate of 20 ^{o}C/min. The temperature at maximum degradation was considered as the peak degradation temperature while the remaining weight percentage of a compound was defined as the residue.

3.4.5 Field Emission Scanning Electron Microscope (FESEM)

FESEM is an useful tool used to determine the morphology, particle size and microstructure of a compound with particle size ~1 nm. Electron beams that emitted from field emission were having energy ranging from few hundred eV to 100 keV. This process involved the scanning of primary electron beam on a sample surface while the secondary electron beam was reflected from the surface of sample. Therefore, the secondary electron beam will be caught by a detector and generate electronic signal. This electronic signal is amplified and converted to a scan-image that can be seen at monitor and for further processing. In principle, magnification range of the FESEM is from 25 × to 1,000,000 ×.

Figure 3.1 show FESEM instrument of JEOL JSM-7600F model and the morphology of PAni naocomposites were investigated. Initially, fine powder of PAni nanocomposites used for FESEM images were distributed evenly on the surface of the conductive tape, which will place on the sample holder. The samples holder was then injected into the instrument in order to obtain the FESEM images with magnification of 30,000 × and 60,000 × at room temperature. For a non-conductive sample, it is required to coat the sample with conducting materials like gold, palladium (Pd), platinum (Pt) and etc. to avoid the accumulation of electrostatic on the surface. Nevertheless, PAni nanocomposites is conductive thus coating with conductive material is unnecessary.

Figure 3.1 FESEM instrument of JEOL JSM-7600F model used for morphology study.

3.5 Microwave absorption study

3.5.1 Electrical conductivity

Electrical conductivities of PAni nanocomposites were measured by four-point probe method on a compressed pellet at room temperature. As shown in Figure 3.2, a constant current (I) was supplied through outer two probes (1 and 4) and then the voltage (V) passing through the inner two probes (2 and 3) were measured. Inter-pin distance (d1) is about 1.5 mm for PSP probe while the inter-pin distance (d2) is about 5 mm for ASP probe. In general, PSP probe can be used to test for the small samples of rectangular and circular samples from 0.001 mm – 9999 mm but ASP probe was only

limited for samples with width greater than 15 mm. Figure 3.2 show the set-up of PSP and ASP probe for conductivity measurement. Then the conductivity (σ) of the compressed sample can be measured using the equation, $\sigma = (\ln 2)(I) / (\pi t V)$. σ is the conductivity of the pellet (in S/cm), I is the current applied through probe 1 and 4 (in mA), V is the voltage passed though probe 2 and 3 (in mV) and t is the thickness of the compressed pellet.

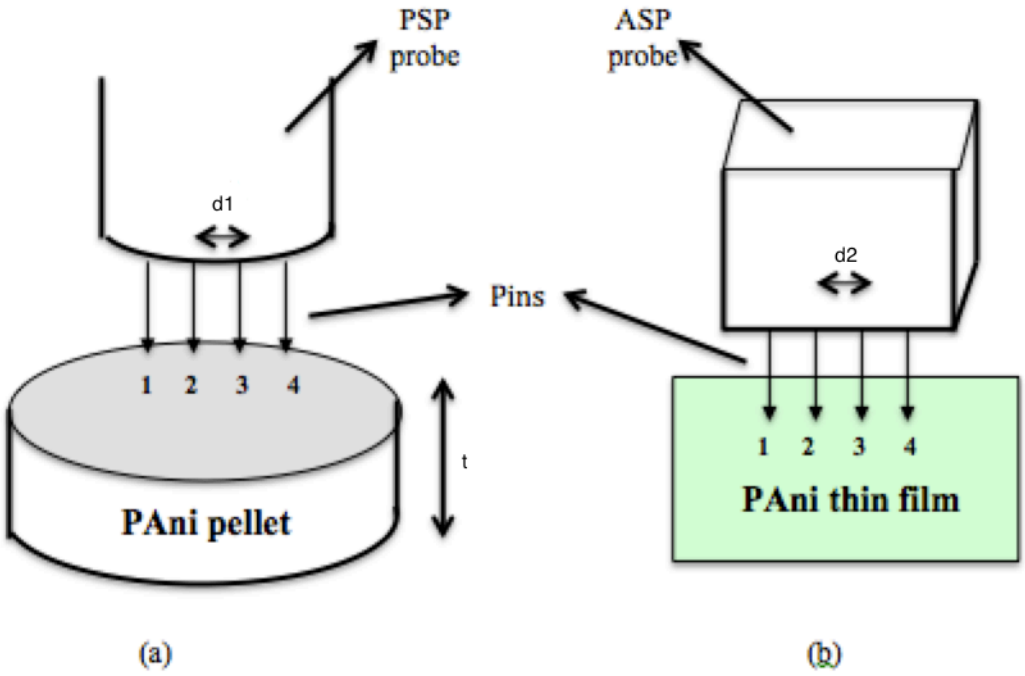

Figure 3.2 Set-up for four-point probe method with different probes: (a) PSP and (b) ASP.

Samples used for the conductivity study was in pellet form with diameter of 10 mm and thickness of ~1 mm. The samples were compressed slowly by a constant load of 625 kg for 10 minutes. The compact densities for these samples were ~1.00 g/cm^3. The electrical conductivity of the PAni was tested by four-point probe (PSP probe) method using Loresta-GP MCP-T610 model at room temperature. Besides, the measurement range of the four-point probe was from 10^{-7} to 10^7 S/cm. It shows an overload reading when the conductivity exceeds the measurement range while the best

condition for this instrument to function was less than 25 ^{o}C with 50 % of air humidity. Three times reading will be taken for the conductivities measurement in order to obtain the average while the thickness of the samples will also significantly affect the result of electrical conductivity.

3.5.2 Vibrating Sample Magnetometer (VSM)

The main purpose of VSM analysis is to measure the magnetic property of a magnetic material. First of all, a sample was put on a rod with constant magnetic field to magnetize the sample and substantially vibrated through the usage of piezoelectric material. The rod was then allocated between the pole pieces of an electromagnet where the detection coils have been fixed. The oscillatory motion of magnetized sample can stimulate the voltage in the coils and the voltage is proportional to the sample's magnetic moment but independent on the strength of the applied magnetic field. A hysteresis loop, which containing saturated magnetization (Ms), remnant magnetization (Mr) and coercive force (Hc) can be determined by measuring the field of an external electromagnet (Burgei, Pechan, & Jaeger, 2003).

Samples used for the magnetization measurements were in pellet form with diameter of 10 mm and thickness of ~1 mm. The samples were compressed slowly by a constant load of 625 kg for 10 minutes and the compact densities for these samples were ~1.00 g/cm^3. Magnetization of the PAni nanocomposites at magnetic field from -1.0 kOe to 1.0 kOe was analyzed by VSM, Lakeshore 7400 Series model at room temperature as shown in Figure 3.3.

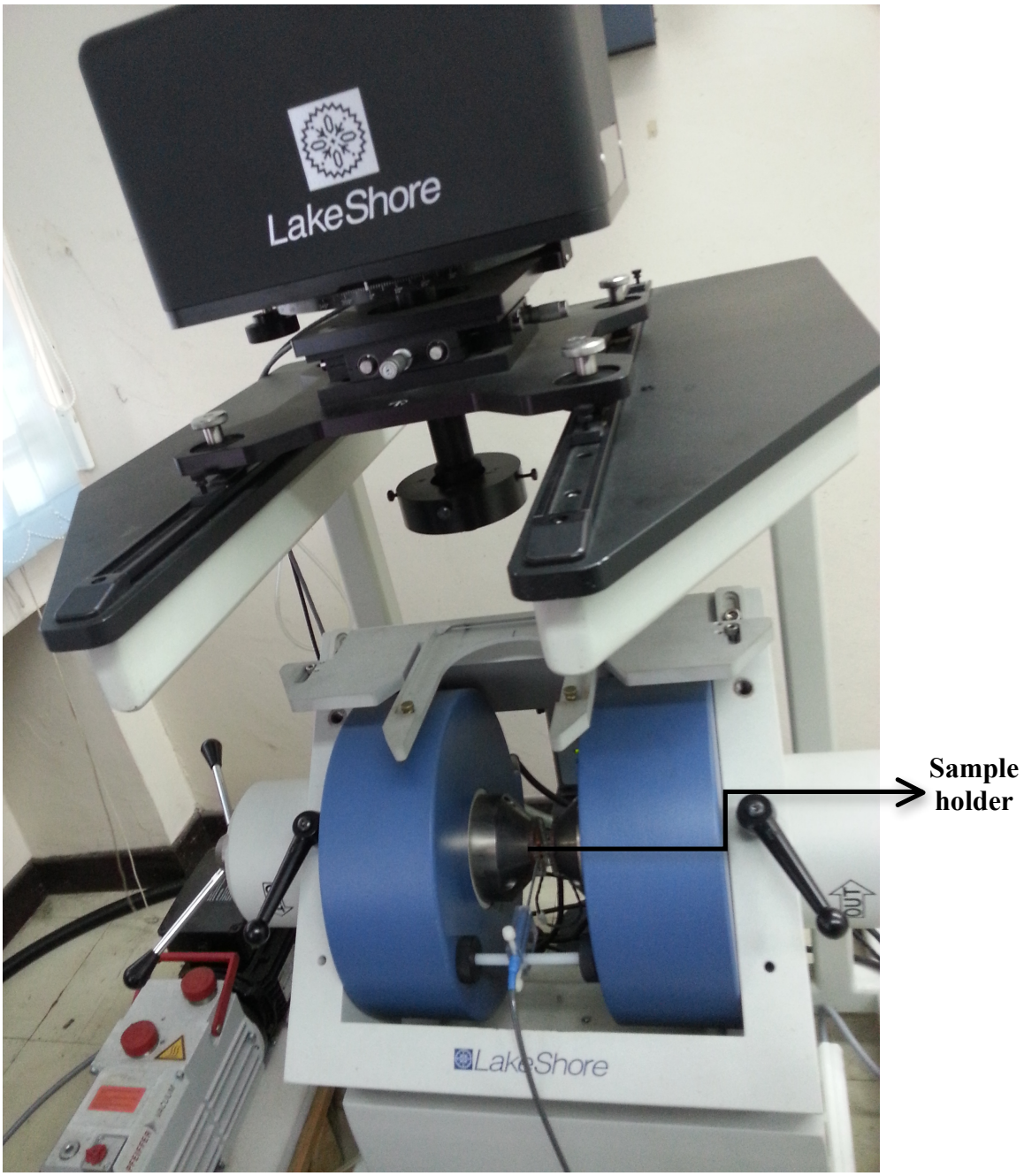

Figure 3.3 VSM instrument of Lakeshore 7400 Series model used for magnetic measurement.

3.5.3 Microwave absorption measurement

Complex reflection and transmission characteristic of two ports devices can be measured by MVNA, in which the incident signal was tested, dividing the reflected and transmitted waves following by displayed the ratios that are directly proportional to the reflection and transmission coefficients. However in this study, one port device was used by metal-backed system.

In order to obtain high precision result, a full cycle of one-port calibration was carried out before measurement to minimize the errors, which will occur during microwave measurement such as load match, isolation, source match, directivity and frequency response. MVNA was calibrated using air as standard where $\varepsilon_r' = 1$, $\varepsilon_r'' = 0$, $\mu_r' = 1$ and $\mu_r'' = 0$ through the frequency range. The complex scattering parameters correlated to reflection (S_{11}*) of transverse electromagnetic (TEM) which rely on a model of single-layered plane wave absorber backed by an excellent conductor were determined. Therefore, the transmission of the microwave was expected as 0 % from 0.4 GHz to 18 GHz (Phang, Daik, & Abdullah, 2004). Additionally, complex dielectric permittivity ($\varepsilon_r^* = \varepsilon_r' - j\varepsilon_r''$) and complex magnetic permeability ($\mu_r^* = \mu_r' - \mu_r''$), in which consist of real (ε_r' or μ_r') and imaginary (ε_r'' or μ_r'') parts were also been studied (Osawa & Kuwabara, 1992).

PAni nanocomposites were measured by MVNA instrument, Anritsu 37369C model (Figure 3.4) from frequency range of 0.5 – 18 GHz by using toroidal samples (Figure 3.5) of PAni nanocomposites with outer diameter of 6.92 - 6.94 mm and inner diameter of 2.8 mm. The samples were compressed up to 750 kg for 35 minutes and the compact densities of the samples were ~1.10 g/cm^3. The reflection loss (RL) of the sample that is due to the interaction between conducting particles in both conducting material and electromagnetic material were calculated using formula, RL = 20 log S_{11}* and loss tangent (tan δ) was measured by using formula, tan $\delta = \varepsilon_r'' / \varepsilon_r'$ (Saini et al., 2009).

Figure 3.4 MVNA instrument of Anritsu 37369C model for microwave measurement.

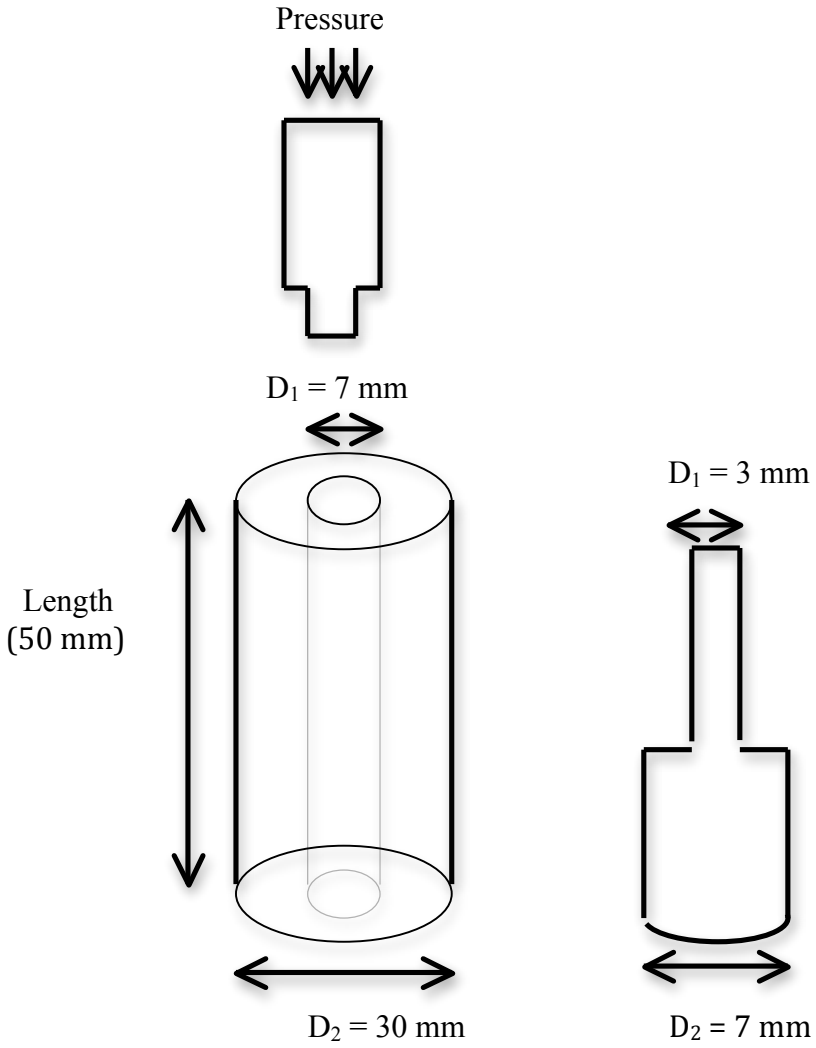

(a)

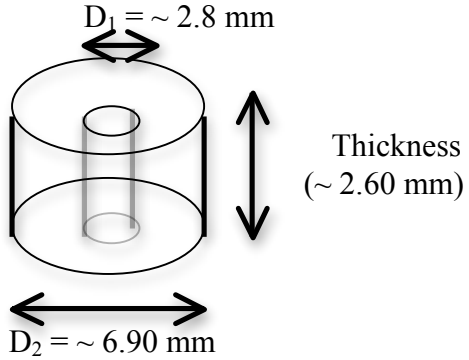

(b)

Figure 3.5 (a) Toroidal mould and (b) toroidal sample used for MVNA measurement.

CHAPTER 4

Results and Discussions

4.1 PAni/HA/TiO_2/Fe_3O_4 nanocomposites

4.1.1 FTIR analysis

FTIR spectra of pristine PAni (PAni/HA) and PAni/HA/TiO_2/Fe_3O_4 nanocomposites (without chemical treatment) with different contents (10 %, 20 % and 40 %) of Fe_3O_4 are shown in Figure 4.1. In general, both pristine PAni and PAni/HA/TiO_2/Fe_3O_4 nanocomposites (with and without chemical treatment) show similar FTIR spectra from 400 – 4000 cm^{-1}. The peaks at 2931 cm^{-1} and 2828 cm^{-1} are characteristic peaks for the CH_3 and CH_2 stretching of PAni while the peaks at 1578 cm^{-1} and 1498 cm^{-1} indicate the quinoid and benzenoid rings, respectively (Lixia Zhang, Zhang, Wan, & Wei, 2006). The peaks at 1301 cm^{-1} and 1248 cm^{-1} show the C-N stretching vibration of PAni while the quinoid unit of doped-PAni appears at 1142 cm^{-1}. Furthermore, the band at 595 cm^{-1} represents the presence of Fe_3O_4 in PAni/HA/TiO_2/Fe_3O_4 nanocomposites (Chen, Wang, Zhao, & Li, 2003).

There is a small vibration of C=O corresponding to HA dopant at 1755 cm^{-1} but it does not show any peak on the spectra due to the overlapping of quinoid ring from pristine PAni and PAni/HA/TiO_2/Fe_3O_4 nanocomposites (Lixia Zhang et al., 2006). As mentioned earlier, pristine PAni and PAni/HA/TiO_2/Fe_3O_4 nanocomposites show almost identical peak in all different contents of PAni/HA/TiO_2/Fe_3O_4 nanocomposites without chemical treatment. Besides, PAni/HA/TiO_2/Fe_3O_4 nanocomposites with chemical treatment show similar spectra as PAni/HA/TiO_2/Fe_3O_4 nanocomposites without chemical treatment (Phang & Kuramoto, 2010).

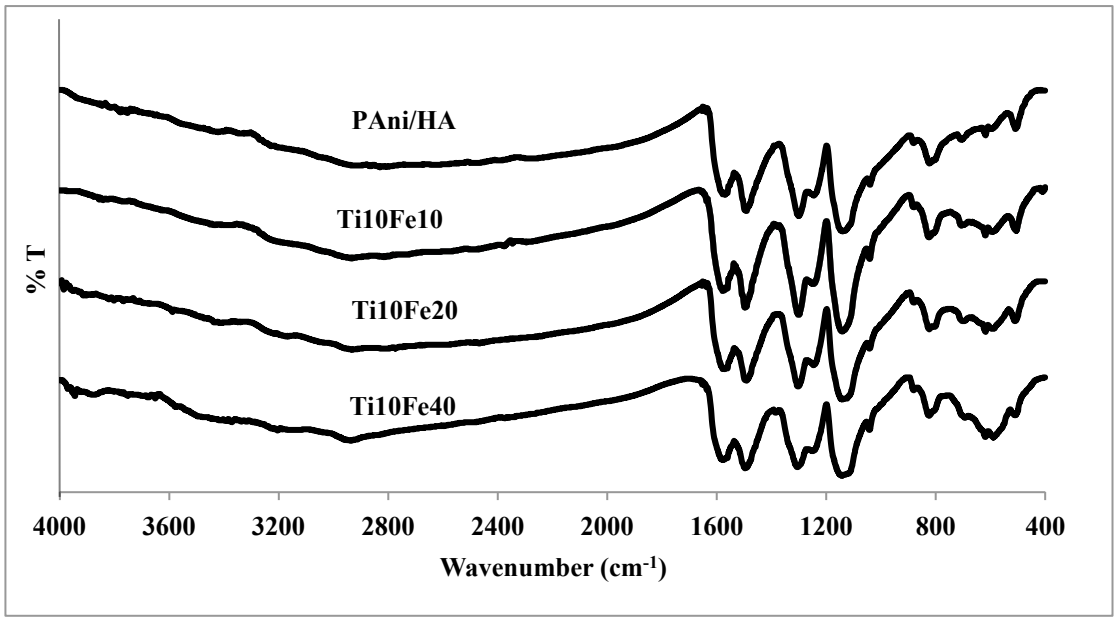

Figure 4.1. FTIR spectra of PAni/HA and PAni nanocomposites (without chemical treatment) with different contents of Fe_3O_4.

4.1.2 UV-vis analysis

The UV-vis absorption spectrum of PAni/HA/TiO_2/Fe_3O_4 nanocomposites (TiO_2: 10%, Fe_3O_4: 10%) without chemical treatment is given in Figure 4.2. The band observes at 375 nm represents the π-π* transition of the benzenoid ring while a shoulder-like peak near 800 nm indicates the emeraldine salt phase of doped-PAni. Generally, all PAni/HA/TiO_2/Fe_3O_4 nanocomposites (with and without chemical treatment) with different contents of Fe_3O_4 content show almost identical peak in UV-vis spectra from 300 nm to 900 nm (Phang, Tadokoro, Watanabe, & Kuramoto, 2009).

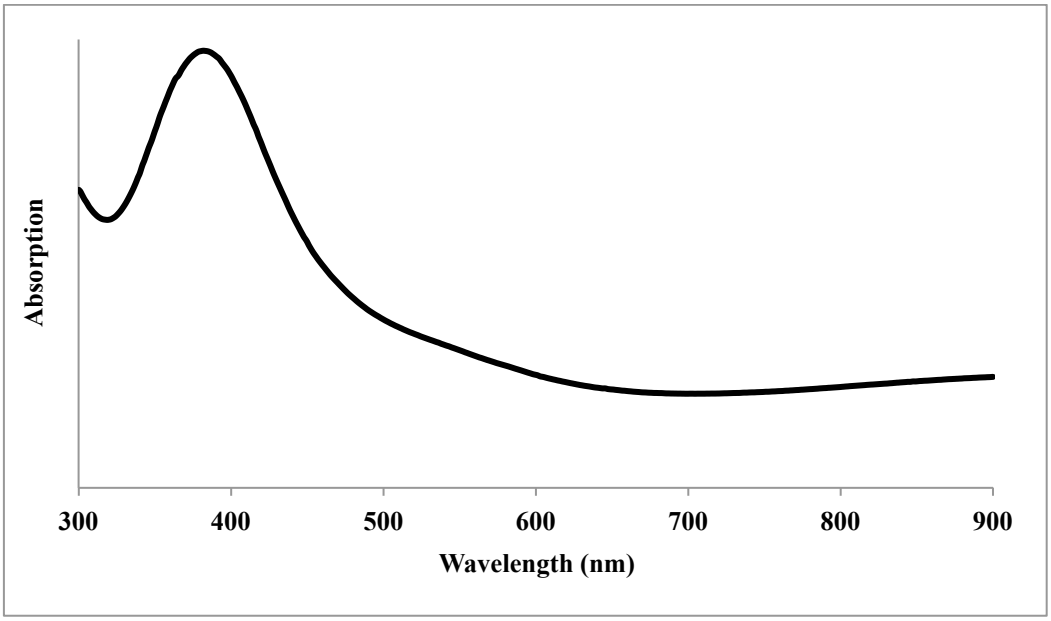

Figure 4.2. UV-vis spectrum of PAni/HA/TiO_2/Fe_3O_4 nanocomposites (without chemical treatment) with 10 % of TiO_2 and 10 % of Fe_3O_4.

4.1.3 XRD analysis

Crystallinity orientations of PAni/HA/TiO_2/Fe_3O_4 nanocomposites are determined by XRD and the results are shown in Figure 4.3. Generally, all PAni/HA/TiO_2/Fe_3O_4 nanocomposites (with and without chemical treatment) with different contents of Fe_3O_4 show similar XRD diffraction pattern from 5 - 60^o. The X-ray diffraction patterns clearly assess that all PAni nanocomposites show amorphous behavior with major peaks at 2θ = 25.1^o which represent the characteristic of doped-PAni. The peak at 25.1^o is attributed to the periodicity parallel and perpendicular of the polymer chain direction of PAni (Martin, 1996; Yang & Wan, 2002).

Besides, all PAni/HA/TiO_2/Fe_3O_4 nanocomposites show the existence of TiO_2 peaks at 2θ = 25.2^o and 48.1^o and the presence of Fe_3O_4 also determined by the characteristic peaks at 2θ = 13.4^o, 30.1^o, 35.6^o, 43.3^o and 57.1^o (Shalini, Subbanna, Chandrasekaran, & Shivashankar, 2003; Y.-k. Sun, Ma, Zhang, & Gu, 2004). Hence, it

can be suggested that addition of the dielectric and magnetic materials such as TiO_2 and Fe_3O_4 do not affect the chemical structure of PAni/HA/TiO_2/Fe_3O_4 nanocomposites (with and without chemical treatment) because all PAni/HA/TiO_2/Fe_3O_4 nanocomposites show almost identical peaks for FTIR, UV and XRD spectra.

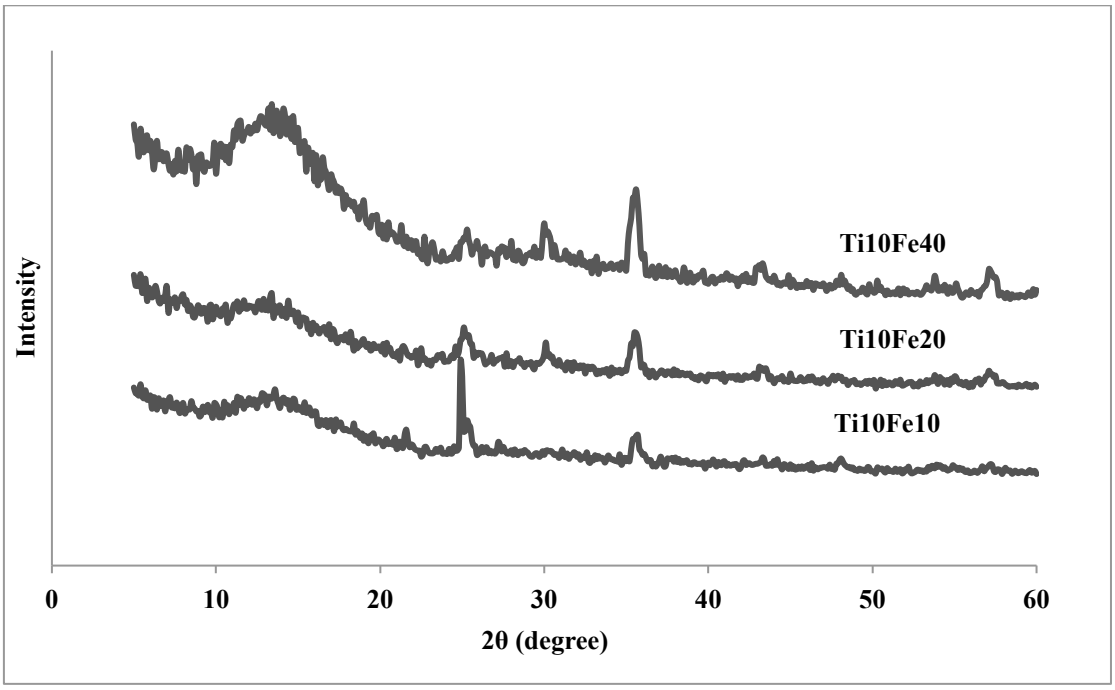

Figure 4.3. X-ray diffraction patterns of PAni/HA/TiO_2/Fe_3O_4 nanocomposites (without chemical treatment) with different contents of Fe_3O_4.

4.1.4 TGA analysis

The TGA thermograms of PAni/HA/TiO_2/Fe_3O_4 nanocomposites without chemical treatment are shown in Figure 4.4 from 50 ^oC to 900 ^oC. From the TGA profiles of PAni/HA/TiO_2/Fe_3O_4 nanocomposites, four major weight losses are observed. The first weight loss from 50 ^oC to 100 ^oC is due to the evaporation of water molecules or moistures. The second weight loss from 100 ^oC to 260 ^oC is corresponding to the loss of HA dopant from PAni chains while the third stage observed from 260 ^oC to 710 ^oC is attributed to the dedoping of HA dopant from backbone of PAni. The last

stage was responsible to the degradation of polymer backbone (Phang, Hino, & Kumamoto, 2008).

Generally, PAni/HA/TiO_2/Fe_3O_4 nanocomposites (with and without chemical treatment) with different contents of Fe_3O_4 content show the same sequence in which the thermal stabilities of PAni/HA/TiO_2/Fe_3O_4 nanocomposites were significantly improved by the addition of Fe_3O_4 nanoparticles, in which 40 % of Fe_3O_4 nanoparticles show the highest thermal stability followed by 20 % and 10 % of Fe_3O_4 nanoparticles (Kulkarni & Viswanath, 2004).

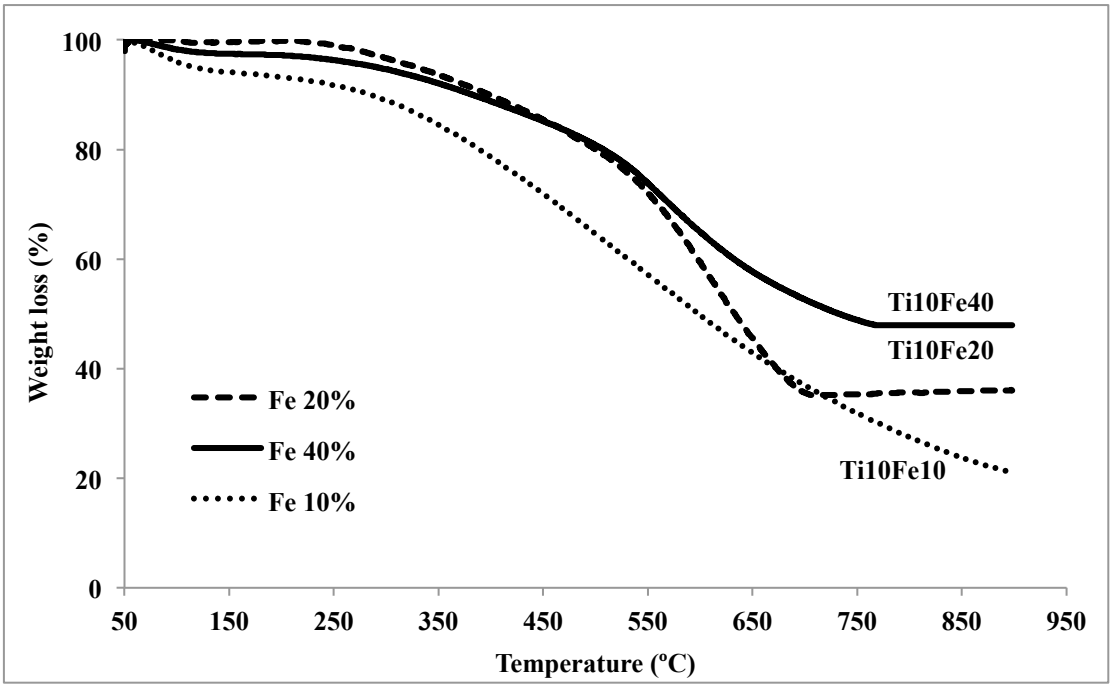

Figure 4.4. TGA thermograms of PAni/HA/TiO_2/Fe_3O_4 nanocomposites (without chemical treatment) with different contents of Fe_3O_4.

4.1.5 Morphology studies

For the template free method, since TiO_2 and Fe_3O_4 nanoparticles were dispersed well in the Ani/HA solution before polymerization, TiO_2 and Fe_3O_4 nanoparticles were assigned as the nucleus of micelles. Moreover, Ani was assessed as the shell of micelles due to its hydrophobicity while HA as the tail of micelles due to the hydrophilic properties of HA which contains –COOH group. Mechanism proposed in Figure 4.5 (a)-(b) for Ani/HA/TiO_2 nanocomposites was agreed by the Ani/salicyclic acid/TiO_2 micelles mechanism as reported by Zhang and coworkers (Lijuan Zhang, Wan, & Wei, 2005).

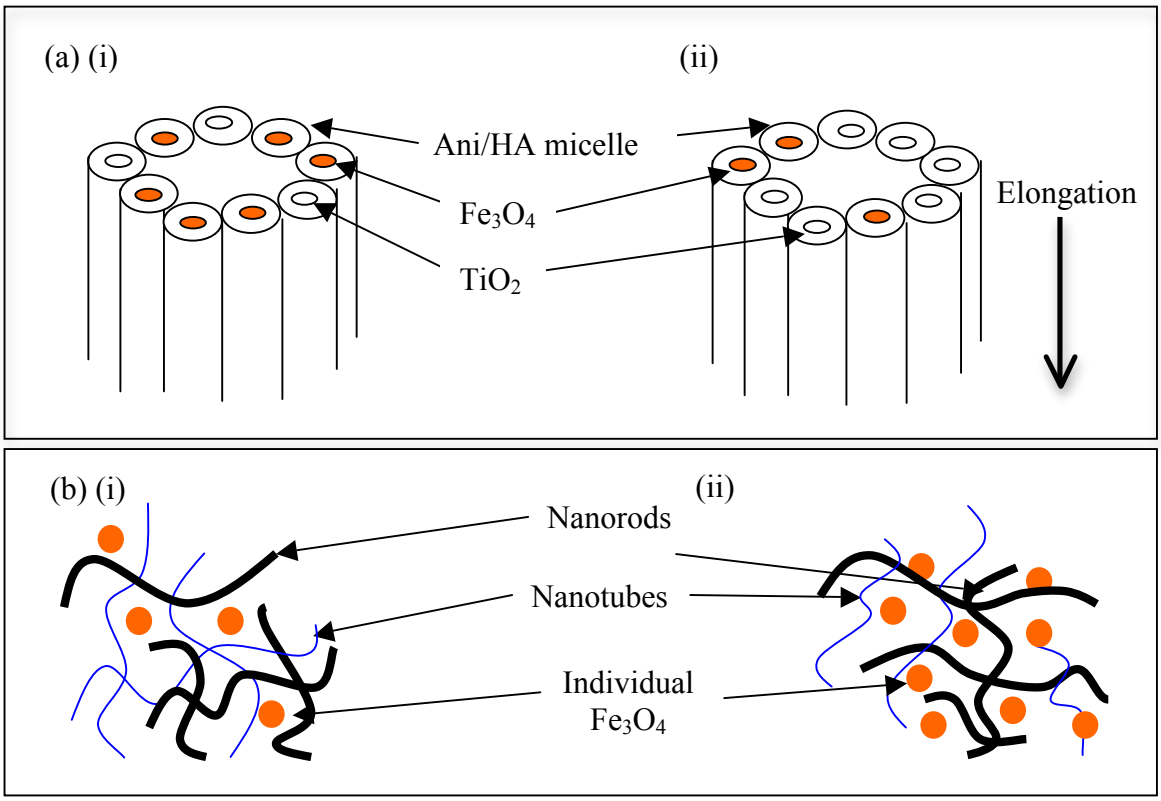

Figure 4.5. (a) Formation of nanorods/nanotubes and (b) physical interaction between nanorods/nanotubes with Fe_3O_4 and TiO_2 nanoparticles for PAni nanocomposites (i) with and (ii) without chemical treatment by template free method.

Due to the repulsive energy of the tail group of micelles, fluid surface will exist and it will form a spherical micelle first through aggregation because of the lowest surface energy. Since Ani/HA/TiO_2/Fe_3O_4 micelles were in undisturbed condition during polymerization, the Ani/HA/TiO_2/Fe_3O_4 micelles performed polymerization

through elongation at the micelle/water interface. Micelles with and without Ani will form nanorods and nanotubes, respectively. Formation of nanorods/nanotubes depends on the synthesis parameters during polymerization such as polymerization time and temperature, types of dopant used, concentration of filler and etc (Wan et al., 2003; Lixia Zhang et al., 2006).

FESEM images in Figure 4.6 show that Ani/HA/TiO_2/Fe_3O_4 micelles undergo elongation process in the micelle/water interface during polymerization in order to produce the nanorods/nanotubes. The formation of nanorods/nanotubes is suggested by the mechanism shown in Figure 4.5. Figure 4.6 clearly indicates that increasing the content of magnetic nanoparticles (Fe_3O_4) will eventually decrease the amount of nanorods/nanotubes because Fe_3O_4 will act as the barrier that impedes the formation of nanorods/nanotubes thus it significantly reduces the amount of nanorods/nanotubes for both PAni/HA/TiO_2/Fe_3O_4 nanocomposites with and without chemical treatment (Figure 4.6 (c)). Besides, the nanorods/nanotubes of PAni/HA/TiO_2/Fe_3O_4 nanocomposites show almost identical size for those with and without chemical treatment.

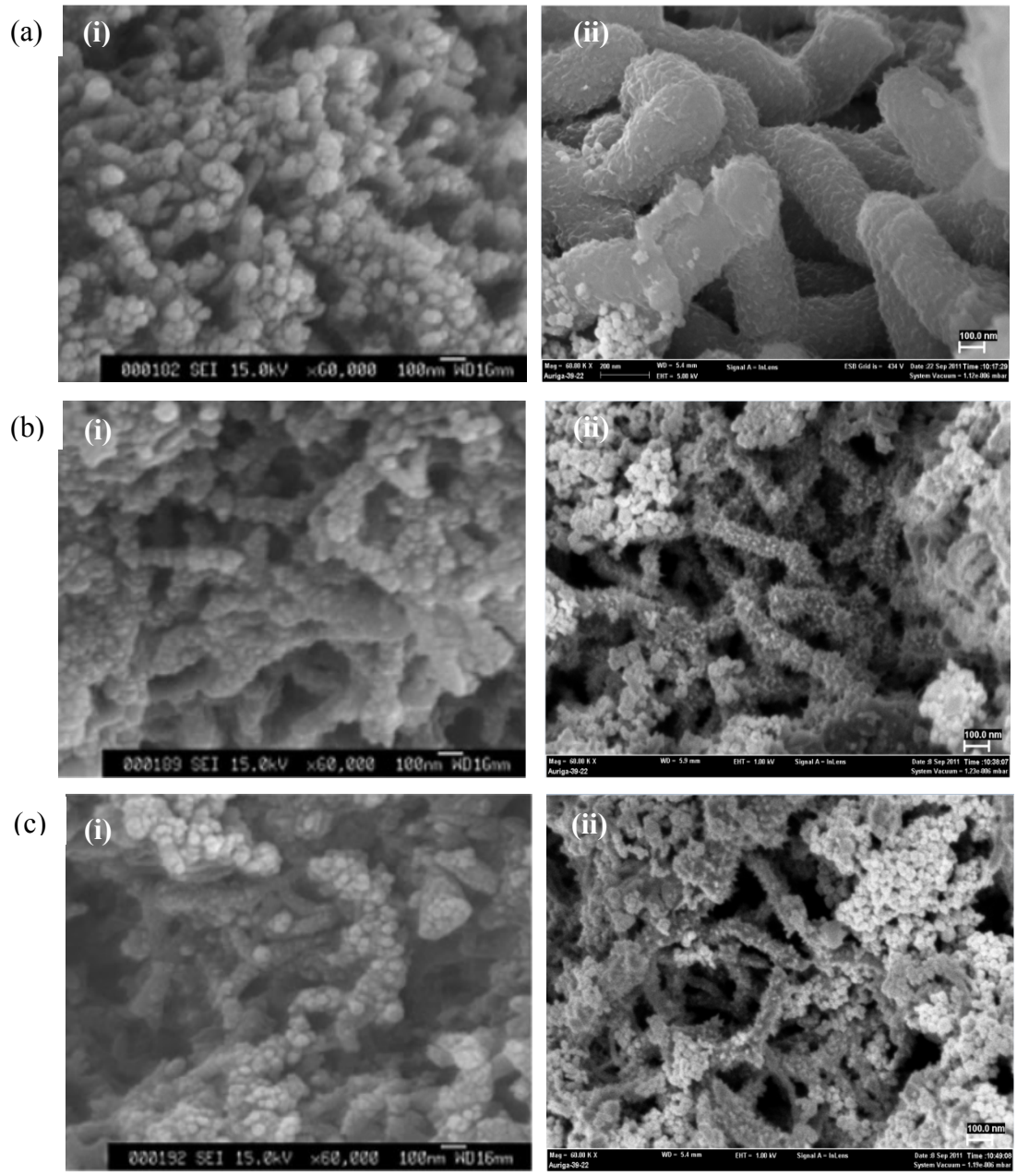

Figure 4.6. FESEM images of PAni/HA/TiO_2/Fe_3O_4 nanocomposites ((i) with and (ii) without chemical treatment) for: (a) 10 %, (b) 20 % and (c) 40 % of Fe_3O_4 nanoparticles (60,000 × magnifications).

However, PAni/HA/TiO_2/Fe_3O_4 nanocomposites with chemical treatment (Figure 4.6 (i)) show higher amount of nanorods/nanotubes if compared to those without chemical treatment (Figure 4.6 (ii)). During the preparation of PAni/HA/TiO_2/Fe_3O_4 nanocomposites with chemical treatment, chemical treatment by using $FeCl_3.6H_2O$ will significantly induce the formation of more Fe_3O_4 encapsulated PAni nanocomposites (Figure 4.6 (b)(i)) and finally increase the amount of

nanorods/nanotubes compared to those without chemical treatment (Figure 4.6 (b)(ii)) (Phang & Kuramoto, 2010).

For PAni/HA/TiO_2/Fe_3O_4 nanocomposites with chemical treatment, $FeCl_3.6H_2O$ will act as oxidant to polymerize Ani but it was not strong enough to polymerize Ani completely, thus APS has been added to start the polymerization. The real oxidant in this study was APS instead of $FeCl_3.6H_2O$ in order to give high efficiency on in situ polymerization (He Yang et al., 2011). Figure 4.7 show the dispersion of Fe_3O_4 after treated with $FeCl_3.6H_2O$. The main function of $FeCl_3.6H_2O$ was to improve the dispersion of Fe_3O_4 in Ani/HA solution after treated with $FeCl_3.6H_2O$ due to the formation of PAni-Fe_3O_4 core shell structure. In this study, Fe_3O_4 nanoparticles were surrounded by Fe^{3+} ions due to the common ion effect. The positive charge at the surface of Fe_3O_4 will prevent the aggregation of Fe^{3+} ions during polymerization process. This proposed model was supported by the formation of PPy-Fe_3O_4 that was reported by Chen and co workers in year 2003 (Chen et al., 2003).

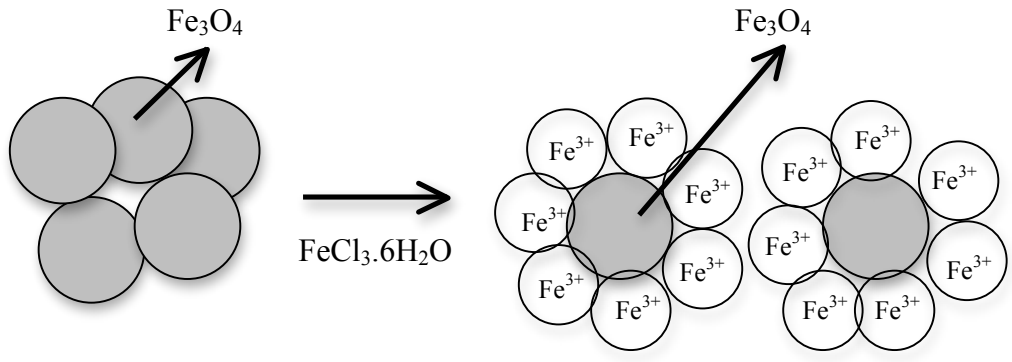

(i) Aggregation of Fe_3O_4 (ii) Common ion effect

Figure 4.7. The dispersion of Fe_3O_4 after treated with $FeCl_3.6H_2O$.

Figure 4.5 (b)(i) shows that PAni/HA/TiO_2/Fe_3O_4 nanocomposites with chemical treatment will induce the formation of more Fe_3O_4 encapsulated PAni and lead to increment in the amount of nanorods/nanotubes. Thus, the existing of individual Fe_3O_4 nanoparticles that physically mixed with nanorods/nanotubes was lesser compared to those without chemical treatment. On the other hand, there was lesser Fe_3O_4 encapsulated PAni in those nanocomposites without chemical treatment as shown in Figure 4.5 (b)(ii). Therefore, it will decrease the formation of nanorods/nanotubes in PAni without chemical treatment (Figure 4.6) as shown in Figure 4.5.

4.1.6 Conductivity studies

Electrical conductivities of PAni/HA/TiO_2/Fe_3O_4 nanocomposites with different contents of Fe_3O_4 nanoparticles (10 %, 20 % and 40 %) were tested by four-point probe and the data are shown in Table 1. The conductivities decreased simultaneously with the increasing of Fe_3O_4 nanoparticles content from 10 % to 40 % for both PAni/HA/TiO_2/Fe_3O_4 nanocomposites with and without chemical treatment. It is due to the increasing amount of Fe_3O_4 content significantly enhances the barrier that blocks the PAni conductive pathway along the PAni chain and thus reduces the conductivity of the PAni/HA/TiO_2/Fe_3O_4 nanocomposites (Phang et al., 2009).

As shown in Table 4.1, electrical conductivities of PAni/HA/TiO_2/Fe_3O_4 nanocomposites with chemical treatment show higher conductivities (3.58 ~ 4.77 x 10^{-2} S/cm compared to those without chemical treatment (8.48 x 10^{-4} ~ 1.23 x 10^{-2} S/cm). Besides, the conductivities of PAni/HA/TiO_2/Fe_3O_4 nanocomposites without chemical treatment are relatively low compared to pure PAni/HA, which exhibits the highest conductivity (2.37 x 10^{-2} S/cm). It had been proposed that Fe_3O_4 shows better dispersion in Ani/HA solution after chemical treatment and thus enhances the

possibility for the formation of Fe_3O_4 encapsulated PAni compared to those without chemical treatment.

This fact is strongly supported by the suggested mechanism as shown in Figure 4.5 (a). So, the poor conductivities as indicated by the PAni/HA/TiO_2/Fe_3O_4 nanocomposites without chemical treatment was due to the formation of more individual Fe_3O_4 nanoparticles that block the movement of free electron between the interchain of PAni besides the blockage of Fe_3O_4 encapsulated PAni along the intrachain of the PAni backbone. Oppositely, PAni/HA/TiO_2/Fe_3O_4 nancomposites with chemical treatment, the conductive pathway is only blocked by the individual Fe_3O_4 nanoparticle between the interchain of PAni backbone if compared to those without chemical treatment. Thus, electrical conductivities of PAni/HA/TiO_2/Fe_3O_4 nancomposites without chemical treatment are lower than those with chemical treatment due to the blockage of conductive pathway at both interchain and intrachain of PAni backbone.

Table 4.1. Conductivity and magnetization data for PAni nanocomposites ((i) with and (ii) without chemical treatment) with different contents of Fe_3O_4 nanoparticles.

Sample	Conductivity (S/cm)	Ms (emu/g)	Mr (emu/g)	Hc (Oe)
a) PAni/HA	2.37×10^{-2}	-	-	-
b) (i) PAni/HA/Ti10/Fe10 (with)	4.77×10^{-2}	6.03	1.09	101.80
(ii) PAni/HA/Ti10/Fe10 (without)	1.23×10^{-2}	8.87	1.44	101.36
c) (i) PAni/HA/Ti10/Fe20 (with)	4.42×10^{-2}	10.10	1.78	96.10
(ii) PAni/HA/Ti10/Fe20 (without)	3.51×10^{-3}	16.69	2.58	98.26
d) (i) PAni/HA/Ti10/Fe40 (with)	3.58×10^{-2}	16.90	3.10	92.60
(ii) PAni/HA/Ti10/Fe40 (without)	8.48×10^{-4}	28.49	4.71	100.55

4.1.7 Magnetization studies

The magnetization data for PAni/HA/TiO_2/Fe_3O_4 nanocomposites (with and without chemical treatments) with different contents (10 %, 20 % and 40 %) of Fe_3O_4 nanoparticles are shown in Table 4.1. The saturated magnetization (Ms), remnant magnetization (Mr) and coercive force (Hc) are determined by the magnetization curves as shown in Figure 4.8.

Ms is a state in which magnetization of a material cannot exceed although external magnetic field is applied while Mr is magnetization that left out after the external magnetic field has been removed. As for Hc, it is the measurement of a ferromagnetic material that can endure external magnetic field. Among all the magnetization data, Ms will be focused in this research study because Ms represents the magnetic property of a nanocomposites. Refer to Table 4.1, PAni/HA/TiO_2/Fe_3O_4 nanocomposites (without chemical treatment) with 10 % of Fe_3O_4 nanoparticles under applied magnetic field of -10 kOe to 10 kOe at room temperature exhibit a hysteric loop (Figure 4.8) with Ms of 8.87 emu/g.

From Table 1, Ms is increased simultaneously from 6.03 emu/g to 28.48 emu/g with the increasing of Fe_3O_4 content for both PAni/HA/TiO_2/Fe_3O_4 nanocomposites (with and without chemical treatments). The increment of Fe_3O_4 contents will significantly improves the magnetic effect and eddy current in the material. This improvement eventually enhance the anisotropy in the materials and thus induce the magnetization of the PAni/HA/TiO_2/Fe_3O_4 nanocomposites (Costa, Valente, Sá, & Henry, 2006).

From the data obtained, PAni/HA/TiO_2/Fe_3O_4 nanocomposites without chemical treatment show better magnetization (Ms = 8.87 – 28.48 emu/g) if compared to those with chemical treatment (Ms = 6.03 – 16.90 emu/g). For PAni/HA/TiO_2/Fe_3O_4 nanocomposites without chemical treatment, more individual Fe_3O_4 nanoparticles exist outside the nanorods/nanotubes that possess high mobility and increase the Ms value of the nanocomposite. As for PAni/HA/TiO_2/Fe_3O_4 nanocomposites with chemical treatment, the mobility/motion of the Fe_3O_4 are restricted because the individual Fe_3O_4 are encapsulated by the PAni layer inside the micelles and thus significantly reduce the Ms value (Phang & Kuramoto, 2010).

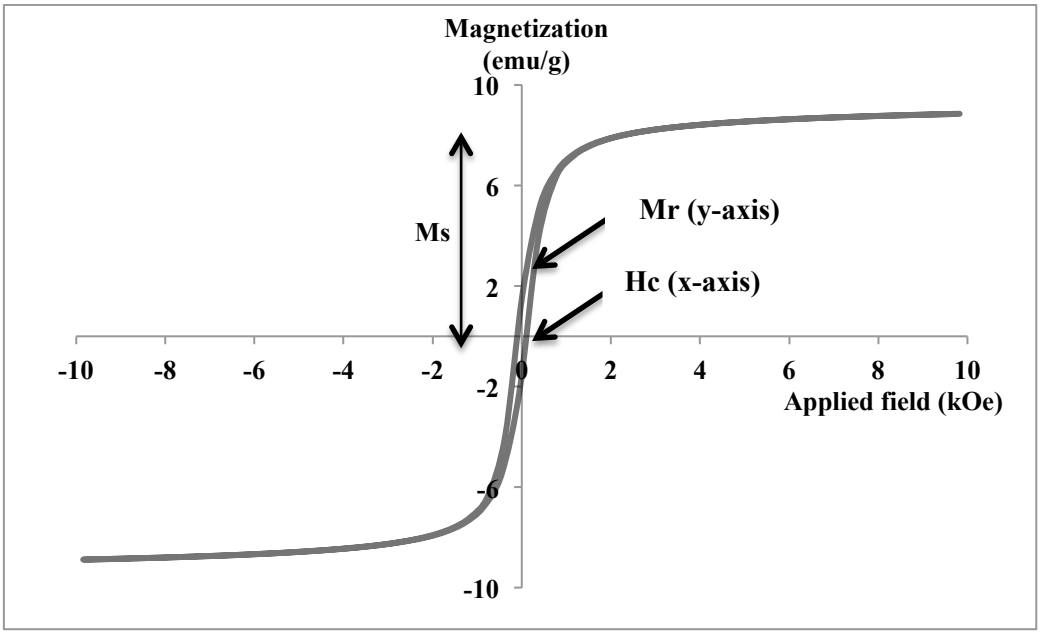

Figure 4.8. Variation of magnetization with the applied magnetic field measured at room temperature for PAni/HA/TiO_2/Fe_3O_4 nanocomposites (without chemical treatment) with 10 % of Fe_3O_4 nanoparticles.

4.1.8 Microwave absorption studies

The complex dielectric permittivity and complex magnetic permeability are tested by MVNA from the range of 0.4 GHz till 18 GHz. In general, RL is used to study the interaction between the conducting particles in both conducting material and electromagnetic material. In this study, RL are calculated using formula, RL = 20 log S_{11}*.

Figure 4.9 shows the RL of PAni/HA/TiO_2/Fe_3O_4 nanocomposites (with and without chemical treatments) with different contents (10 %, 20 % and 40 %) of Fe_3O_4 nanoparticles. The dip in the RL curve indicates the appearances of absorption and reflection of the microwave. Refer to Figure 4.9, PAni/HA/TiO_2/Fe_3O_4 nanocomposites without chemical treatment exhibit the broad RL peak with poor absorption (RL = -11 dB to -13 dB) in frequency range of 11-12 GHz. By comparison, PAni/HA/TiO_2/Fe_3O_4 nanocomposites after chemical treatment possesses the narrow and sharp RL peak with high absorption (-35.6 dB to -48.9 dB) at lower frequency range of 10-11 GHz (Wan, Liu, Qiu, Li, & Li, 2001).

Generally, polymer exhibits a broad absorption peak due to its various conductivities along the long molecular chain. However, the traditional microwave absorption materials such as metals possess the sharp RL peak due to its constant conductivity value. The narrow conductivity range of PAni/HA/TiO_2/Fe_3O_4 nanocomposites with chemical treatment that rise from the majority of Fe_3O_4 encapsulated by PAni inside the nanorods/nanotubes (Figure 4.5 (i)) contribute to the narrow sharp RL peak with high absorption (Figure 4.9 (i)). However, the broad conductivity range for those without chemical treatment that due to the minimum

amount of Fe_3O_4 encapsulated by PAni inside the nanorods/nanotubes (Figure 4.5 (ii)) gives rise to the broad RL peak with poor absorption (Figure 4.9 (ii)).

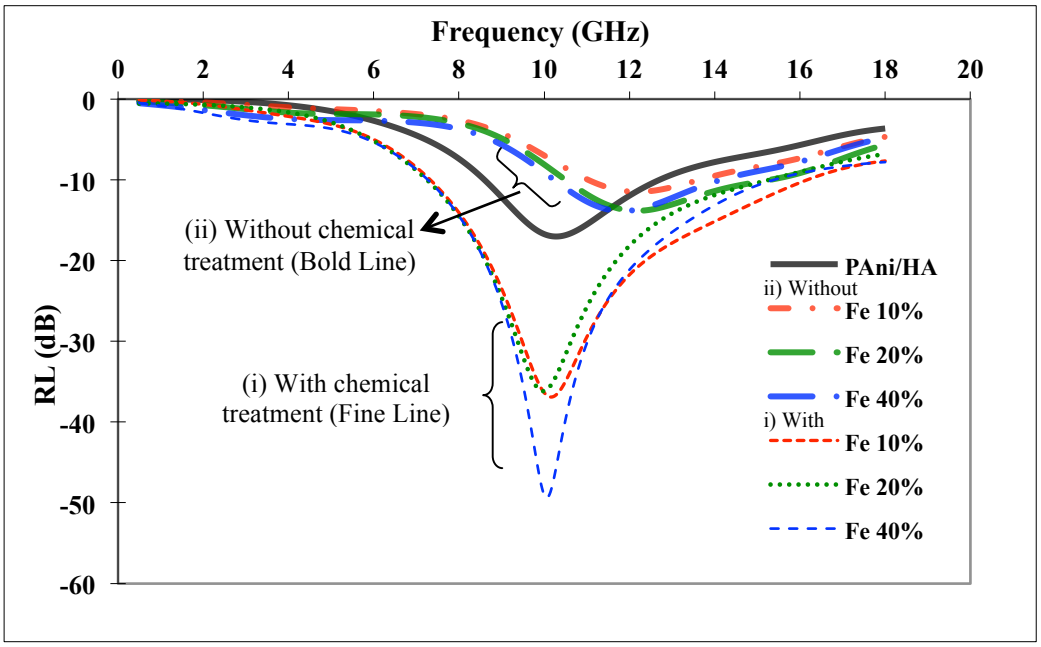

Figure 4.9. Reflection loss (RL) for both PAni/HA/TiO_2/Fe_3O_4 nanocomposites ((i) with and (ii) without chemical treatment) with different contents (10%, 20% and 40%) of Fe_3O_4.

When the electromagnetic radiation collides with the surface of certain material, some of the radiation will be transmitted and some will be reflected. Generally, an insulator will transmit almost all of the radiation but will not reflect from the surface, which shows the low value in surface resistivity and conductivity. For the conductive materials like metals, the high value in both surface resistivity and conductivity will reflect almost all of the radiation. Therefore, the proposed PAni/HA/TiO_2/Fe_3O_4 nanocomposites in this study not only show the combination behavior of low surface resistivity and high conductivity but also indicate their good reflection behavior together with their best microwave absorption property (Håkansson et al., 2007).

The loss tangent (tan δ) of the samples (Figure 4.10) can be calculated from the real and imaginary part of complex dielectric permittivity using formula, tan $\delta = \varepsilon_r''/\varepsilon_r'$. Commonly, strong absorption can be identified through tan δ where higher tan δ was considered as lossy material. Thus, the value of loss tangent can estimate the microwave absorbance of PAni/HA/TiO_2/Fe_3O_4 nanocomposites in this study (Makeiff & Huber, 2006).

From Figure 4.10, PAni/HA/TiO_2/Fe_3O_4 nanocomposites with chemical treatment shows higher tan δ (0.39 – 0.67) if compared with those without chemical treatment (0.37 – 0.47), thus it can be considered as lossy material, which will induce the microwave absorbance properties. Higher tan δ that obtained from the PAni/HA/TiO_2/Fe_3O_4 nanocomposites after chemical treatment strongly proved by the strong absorption peak as shown in Figure 4.9(i).

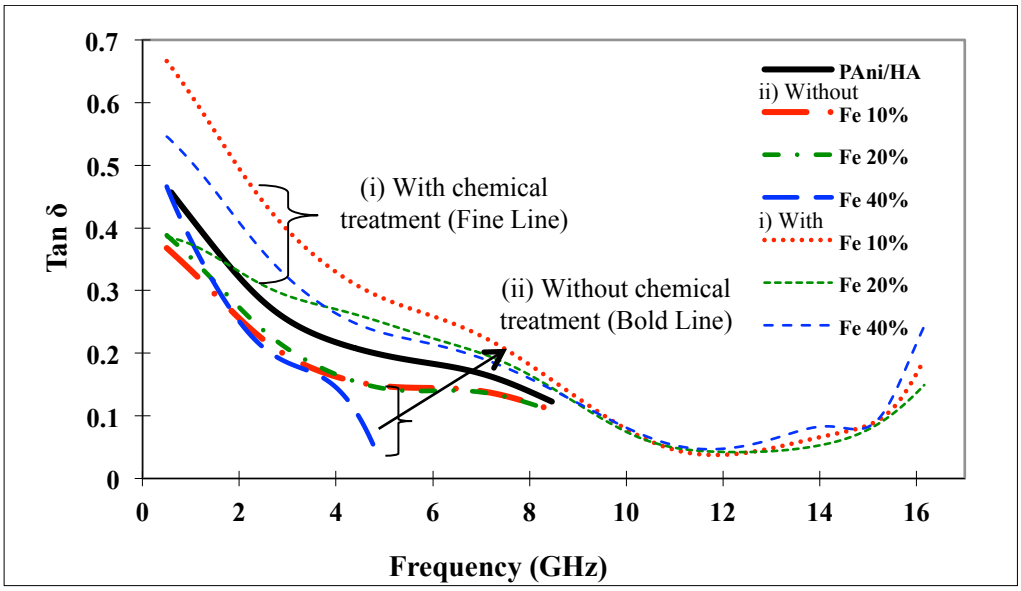

Figure 4.10. Loss tangent of PAni/HA/TiO_2/Fe_3O_4 nanocomposites ((i) with and (ii) without chemical treatment) with different contents (10 %, 20 % and 40 %) of Fe_3O_4.

Furthermore, electronic, ionic, orientation and space charge polarization are the four factors that will contribute to the dielectric behavior of a certain material. The space-charge polarization relies on the homogeneity or heterogeneity of a material (Abdul Hamid, Abdullah, Ahmad, Mansor, & Yusoff, 2002). Heterogeneity depends on the amount of nanorods/nanotubes where the higher heterogeneity will enhance the dielectric permittivity of the materials that lead to a better microwave absorbing and shielding property.

From the FESEM images (Figure 4.6), PAni/HA/TiO_2/Fe_3O_4 nanocomposites with chemical treatment show larger amount of nanorods/nanotubes. It is because the formation of more Fe_3O_4 encapsulated PAni (Figure 4.5) in PAni/HA/TiO_2/Fe_3O_4 nanocomposites with chemical treatment will activate the production of more Ani/HA micelles if compared with those without chemical treatment. This fact was strongly agreed by the mechanism that proposed in Figure 4.5. Finally, the larger amount of nanorods/nanotubes observed in the PAni/HA/TiO_2/Fe_3O_4 nanocomposites with chemical treatment significantly enhance the dielectric permittivity (heterogeneity) and thus improve the microwave absorption of the material.

In general, high conductivity, dielectric permittivity and magnetic permeability of a material will contribute to good microwave absorption and high EMI shielding efficiency (Su & Kuramoto, 2000). PAni/HA/TiO_2/Fe_3O_4 nanocomposites with chemical treatment possesses high conductivity (3.58×10^{-2} – 4.77×10^{-2} S/cm), high heterogeneity (larger amount of nanorods/nanotubes as shown in Figure 4.5) and moderate magnetization (Ms = 6.03 – 16.90 emu/g) as agreed by the proposed mechanism in Figure 4.5.

On the other hand, PAni/HA/TiO_2/Fe_3O_4 nanocomposites without chemical treatment show low conductivity (8.48×10^{-4} – 1.23×10^{-2} S/cm), low heterogeneity (Figure 4.5) and moderate magnetization (Ms = 8.87 – 28.48 emu/g) due to the formation of more individual Fe_3O_4 nanoparticles than the Fe_3O_4 encapsulated PAni. These are the main factors that might cause more disordered motion of charge carriers among the polymer and lead to the best microwave absorption and shielding behavior in PAni/HA/TiO_2/Fe_3O_4 nanocomposites with chemical treatment (RL = -35.6 dB to -48.9 dB) if compared with those without chemical treatment (RL = -11 dB to -13 dB).

Furthermore, high content (40 %) of Fe_3O_4 nanoparticles give rise to the best microwave absorption in both PAni/HA/TiO_2/Fe_3O_4 nanocomposites with (-48.9 dB) and without chemical treatment (-13 dB) if compared with those lower content (10 %) of Fe_3O_4 (with: -35.6 dB, without: -11 dB). The microwave absorption of PAni/HA/TiO_2/Fe_3O_4 nanocomposites significantly improved with the increasing of Fe_3O_4 content (10 % to 40 %) due to the increase in conductivity, tan δ, amount of nanorods/nanotubes and magnetization in which the improvement of eddy current of a materials will lead to a better microwave absorbing and shielding behavior for PAni/HA/TiO_2/Fe_3O_4 nanocomposites (with and without chemical treatments).

4.2 PAni/HA/TiO_2/MWNT nanocomposites

4.2.1 FTIR analysis

Figure 4.11 shows the FTIR spectra of PAni/HA/TiO_2/MWNT nanocomposites with different diameter (D = 10-20 nm; D = 60-100 nm) and length (l = 1-2 μm; 5-15 μm) of MWNT. The characteristic bands of PAni/HA/TiO_2/MWNT nanocomposites with different diameter and length of MWNT exhibit the similar peaks as pristine PAni as shown in Figure 4.1. The quinoid (C=N) and benzenoid (C=C) ring occur at 1586 cm^{-1} and 1509 cm^{-1} respectively attribute to the emeraldine salt form of PAni. The peaks at 1312 cm^{-1} and 1274 cm^{-1} indicate the C-N stretching mode of benzenoid ring while the 1160 cm^{-1} peak show the characteristic peak for quinoid ring of doped-PAni as reported by MacDiarmid and coworkers (Quillard, Louarn, Lefrant, & Macdiarmid, 1994).

In general, PAni/HA/TiO_2/MWNT nanocomposites show a significant decrease in peak intensity if compared to the pristine PAni (PAni/HA). During polymerization process, Ani will absorb on the MWNT that dispersed in the solution and the polymerization will start on the surface of MWNT after APS was added into the reaction mixture. There was a constrained growth of polymer on the surface of MWNT and the constrained motion of chain will restrict the vibration in PAni and thus reduce the intensity in FTIR spectrum (Feng et al., 2003). This change shows that there is some interaction occur between PAni and MWNT where the interaction may help the charge transfer process of PAni and MWNT, in which affect the transport properties of electron.

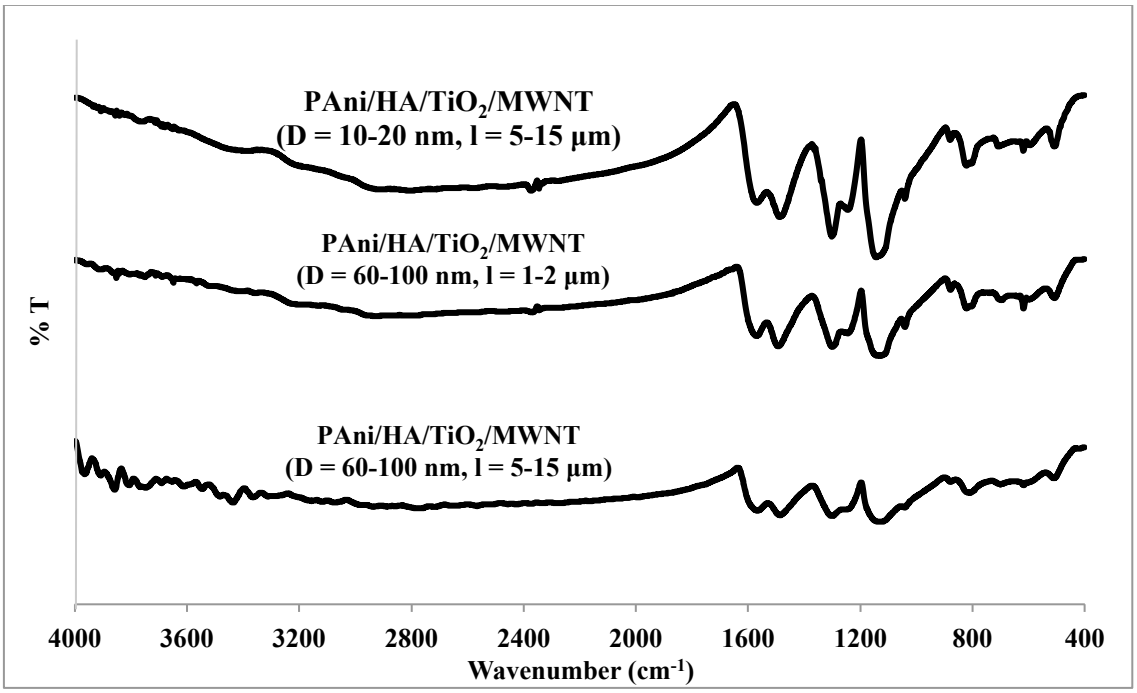

Figure 4.11. FTIR spectra for PAni/HA/TiO_2/MWNT nanocomposites with different diameter and length of MWNT.

4.2.2 UV-vis analysis

UV-vis spectrum in Figure 4.12 shows the PAni/HA/TiO_2/MWNT nanocomposites with MWNT (D = 60-100 nm, l = 1-2 µm). Generally, all the PAni/HA/TiO_2/MWNT nanocomposites with different diameter and length of MWNT possesses two bands at 364 nm and a free carrier tail near 806 nm, which indicate the π-π* transition of the benzenoid and n-π* transition of quinoid (emeraldine salt of PAni), respectively. Besides, it also shows a shoulder-like peak at 464 nm, which indicate the bipolaron peak of PAni (Y. H. Kim, Foster, Chiang, & Heeger, 1989). However, there is no new peak has been observed for pristine MWNT in PAni nanocomposites in wavenumber range of 300 – 900 nm.

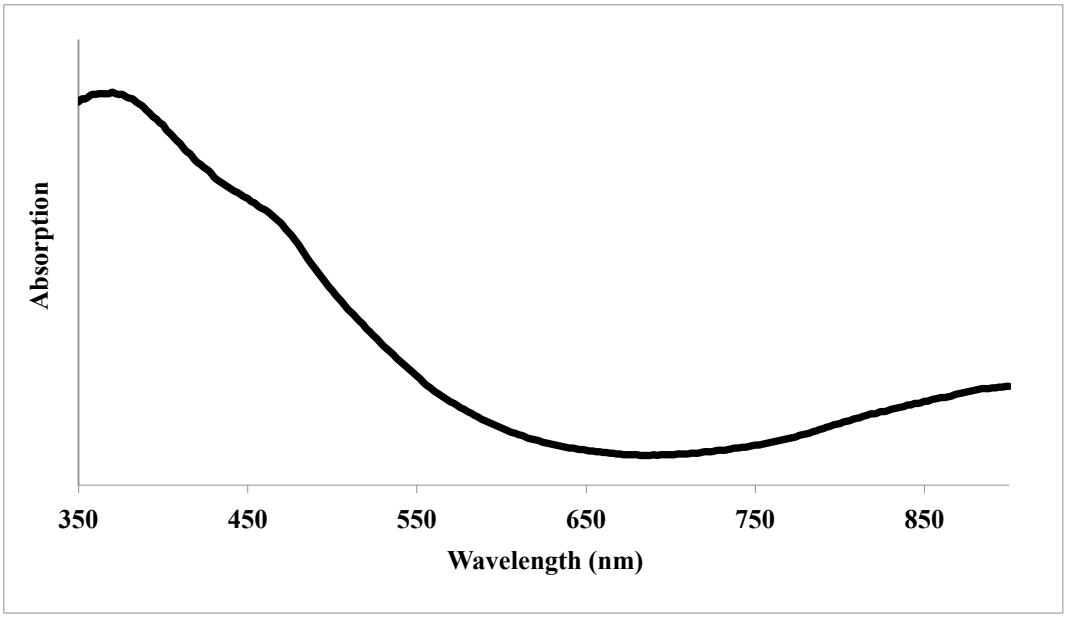

Figure 4.12. UV-vis spectrum of PAni/HA/TiO_2/MWNT nanocomposites with MWNT (D = 60-100 nm, l = 1-2 μm).

4.2.3 XRD analysis

The result of crystallinity orientations for PAni/HA/TiO_2/MWNT nanocomposites with MWNT (D = 60-100 nm, l = 1-2 μm) are shown in Figure 4.13. In general, all PAni/HA/TiO_2/MWNT nanocomposites with different diameter and length of MWNT show almost similar X-ray diffraction pattern. The diffraction peaks at 2θ = 25.2^o and 42.1^o are corresponding to the graphite-like structure and small amount of catalytic particles encapsulated inside the wall of MWNT (Endo et al., 1997). Moreover, all PAni/HA/TiO_2/MWNT nanocomposites show amorphous behavior with characteristic peaks at 2θ =6.3^o, 22.7^o and 25.2^o which represent the characteristic of doped-PAni.

Besides, the band at 25.2^o is attributed to the periodicity parallel and perpendicular of the polymer chain direction of PAni (Lijuan Zhang et al., 2005). Besides, all PAni/HA/TiO_2/MWNT nanocomposites exhibit the existence of TiO_2 peaks at 2θ = 35.1^o, 37.5^o, 47.8^o, 53.3^o, 54^o, 61.9^o, 67.9^o, 69.2^o and 74.0^o. In summary, it can

be proposed that the addition of dielectric and magnetic materials such as TiO_2 and MWNT do not affect the chemical structure of PAni because all PAni/HA/TiO_2/MWNT nanocomposites with different diameter and length of MWNT show almost identical peaks for FTIR, UV-vis and XRD spectra.

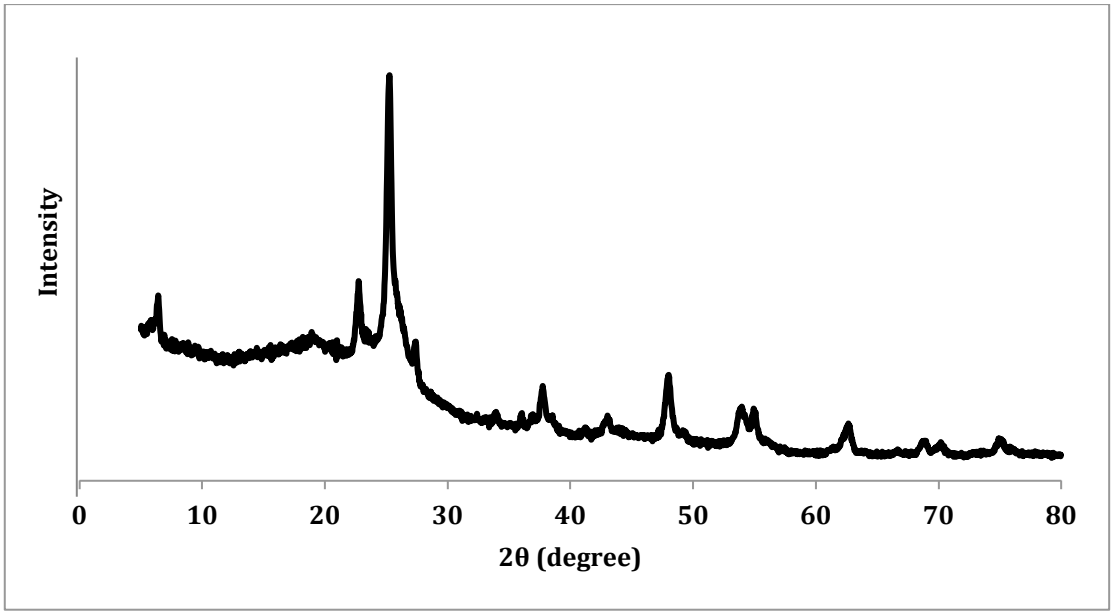

Figure 4.13. X-ray diffraction patterns of PAni/HA/TiO_2/MWNT nanocomposites with MWNT (D = 60-100 nm, l = 1-2 μm).

4.2.4 TGA analysis

Figure 4.14 indicates the TGA thermogram of PAni/HA/TiO_2/MWNT nanocomposites with different diameter and length of MWNT from 50 ^oC to 900 ^oC. There are four major weight losses can be observed from the TGA profiles. The first step loss below 100 ^oC is due to the evaporation of water molecules while the second step loss from 100 ^oC to 270 ^oC is corresponding to the loss of HA dopant from PAni chains. The third stage (steepest weight loss) observed from 270 ^oC to 750 ^oC is attributed to the dedoping of HA dopant from the PAni backbone. Finally, the last stage is responsible to the degradation of PAni backbone (Phang, Hino, et al., 2008). The

remaining residues (after 750 ^{o}C) are mainly contributed to the high thermally stable MWNT.

From the TGA thermograms, PAni/HA/TiO_2/MWNT nanocomposites with longer length (l = 5-15 μm) of MWNT show the highest thermal stabilities compared to those with shorter length (l = 1-2 μm). It is because the longer length of MWNT provides more active site to initiate the polymerization at the surface of MWNT in order to form more PAni/MWNT nanorods/nanotubes (Wu & Lin, 2006). Oppositely, PAni/HA/TiO_2/MWNT nanocomposites with different diameter possess almost similar TGA thermogram as shown in Figure 4.14. Thus, length of MWNT plays an important role in thermal stability instead of the diameter of MWNT.

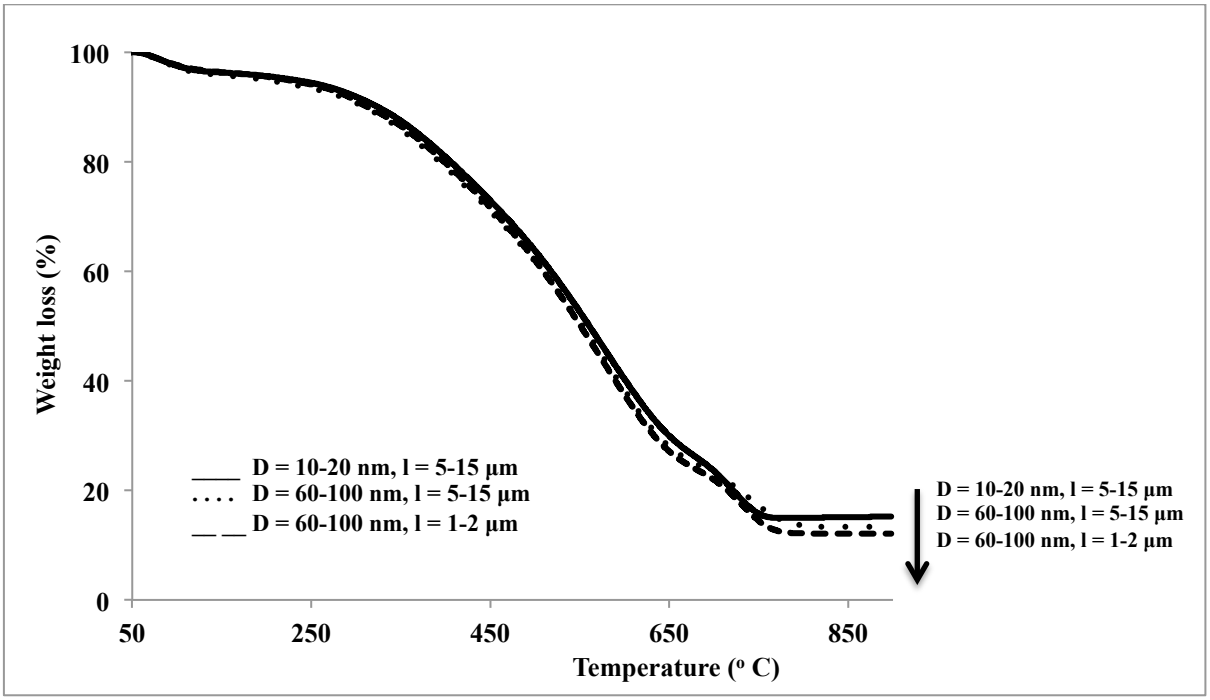

Figure 4.14. TGA thermogram of PAni/HA/TiO_2/MWNT nanocomposites with different diameter and length of MWNT.

4.2.5 Morphology studies

Figure 4.15 shows the proposed micelle mechanism of PAni/HA/TiO_2/MWNT nanocomposites with different diameter and length of MWNT. During the polymerization process, TiO_2 and MWNT will act as the nucleus of the micelles because TiO_2 and MWNT were dispersed well in Ani/HA solution where Ani/HA/TiO_2/MWNT mixture was stirred vigorously for 24 hours before polymerization. Besides, Ani will assign as shell of the micelle due to the hydrophobic property of Ani and HA will act as tail of the micelle owing to the hydrophilicity of –COOH group in HA dopant.

The core-shell structure that proposed in Figure 4.15 for Ani/HA/TiO_2/MWNT nanocomposites was agreed by the Ani/salicyclic acid/TiO_2 micelles mechanism as reported by Zhang and coworkers (Lijuan Zhang et al., 2005). In general, nanosphere will be formed if a solution was stirred vigorously during polymerization, Since Ani/HA/TiO_2/MWNT micelles were in undisturbed condition during polymerization, therefore Ani/HA/TiO_2/MWNT micelles polymerized through elongation at the micelle/water interface to form the nanorods/nanotubes.

FESEM images in Figure 4.16 show that Ani/HA/TiO_2/MWNT micelles undergo elongation process in the micelle/water interface during polymerization in order to form the nanorods/nanotubes. The formation of nanorods/nanotubes is proposed by the mechanism shown in Figure 4.15.

From the FESEM images, longer length of MWNT (l = 5-15 μm) forms more nanorods/nanotubes if compared to shorter length of MWNT (l = 1-2 μm) in PAni/HA/TiO_2/MWNT nanocomposites. It is because longer length of MWNT will provide more active sites for Ani to initiate the polymerization and this eventually increase the amount of nanorods/nanotubes. However, MWNT with different diameter does not show an obvious change in amount of nanorods/nanotubes because longer length of MWNT will prove more absorption site if compared to those with bigger diamter (Wu & Lin, 2006). Moreover, nanorods/nanotubes with smaller diameter (D = 10-20 nm) of MWNT will exist in agglomerated form if compared to bigger diameter (D = 60-100 nm) where the nanorods/nanotubes are aligned well in the reaction system.

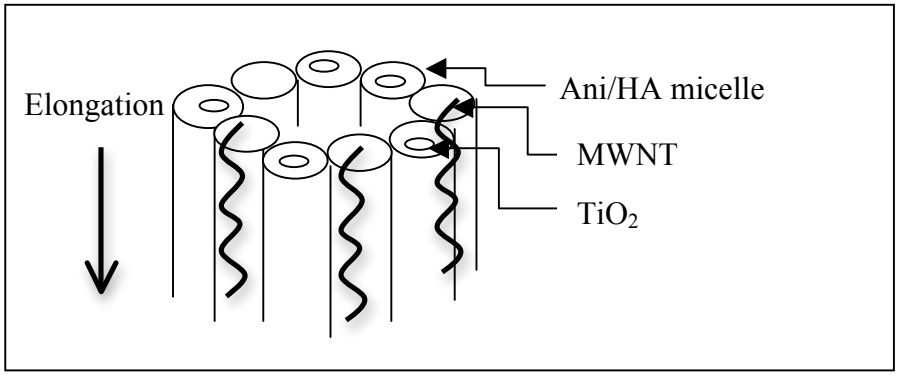

Figure 4.15. Formation of nanorods/nanotubes in PAni/HA/TiO_2/MWNT nanocomposites with different diameter and length of MWNT by template free method.

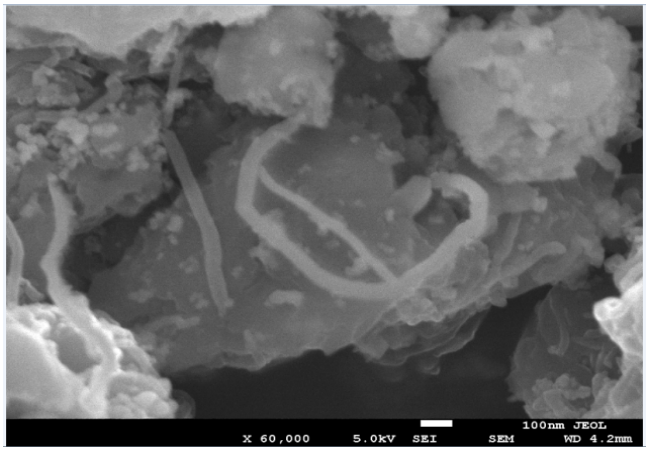

a) PAni/HA/TiO_2/MWNT (D = 60-100 nm, l = 1-2 μm)

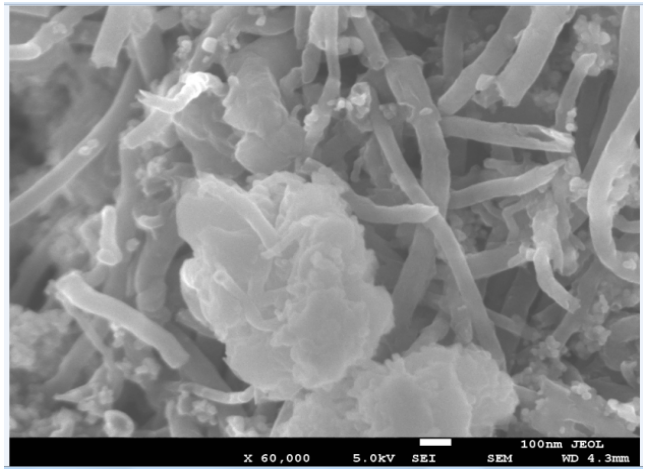

b) PAni/HA/TiO_2/MWNT (D = 60-100 nm, l = 5-15 μm)

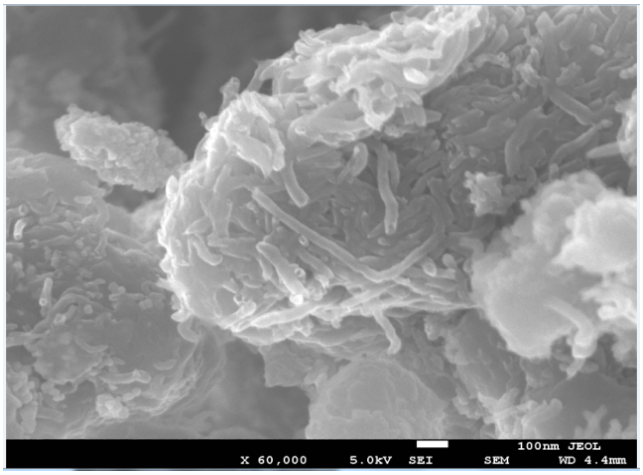

c) PAni/HA/TiO_2/MWNT (D = 10-20 nm, l = 5-15 μm)

Figure 4.16. FESEM images for PAni/HA/TiO_2/MWNT nanocomposites with different diameter and length of MWNT. (Magnification: 60, 000 ×)

4.2.6 Conductivity studies

Figure 4.17 shows the electrical conductivities of PAni/HA/TiO_2/MWNT nanocomposites with different diameter and length of MWNT. PAni/HA/TiO_2/MWNT nanocomposites (D = 60-100 nm, l = 5-15 μm) with longer length and bigger diameter of MWNT possess the highest conductivity (1.51 x 10^{-2} S/cm) if compared to those with shorter length and smaller diameter of MWNT (1.11 x 10^{-2} – 6.53 x 10^{-3} S/cm). It is because the bigger diameter and longer length of MWNT provide high surface area that will facilitate both intrachain charge transfer along the MWNT and interchain charge transfer between MWNT and PAni (Saini et al., 2009).

In general, the electrical conductivity of a conducting polymer mainly related on the conjugated length or chain length, doping level, synthesis method, polymer type, aspect ratio of CNT, degree of alignment, disentanglement of CNT agglomerated and etc. (Tishkova et al., 2011). Thus, high aspect ratio (bigger diameter and longer length) of MWNT will serve as the connecting bridge (interchain charge transfer) between the two components and thus significantly enhance the electrical conductivities (Nagaraja et al., 2012).

Based on the data obtained, PAni/HA/TiO_2/MWNT nanocomposites (D = 60-100 nm, l = 5-15 μm) with longer length and bigger diameter of MWNT that show the highest amount of nanorods/nanotubes (Figure 4.16 (b)) will possess the highest electrical conductivity. The highest amount of nanorods/nanotubes indicate that large amount of MWNT cores are enwrapped by PAni layer and induce more π-π* interaction between the surface of MWNT and the quinoid ring of PAni chain. Thus, it significantly facilitates the conductivity of PAni/HA/TiO_2/MWNT nanocomposites (D = 60-100 nm, l = 5-15 μm) with bigger diameter and longer length of MWNT if compared to those

with smaller diameter and shorter length (Jeevananda, Siddaramaiah, Kim, Heo, & Lee, 2008).

For the MWNT with small diameter and longer length, it is clearly show that nanorods/nanotubes (Figure 4.16 (c)) of PAni/HA/TiO_2/MWNT nanocomposites (D = 10-20 nm, l = 5-15 μm) were entangled and block the movement of electron along the intrachain of nanords/nanotubes. Hence, it significantly reduces the electrical conductivities although it shows the almost similar amount of nanorods/nanotubes with PAni/HA/TiO_2/MWNT nanocomposites (D = 60-100 nm, l = 5-15 μm). Thus, it can be concluded that higher amount of nanorods/nanotubes (high heterogeneity) will give rise to a better electrical conductivity in the situation of nanorods/nanotubes are not entangled together.

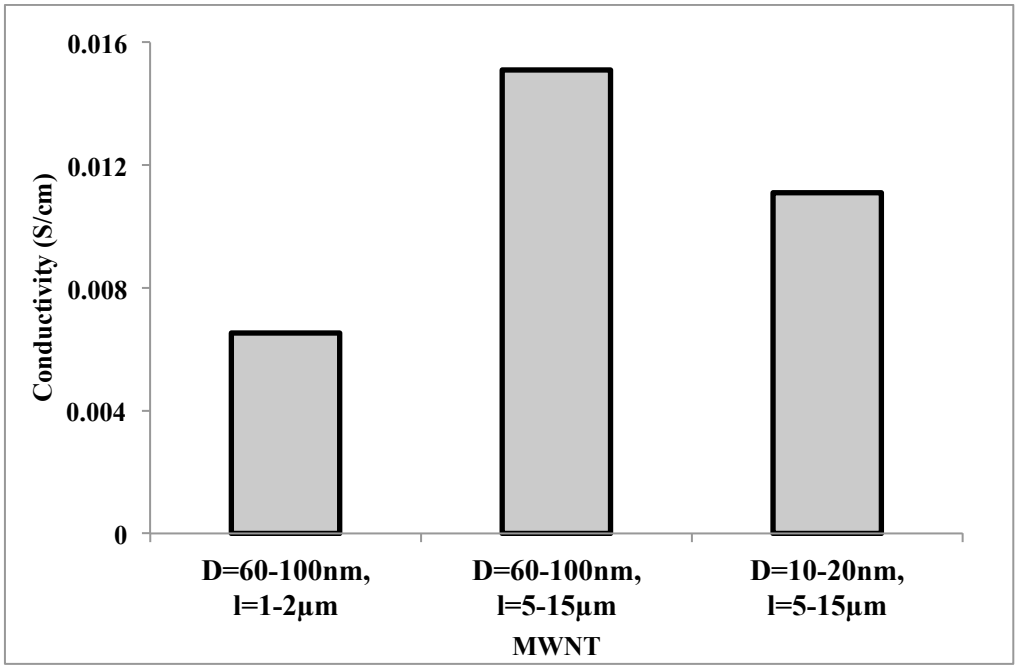

Figure 4.17. Electrical conductivities of PAni/HA/TiO_2/MWNT nanocomposites with different diameter and length of MWNT.

4.2.7 Magnetization studies

The saturated magnetization (Ms) result of PAni/HA/TiO_2/MWNT nanocomposites with different diameter and length of MWNT can be determined by the hysteresis loop as shown in Figure 4.18. Generally, PAni is not a magnetic material. So, the Ms value of the PAni nanocomposites are mainly attributed to the existence of MWNT (Y.-J. Zhang, Lin, Chang, & Wu, 2011). As shown in Figure 4.19, PAni/HA/TiO_2/MWNT nanocomposites with MWNT (D = 10-20 nm, l = 5-15 μm) exhibit the highest Ms (0.074 emu/g) if compared to PAni/HA/TiO_2/MWNT nanocomposites with MWNT (D = 60-100 nm, l = 5-15 μm) and MWNT (D = 60-100 nm, l = 1-2 μm).

In principle, agglomeration and interparticle distance between PAni/HA/TiO_2/MWNT nanorods/nanotubes play important roles in magnetization property. From the FESEM images (Figure 4.16 (c)), it is clearly indicate that the larger amount of nanorods/nanotubes in PAni/HA/TiO_2/MWNT nanocomposites with shorter diameter and longer length of MWNT (D = 10-20 nm, l = 5-15 μm) would induce the agglomeration and shorten the interparticle distance between the nanorods/nanotubes. Therefore, it will significantly increase the charge mobility between nanorods/nanotubes and lead to a better eddy current with higher Ms value (0.074 emu/g) (Bhatia, Prasad, & Menon, 2010).

Oppositely, both PAni/HA/TiO_2/MWNT nanocomposites with MWNT (D = 60-100 nm, l = 1-2 μm) and MWNT (D = 60-100 nm, l = 5-15 μm) possesses similar and lower Ms value of 0.026 emu/g and 0.03 emu/g, respectively. For PAni/HA/TiO_2/MWNT nanocomposites with MWNT (D = 60-100 nm, l = 1-2 μm), individual MWNT with shorter length will reduce the eddy current between individual

MWNT and thus lower the Ms value. While for those with longer length of MWNT (D = 60-100 nm, l = 5-15 μm), the fewer amounts of nanorods/nanotubes will significantly reduce the mobility charge transfer between nanorods/nanotubes. Hence, it will reduce the eddy current and the Ms value.

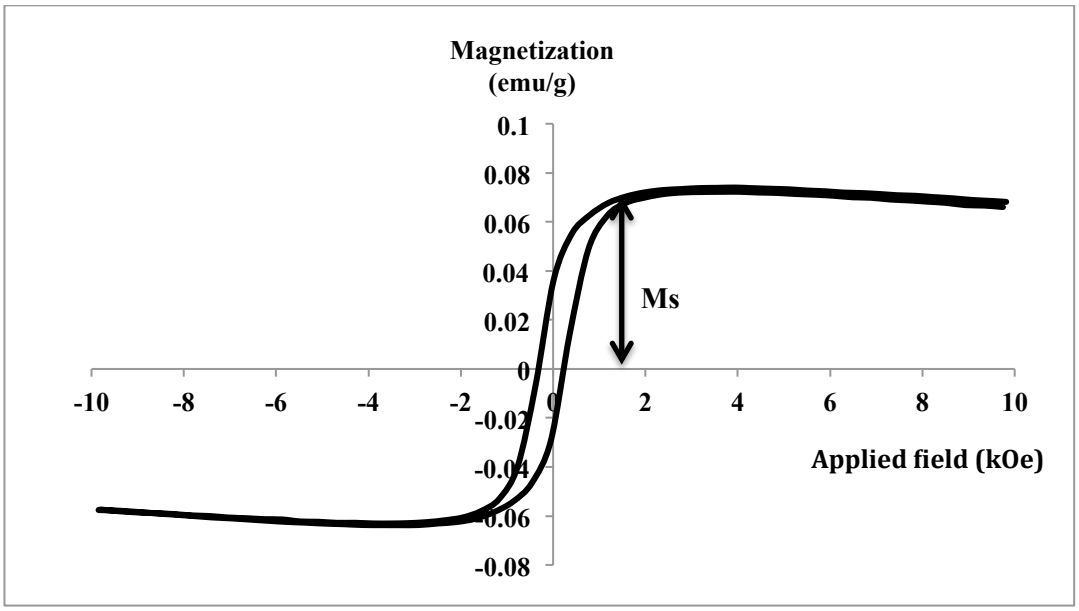

Figure 4.18. Variation of magnetization with the applied magnetic field measured at room temperature for PAni/HA/TiO_2/MWNT nanocomposites with MWNT (D = 10-20 nm, l = 5-15 μm).

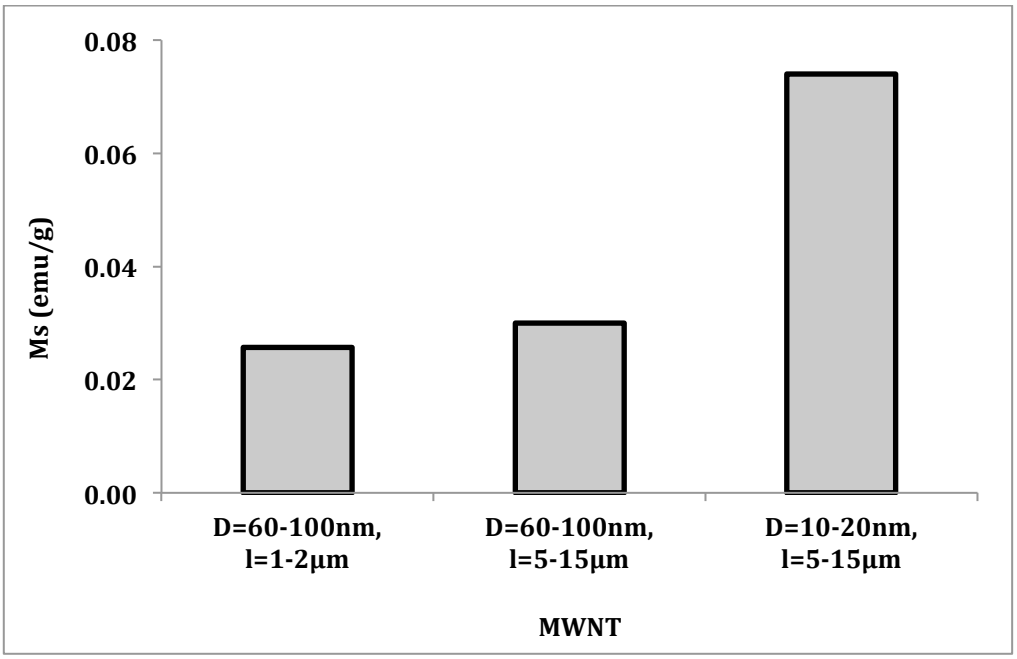

Figure 4.19. Saturation magnetization (Ms) of PAni/HA/TiO_2/MWNT nanocomposites with different diameter and length of MWNT.

4.2.8 Microwave absorption studies

For the microwave absorption study, complex dielectric permittivity ($\varepsilon_r^* = \varepsilon_r' - j\varepsilon_r''$) and complex magnetic permeability ($\mu_r^* = \mu_r' - \mu_r''$) in which consist of real (ε_r' or μ_r') and imaginary (ε_r'' or μ_r'') part of PAni nanocomposites can be determined by scattering parameters (S_{11}) from the range of 0.4 GHz till 18 GHz using MVNA. Full cycle of one-port calibration was achieved before the measurement in order to reduce the measurement errors occurred.

RL of PAni/HA/TiO_2/MWNT nanocomposites with different diameter and length of MWNT are shown in Figure 4.20 in the frequency range of 0.4 GHz – 18 GHz and RL is calculated using formula, RL = 20 log S_{11}*. Furthermore, strong absorption of microwave absorbing materials can be identified by tan δ (Figure 4.21) of the samples, in which is calculated from the real and imaginary part of complex dielectric permittivity using formula, $\tan \delta = \varepsilon_r''/\varepsilon_r'$ (Makeiff & Huber, 2006).

As refer to RL graph in Figure 4.20, PAni/HA/TiO_2/MWNT nanocomposites with MWNT (D = 10-20 nm, l = 5-15 μm) possess a sharp and narrow peak with high absorption (RL = -58 dB) at 7 GHz while MWNT (D = 60-100 nm, l = 5-15 μm) exhibits a broad RL peak with moderate absorption (RL = -19 dB) at 6 GHz. In general, microwave absorption property of a material mainly depend on the dielectric and magnetic properties as well as electrical conductivity of the sample (Table 4.2) (Zhao, Li, & Shen, 2008). PAni/HA/TiO_2/MWNT nanocomposites with MWNT (D = 10-20 nm, l = 5-15 μm) exhibit the highest absorption due to three main factors which are highest Ms (0.074 emu/g), highest heterogeneity (large amount of nanorods/nanotubes) and moderate electrical conductivity (1.11×10^{-2} S/cm) that lead to a more disordered

motion of charge carrier along the backbone of PAni. Thus, it possesses the highest RL value among all the PAni nanocomposites.

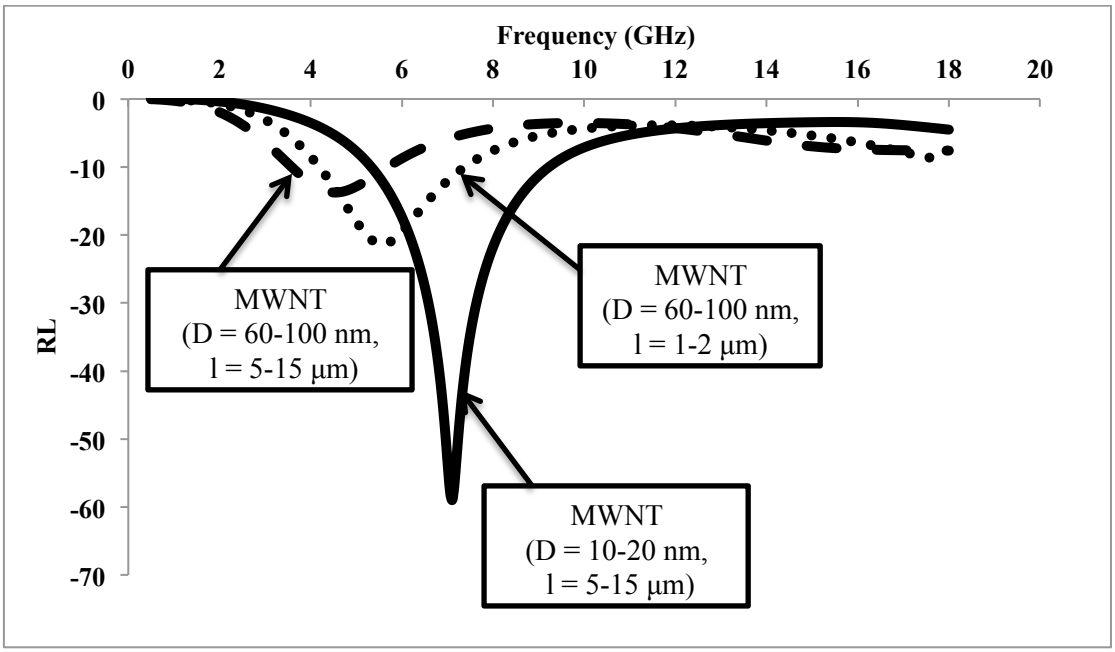

Figure 4.20. RL for PAni/HA/TiO_2/MWNT nanocomposites with different diameter and length of MWNT.

Table 4.2. Comparison among conductivity (σ), saturation magnetization (Ms) and heterogeneity (ε') for PAni/HA/TiO_2/MWNT nanocomposites with different diameter and length of MWNT.

	MWNT (D=60-100nm, l =1-2μm)	**MWNT (D=60-100nm, l =5-15μm)**	**MWNT (D=10-20nm, l =5-15μm)**
σ	↑	↑ ↑ ↑	↑ ↑
Ms	↑	↑ ↑	↑ ↑ ↑
ε'	↑ ↑	↑ ↑ ↑	↑ ↑ ↑

Generally, dielectric behavior of a material is mainly associated with electronic, ionic, orientational and space charge polarization (heterogeneity) (Abdul Hamid et al., 2002). Refer to the FESEM images (Figure 4.16), PAni/HA/TiO_2/MWNT nanocomposites with MWNT (D = 10-20 nm, l = 5-15 μm) exhibit the largest amount of entangled nanorods/nanotubes will eventually enhance the heterogeneity of the nanocomposites. Thus, it will significantly induce the space charge polarization along the PAni backbone and finally PAni/HA/TiO_2/MWNT nanocomposites with MWNT (D = 10-20 nm, l = 5-15 μm) indicate the strongest microwave absorption among all PAni nanocomposites.

Furthermore, the diameter of MWNT play an important role to indicate the strongest absorption that shown by PAni/HA/TiO_2/MWNT nanocomposites with MWNT (D = 10-20 nm, l = 5-15 μm). PAni/HA/TiO_2/MWNT nanocomposites with smaller diameter of MWNT (D = 10-20 nm) will induce the electronic transport among the MWNT and eventually facilitate the hopping conduction of electron between the MWNT because the MWNT are adequately closed together (10 nm) (Wang, Guo, Han, & Zhang, 2013). Hence, it will significantly improve the charge transfer process (intrachain) among the MWNT layer and possess a better microwave absorption if compared to those with bigger diameter of MWNT.

Figure 4.21 and 4.22 show the real (μ_r') and imaginary (μ_r'') part of magnetic permeability, respectively for PAni/HA/TiO_2/MWNT nanocomposites with different diameter and length of MWNT. This figure clearly indicates that μ_r' and μ_r'' of complex magnetic permeability possess the same trend as RL in Figure 4.20 follow the sequence of MWNT (D = 10-20 nm, l = 5-15 μm) > MWNT (D = 60-100 nm, l = 1-2 μm) > MWNT (D = 60-100 nm, l = 5-15 μm).

From the result obtained, RL of PAni/HA/TiO_2/MWNT nanocomposites with MWNT (D = 60-100 nm, l = 1-2 μm) is higher than those with MWNT (D = 60-100 nm, l = 5-15 μm). Among the three main factors, magnetic property especially μ_r' and μ_r'' of complex magnetic permeability of PAni/HA/TiO_2/MWNT nanocomposites with MWNT (D = 60-100 nm, l = 1-2 μm) and MWNT (D = 60-100 nm, l = 5-15 μm) play a significant roles that will eventually affect the RL of PAni nanocomposites. Based on Figure 4.21 and 4.22, μ_r' and μ_r'' of MWNT (D = 60-100 nm, l = 1-2 μm) show a higher value of -2.7 and 3.7 at 7 GHz, respectively will eventually induce higher eddy current and improve the interaction between PAni and MWNT, thus indicate good absorption if compared to those MWNT (D = 60-100 nm, l = 5-15 μm).

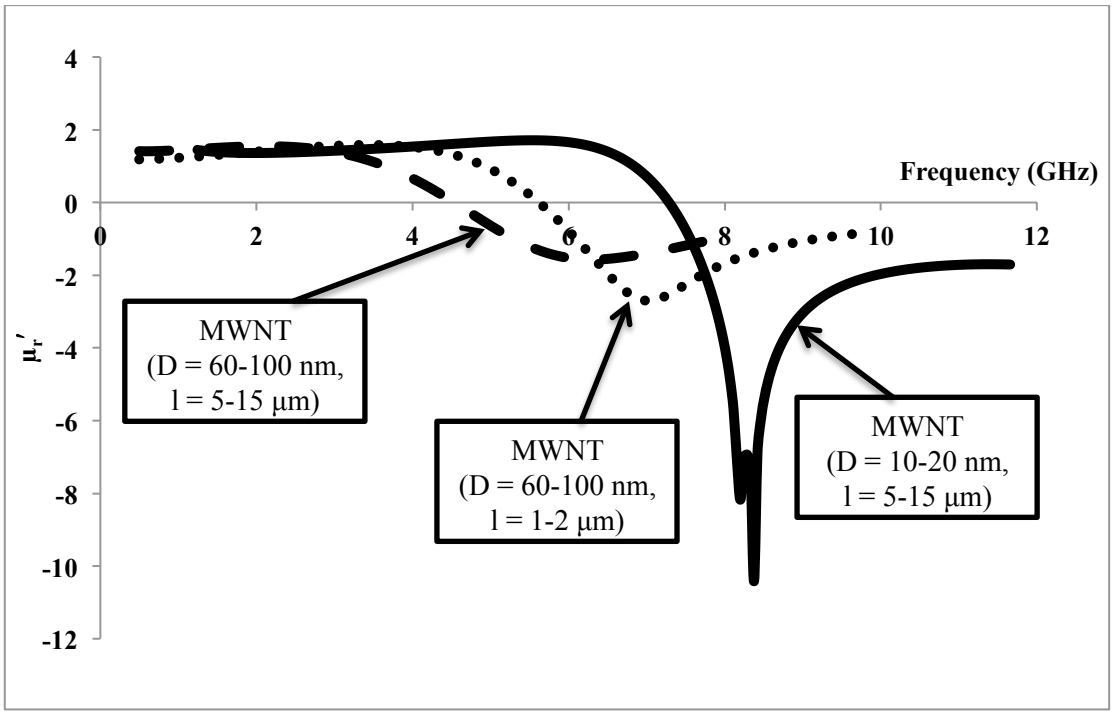

Figure 4.21. Real (μ_r') part of magnetic permeability for PAni/HA/TiO_2/MWNT nanocomposites with different diameter and length of MWNT.

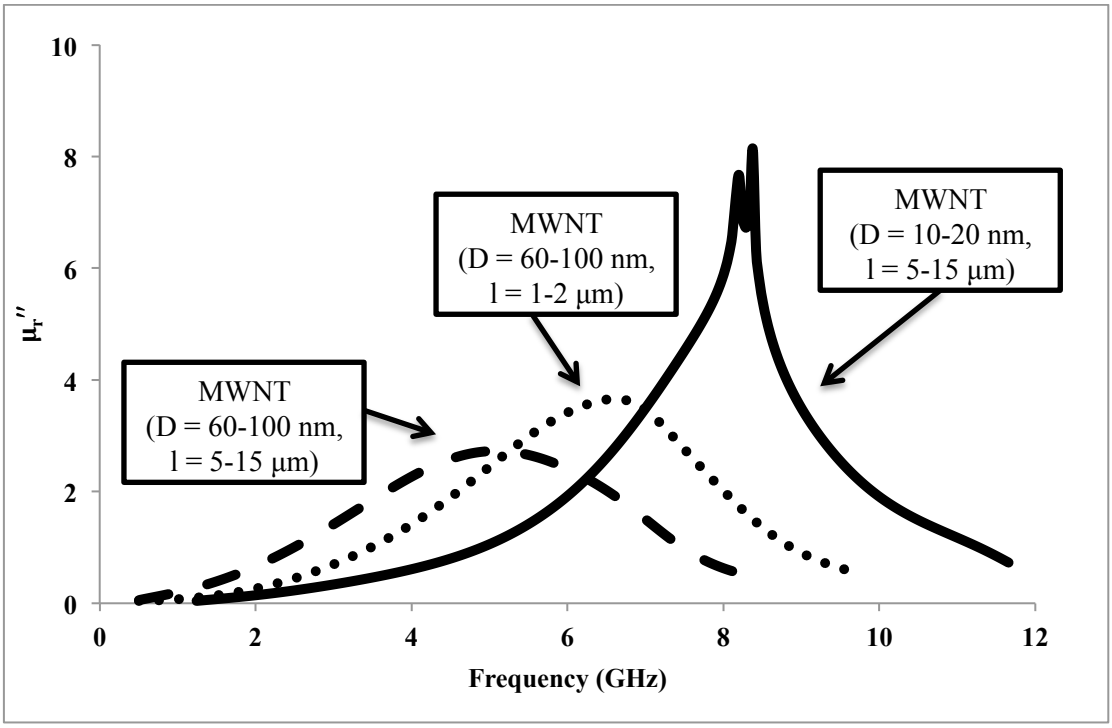

Figure 4.22. Imaginary (μ_r'') part of magnetic permeability for PAni/HA/TiO_2/MWNT nanocomposites with different diameter and length of MWNT.

As refer to Figure 4.23, tan δ show the same trend as RL in Figure 4.20 in which it follows the trend of MWNT (D = 10-20 nm, l = 5-15 μm) > MWNT (D = 60-100 nm, l = 1-2 μm) > MWNT (D = 60-100 nm, l = 5-15 μm). This data significantly proves that PAni/HA/TiO_2/MWNT nanocomposites with MWNT (D = 10-20 nm, l = 5-15 μm) exhibit the highest RL value (RL = -58 dB) which indicate strongest absorption as confirmed by the highest tan δ of 0.18 – 0.32. Oppositely, PAni/HA/TiO_2/MWNT nanocomposites with MWNT (D = 60-100 nm, l = 5-15 μm) show the lowest RL value (RL = -18.9 dB) which indicate the lowest absorption as proven by the lowest tan δ of 0.01 – 0.29.

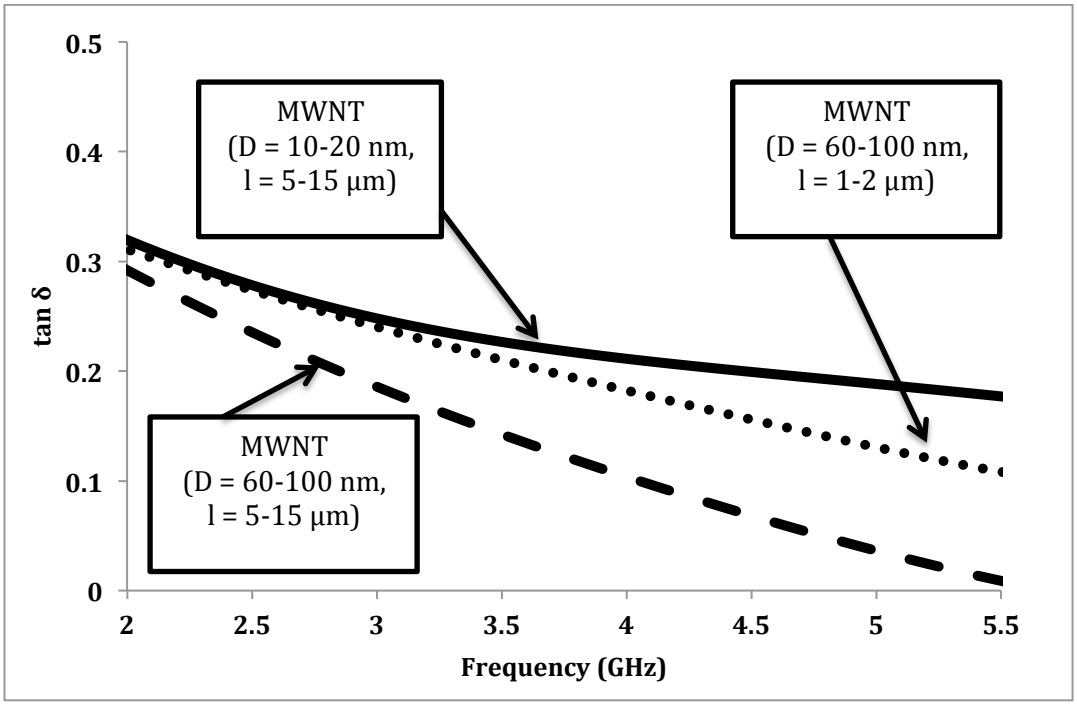

Figure 4.23. Loss tangent for PAni/HA/TiO_2/MWNT nanocomposites with different diameter and length of MWNT.

4.3 PAni/HA/TiO_2/DWNT nanocomposites

4.3.1 FTIR analysis

FTIR spectra of PAni/HA/TiO_2/DWNT nanocomposites with different contents (10 %, 20 % and 60 %) of untreated double wall carbon nanotubes (u-DWNT) and carboxylic treated double wall carbon nanotubes (c-DWNT) are shown in Figure 4.24. The peaks at 1594 cm^{-1} and 1492 cm^{-1} are the characteristic stretching bands of nitrogen quinoid and benzenoid. These are owing to the conducting state of the polymer. The C-N stretching vibration of PAni is shown by the peaks at 1303 cm^{-1} and 1279 cm^{-1} while quinoid unit of doped-PAni at 1134 cm^{-1} (Yang & Wan, 2002).

The strong characteristic band at 1134 cm^{-1} is the "electron-like band" that described by MacDiarmid and coworkers that it is the measure of delocalization of electrons, in which related to the conductivity of PAni/HA/TiO_2/DWNT nanocomposites (Quillard et al., 1994). There is a small vibration of C=O corresponding to HA dopant at 1755 cm^{-1} but it does not show any peak on the spectra due to the overlapping of quinoid ring (1594 cm^{-1}) from PAni/HA/TiO_2/DWNT nanocomposites (Lixia Zhang et al., 2006). The peaks mentioned above show almost identical peak for all PAni/HA/TiO_2/DWNT nanocomposites (u-DWNT and c-DWNT) but all the PAni characteristic peak become subtle when the contents of u-DWNT and c-DWNT increasing.

By comparing the FTIR spectrum of PAni/HA/TiO_2/DWNT nanocomposites with pristine PAni, it shows a significant decreasing in intensity when introducing the DWNT into the PAni. These differences can be explained as following. When introduce the DWNT into the reaction system, Ani was absorbed by the DWNT and the

polymerization was carried out on the surface of DWNT, which will lead to a constrained growth around the DWNT. Such absorption and constrain growth will restrict the vibrations of PAni that significantly reduce the intensity of PAni (Nagaraja et al., 2012).

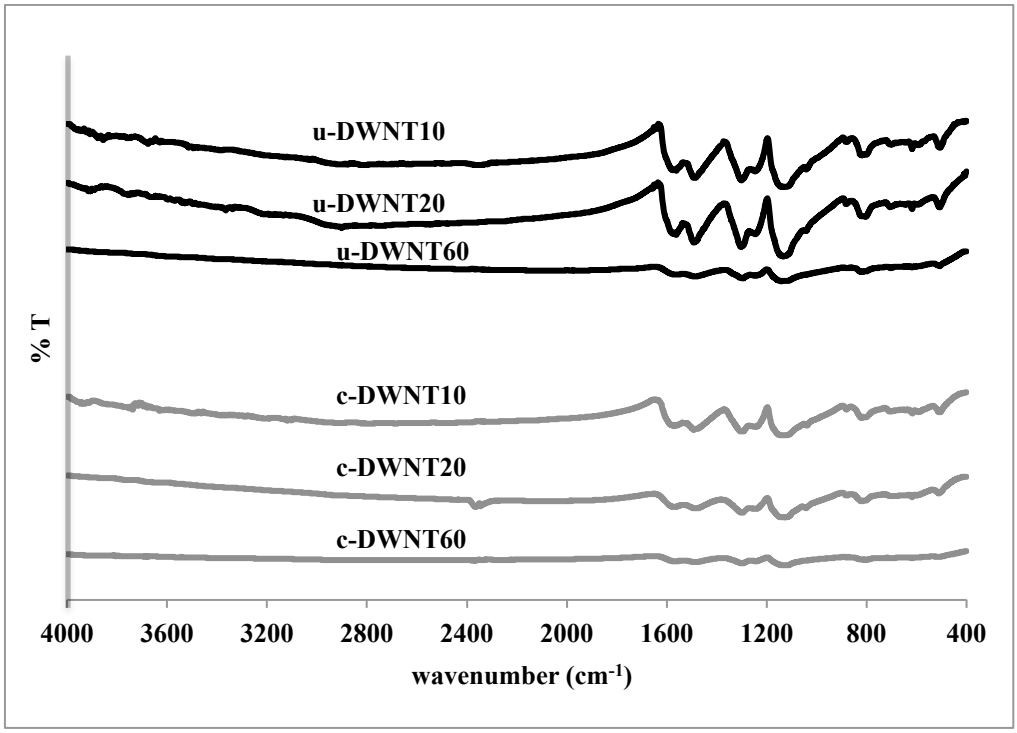

Figure 4.24. FTIR spectra of PAni/HA/TiO_2/DWNT nanocomposites with different contents of u-DWNT and c-DWNT.

4.3.2 UV-vis analysis

The UV-vis absorption spectrum of PAni/HA/TiO_2/DWNT nanocomposites (TiO_2: 10%, c-DWNT: 10%) is given in Figure 4.25. All the PAni/HA/TiO_2/DWNT nanocomposites with different contents of u-DWNT and c-DWNT show almost identical peak in UV-vis spectra from 300 nm to 900 nm. The UV-vis spectrum shows the presence of peaks at 368 nm (π-π* transition of the benzenoid ring) while shoulder-like peak near 466 nm indicates the bipolaron peak. It shows a free carrier tail near 800

nm (quinoid ring) due to the emeraldine salt phase of doped-PAni (Lixia Zhang et al., 2006).

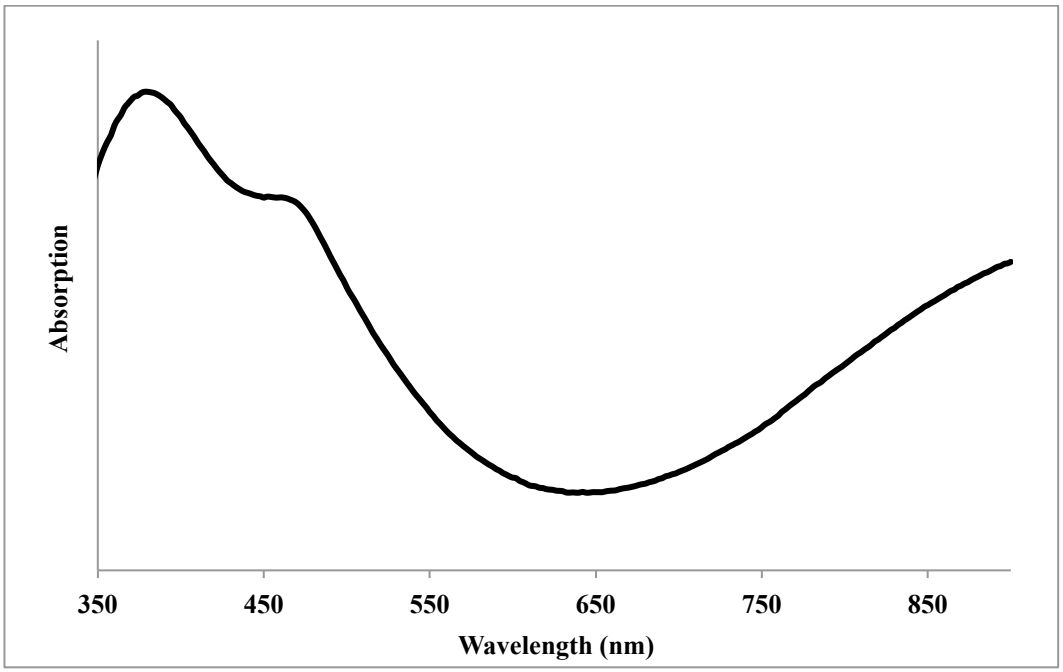

Figure 4.25. UV-vis spectrum of PAni/HA/TiO_2/DWNT nanocomposites with 10 % of c-DWNT.

4.3.3 XRD analysis

Figure 4.26 shows the crystallinity orientations of PAni/HA/TiO_2/DWNT nanocomposites with 10% of c-DWNT. The X-ray diffraction patterns clearly assess that all PAni/HA/TiO_2/DWNT nanocomposites show amorphous behavior with characteristic peaks at $2\theta = 22.7^o$ and 25.3^o which represent the characteristic of doped-PAni. The band at 25.3^o was attributed to the periodicity parallel and perpendicular of the polymer chain direction of PAni (Lijuan Zhang et al., 2005).

Besides, all the PAni/HA/TiO_2/DWNT nanocomposites show the existence of TiO_2 peaks at $2\theta = 35.8^o$, 37.6^o, 47.8^o, 53.6^o, 53.8^o, 62^o, 67.8^o, 69.2^o and 74.1^o. The presence of DWNT in PAni nanocomposites also determined by the characteristic peaks

at 2θ = 25.3° and 42.1° (Sharma et al., 2009). Similar FTIR, UV-vis and XRD spectra are obtained after addition of DWNT. Hence, it can be suggested that dielectric (TiO_2) and magnetic (DWNT) materials do not affect the chemical structure of PAni/HA/TiO_2/DWNT nanocomposites.

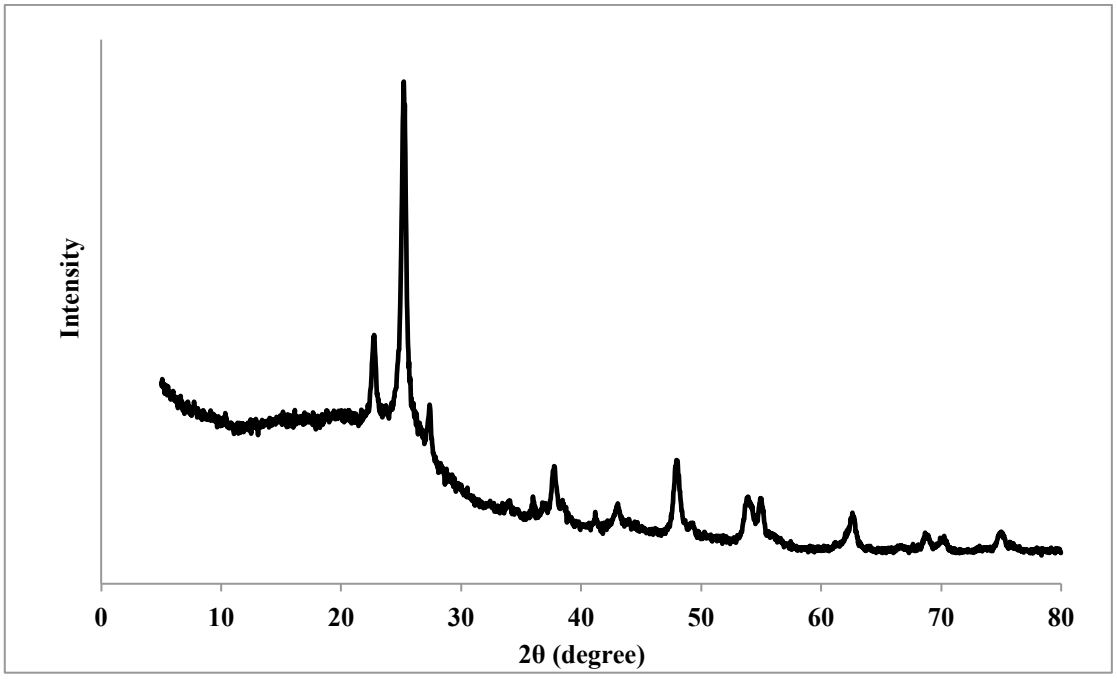

Figure 4.26. X-ray diffraction patterns of PAni/HA/TiO_2/DWNT nanocomposites with 10% of c-DWNT.

4.3.4 TGA analysis

The TGA analysis was conducted to identify the thermal stability of PAni nanomcomposites. Figure 4.27 shows the thermogram of PAni/HA/TiO_2/DWNT nanocomposites with different contents of u-DWNT and c-DWNT from 50 °C to 900 °C. From the TGA profiles of PAni/HA/TiO_2/DWNT nanocomposites, it possesses four stages. The first region from 50 °C to 100 °C may be attributed to the evaporation of water molecules or moistures. The second loss step from 100 °C to 260 °C is corresponding to the loss of organic decomposition for the carboxylic acid groupfrom both the c-DWNT and HA dopant along the PAni chains (Trchová, Šeděnková,

Tobolková, & Stejskal, 2004). While the third stage observed from 260 ^{o}C to 710 ^{o}C is attributed to the dedoping of HA dopant from backbone of PAni. The last stage is responsible to the degradation of the PAni backbone (Phang et al., 2004).

Thermal stability of PAni/HA/TiO_2/DWNT nanocomposites with 60 % od c-DWNT and u-DWNT possess the highest thermal stability while the PAni nanocomposites with 10 % and 20% of DWNT (c-DWNT and u-DWNT) show the almost similar thermal stability due to the lower contents of DWNT. Besides, PAni/HA/TiO_2/DWNT nanocomposites with c-DWNT show a better thermal stability if compared with those consist of u-DWNT because more heat is required to decompose the –COOH groups in c-DWNT.

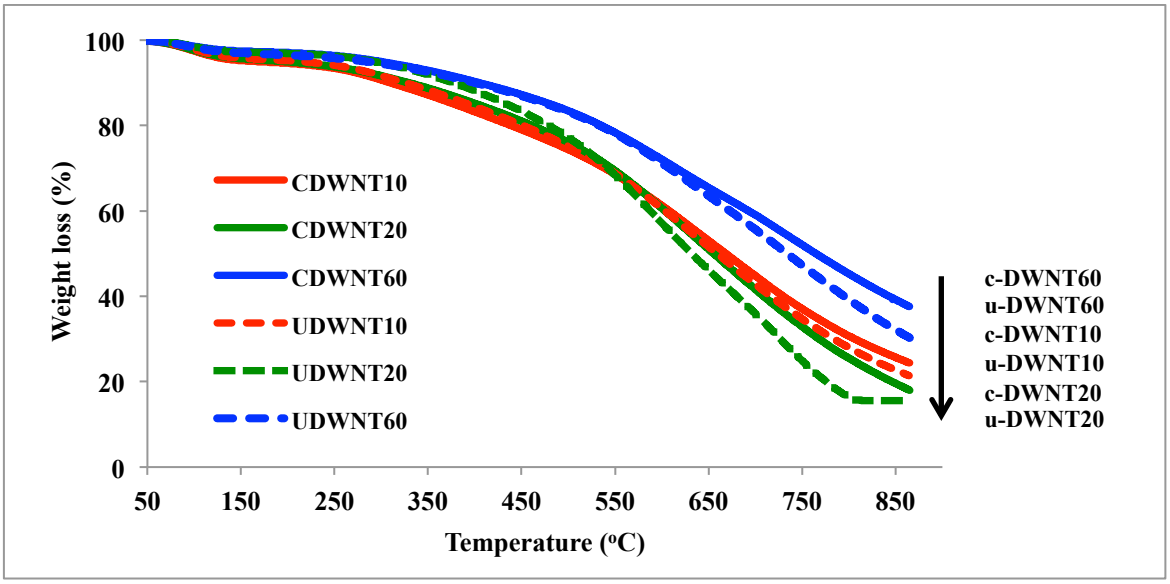

Figure 4.27. TGA thermograms of PAni/HA/TiO_2/DWNT nanocomposites with different contents of c-DWNT and u-DWNT.

4.3.5 Morphology studies

FESEM images in Figure 4.28 show that Ani/HA/TiO_2/DWNT micelles have formed the nanorods/nanotubes and the formation of nanorods/nanotubes is proposed by the mechanism shown in Figure 4.29. As shown in proposed micelle in Figure 4.29, TiO_2 and DWNT were act as the nucleus of the micelles during polymerization owing to TiO_2 and DWNT were dispersed well in Ani/HA solution where Ani/HA/TiO_2/DWNT mixture was stirred vigorously for 24 hours before polymerization. Ani will assign as shell of the micelle due to the hydrophobic property of Ani and HA will act as tail of the micelle owing to the hydrophilicity of –COOH group in HA dopant.

Since Ani/HA/TiO_2/DWNT micelles were in undisturbed condition during polymerization, thus Ani/HA/TiO_2/DWNT micelles will polymerize through elongation at the micelle/water interface to form the nanorods/nanotubes. Besides the formation of nanorods/nanotubes through the proposed mechanism (Figure 4.29), some of the DWNTs just physically mixed (Figure 4.28) with PAni/HA layer and nanorods/nanotubes as shown in proposed mechanism in Figure 4.29 (b).

Furthermore, Figure 4.28 clearly indicates that increasing amount of dielectric (TiO_2) and magnetic (DWNT) materials will significantly enhance the formation of PAni/HA/TiO_2/DWNT nanorods/nanotubes in both u-DWNT and c-DWNT until it reach its optimum at 20% of u-DWNT and c-DWNT where it will act as the barrier that impedes the formation of nanorods/nanotubes. From the FESEM images for PAni/HA/TiO_2/DWNT nanocomposites with different contents of u-DWNT (Figure 4.28 (i)), it was clearly indicated that small amount of u-DWNT has been enwrapped by PAni layer while there was more individual u-DWNT outside the nanorods/nanotubes as proposed by the mechanism (Figure 4.29 (b)(i)).

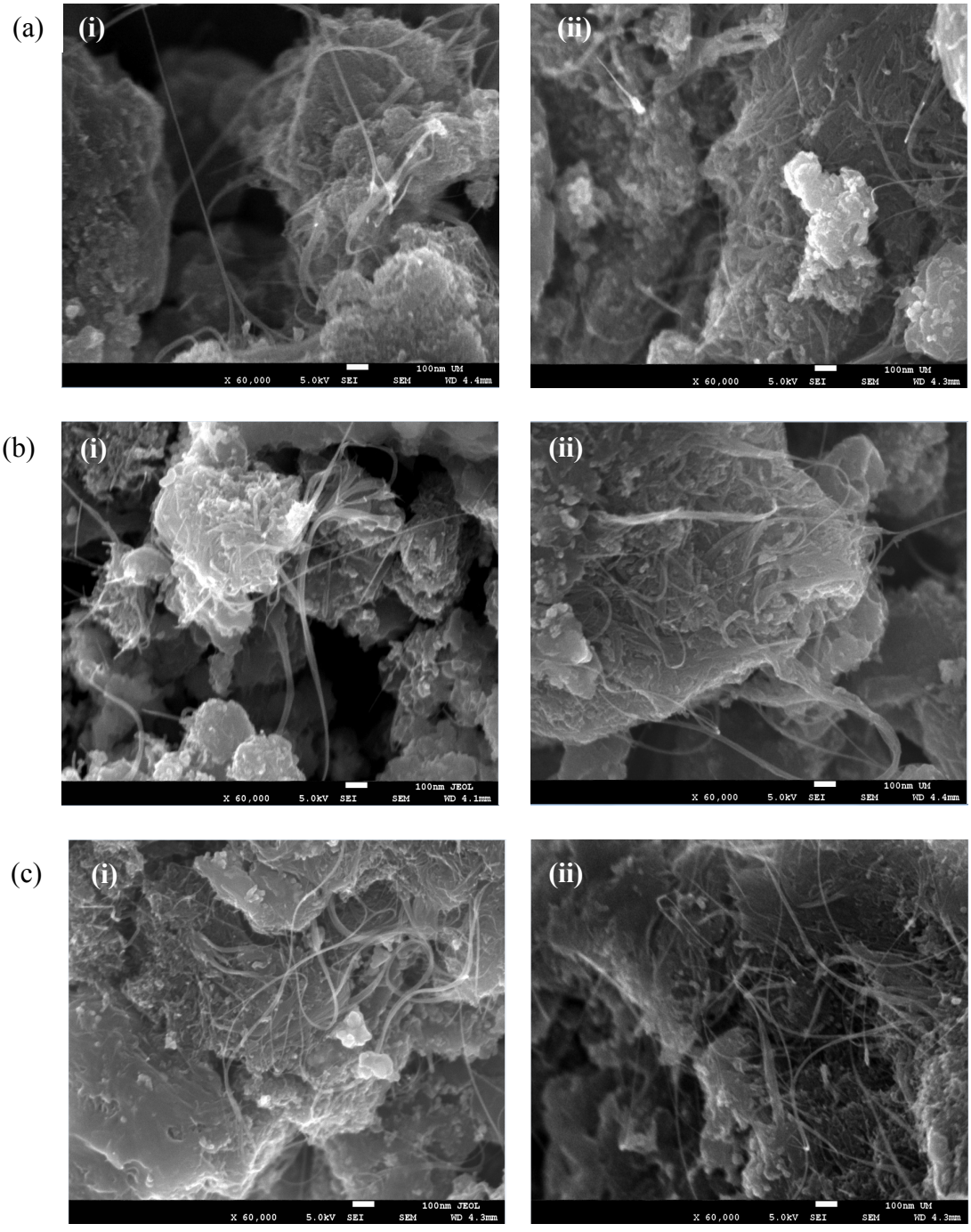

Figure 4.28. FESEM images of PAni/HA/TiO_2/DWNT nanocomposites with ((i) u-DWNT and (ii) c-DWNT) for: (a) 10 %, (b) 20 % and (c) 60 % of DWNT (60,000 × magnifications).

Oppositely, PAni/HA/TiO_2/DWNT nanocomposites with different contents of c-DWNT show that most of the c-DWNT is enwrapped by PAni layer (to form big amount of nanorods/nanotubes) while less individual c-DWNT exist outside the nanorods/nanotubes (Figure 4.29 (b)(ii)). The formation of more nanorods/nanotubes with different contents of c-DWNT can be explained by the strong interaction between Ani and c-DWNT caused by the presence of the π-π* electron interaction between DWNT and Ani as well as the formation of hydrogen bond between –COOH groups from c-DWNT and the amino groups of Ani (Jeevananda et al., 2008; Star et al., 2001).

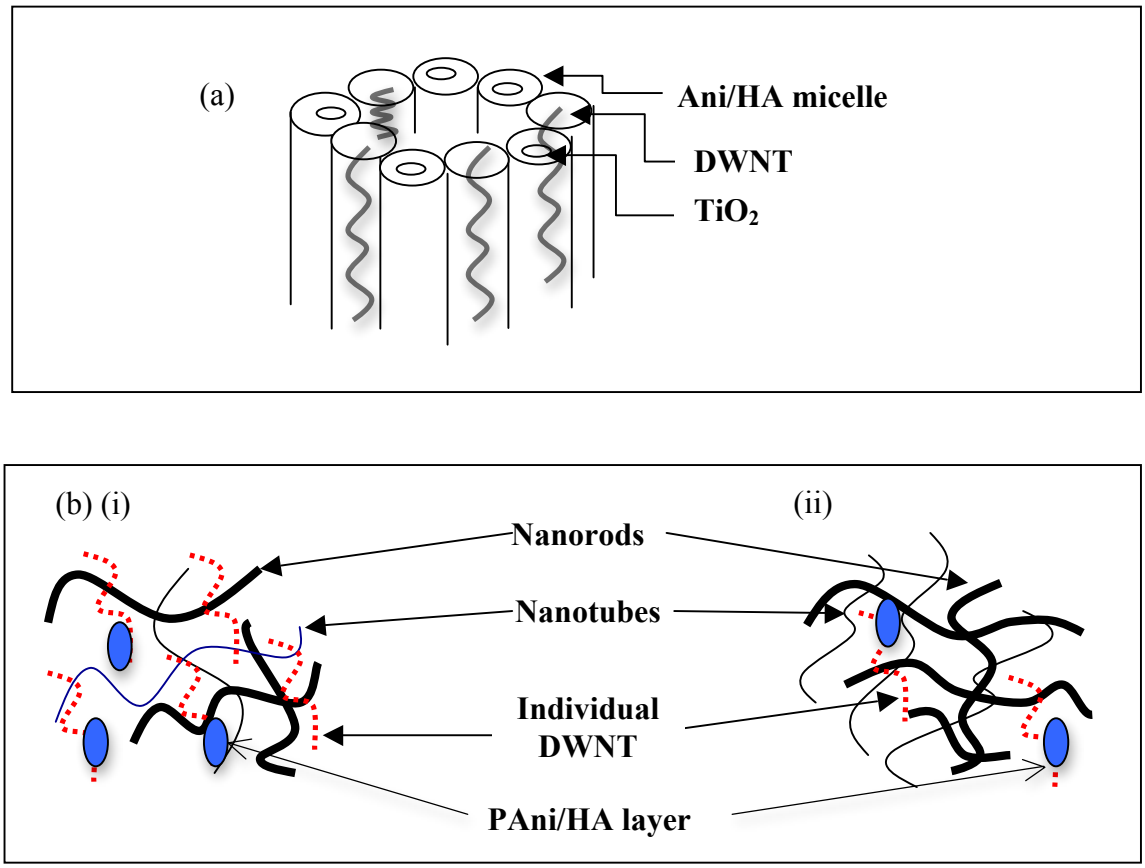

Figure 4.29. (a) Formation of nanorods/nanotubes and (b) physical interaction between individual DWNT with nanorods/nanotubes and PAni/HA layer with (i) u-DWNT and (ii) c-DWNT by template free method.

4.3.6 Conductivity studies

The electrical conductivities of PAni/HA/TiO_2/DWNT nanocomposites are measured according to standard four-probe technique at room temperature. The room-temperature conductivities with different contents of u-DWNT and c-DWNT nanoparticles (10 %, 20 % and 60 %) results are shown in Figure 4.30.

The electrical conductivities increased simultaneously with the increasing of DWNT nanoparticles content from 10 % to 60 % for both PAni/HA/TiO_2/DWNT nanocomposites with u-DWNT (1.23×10^{-1} – 1.13 S/cm) and c-DWNT (3.43×10^{-2} – 4.48×10^{-1} S/cm). In general, the electrical conductivity is depended on the doping level, conjugated length or chain length, interchain or intrachain distance, but also upon some external factors such as orientation of the particles (Feng et al., 2003). PAni can be considered as good electron donor, while the DWNT is relatively good electron acceptor (Y. Sun, Wilson, & Schuster, 2001).

In general, electrical conductivity of PAni nanocomposites is higher than pristine PAni (2.37×10^{-2}). The improvement in conductivity after addition of DWNT may be attributed to the π-π^* interaction between the surface of DWNT and the quinoid ring of PAni chain. This significantly improved the degree of delocalization of electron in the nanocomposites, as proved by the FTIR spectra (Figure 4.24). Besides, when increasing the contents of DWNT for both u-DWNT and c-DWNT (10 % to 60 %), dopant effect became dominant and more charge transfer from quinoid unit of PAni to DWNT (Cochet et al., 2001).

However, the electrical conductivities of PAni/HA/TiO_2/DWNT nanocomposites with c-DWNT (3.43×10^{-2} – 4.48×10^{-1} S/cm) are relatively low if

compared to those with u-DWNT (1.2 x 10^{-1} – 1.13 S/cm). As refer to FESEM images (Figure 4.28 (i)), it can strongly prove that most of the free individual u-DWNT exist outside the PAni/HA/TiO_2/DWNT nanorods/nanotubes if compared to those with c-DWNT. This fact is also strongly supported by the suggested mechanism as shown in Figure 4.29 (b)(i) – (ii). Thus, the large aspect ratio (Length/Diameter) of individual u-DWNT and c-DWNT plays a significant role in the electrical conductivity.

The high aspect ratio of individual u-DWNT will serve as a conducting bridge (without any barrier) that facilitates the movement of electron betweenthe interchain of individual DWNT. Thus it will lead to an improvement in conductivity (Wu & Lin, 2006). PAni/HA/TiO_2/DWNT nanocomposites with c-DWNT show a poor conductivities owing to the electron jumping (interchain) among free individual c-DWNT has been restricted by the –COOH groups (barrier) on the c-DWNT as proposed mechanism suggested in Figure 4.30.

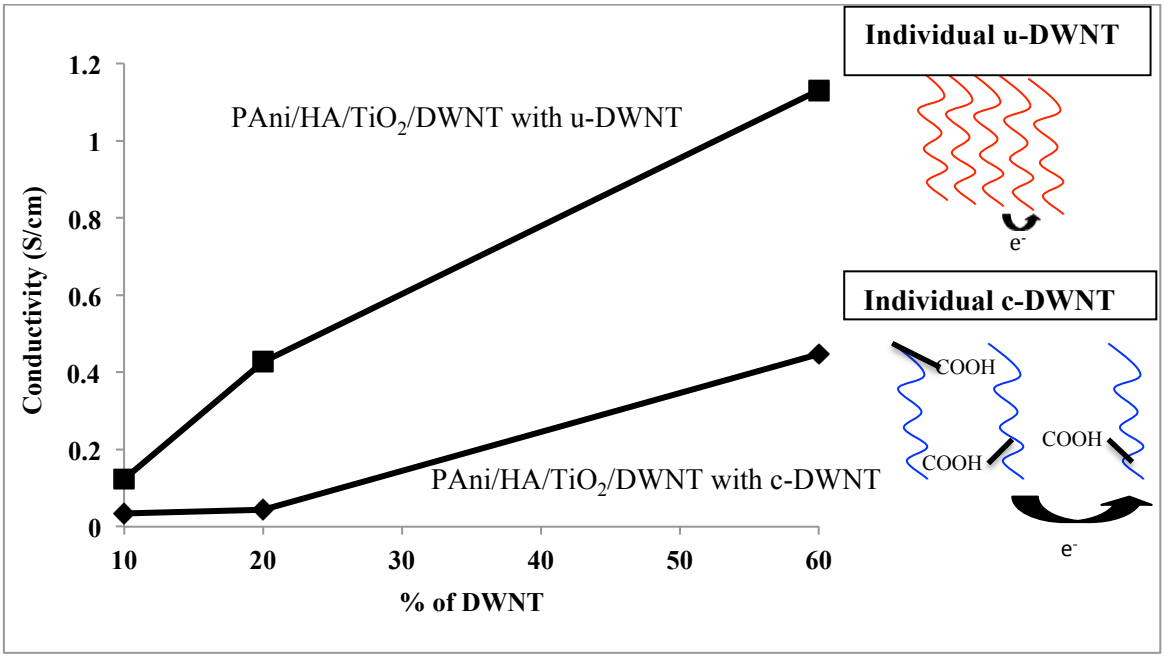

Figure 4.30. Electrical conductivities of PAni/HA/TiO_2/DWNT nanocomposites with different contents of u-DWNT and c-DWNT.

4.3.7 Magnetization studies

The Ms, Mr and Hc are determined by the magnetization curves in Figure 4.31. All the PAni/HA/TiO_2/DWNT nanocomposites with different contents of u-DWNT and c-DWNT under applied magnetic field of -10 kOe to 10 kOe at room temperature exhibit the hysteric loops (Figure 4.31).

As seen in Figure 4.32, increasing the contents of DWNT from 10 % to 60 % will significantly increase the Ms value for both PAni/HA/TiO_2/DWNT nanocomposites with u-DWNT (0.07 – 0.29 emu/g) and c-DWNT (0.07 – 0.24 emu/g). It is because the increment of DWNT contents not only enhances the eddy current (anisotropy) but also induces the interaction between PAni with DWNT. Thus, it eventually improves the magnetic effect of the nanocomposites and lead to a higher Ms value for both PAni/HA/TiO_2/DWNT nanocomposites with 60 % of u-DWNT and c-DWNT (Costa et al., 2006).

However, PAni/HA/TiO_2/DWNT nanocomposites with u-DWNT show better magnetization (0.07 – 0.29 emu/g) if compared to those with c-DWNT (0.07 – 0.24 emu/g). It is because PAni/HA/TiO_2/DWNT nanocomposites with u-DWNT exhibits higher amount of free individual u-DWNT outside the nanorods/nanotubes (Figure 4.29 (b)(i)) that will improve the mobility to align the u-DWNT (spin magnet) and eventually enhance the Ms value. On the other hand, most of the c-DWNT has been enwrapped by the PAni layer as shown in FESEM images (Figure 4.28 (ii)) where the mobility of c-DWNT is restricted and lastly lead to a poorer magnetization (Phang & Kuramoto, 2010).

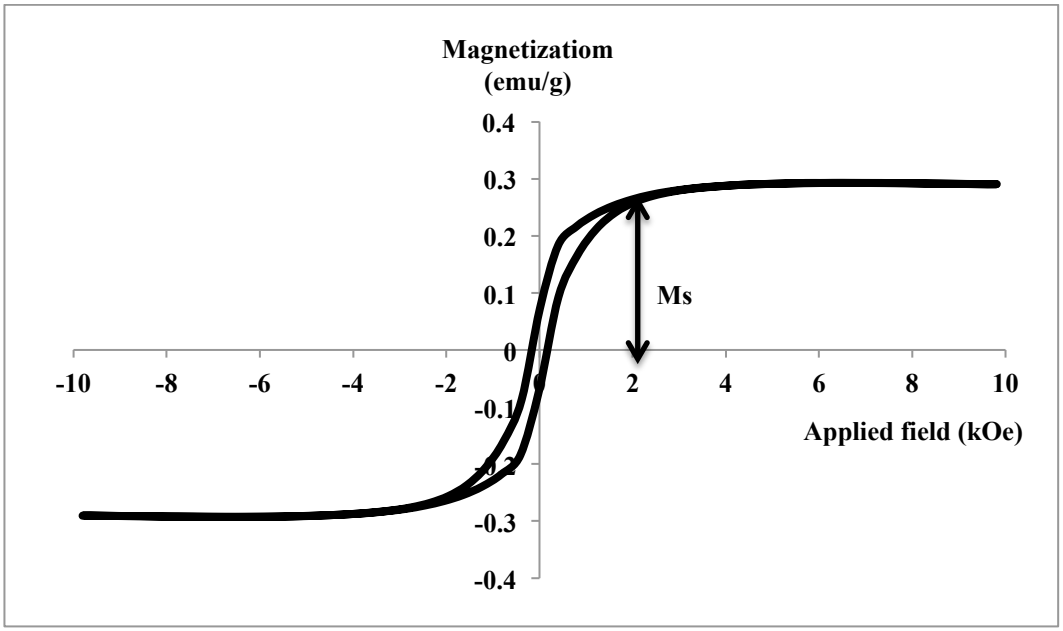

Figure 4.31. Variation of magnetization with the applied magnetic field measured at room temperature for PAni/HA/TiO_2/DWNT nanocomposites with 10 % of c-DWNT.

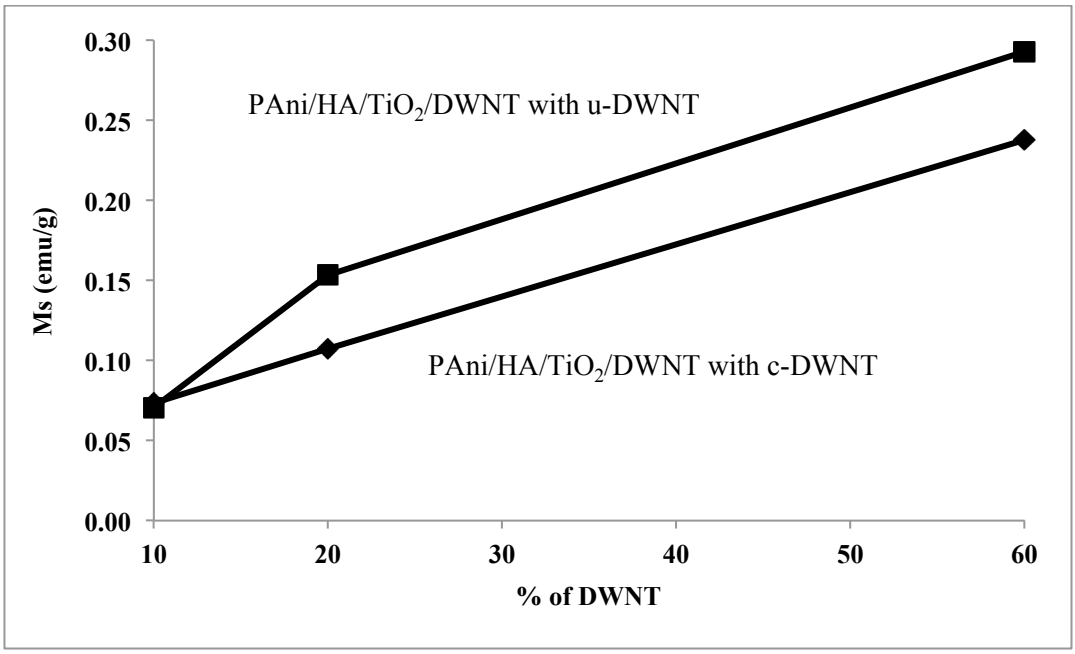

Figure 4.32. Saturation magnetization (Ms) for PAni/HA/TiO_2/DWNT nanocomposites with different contents of u-DWNT and c-DWNT.

4.3.8 Microwave absorption studies

Figure 4.33 shows the RL for both PAni/HA/TiO_2/DWNT nanocomposites with different contents (10%, 20% and 60%) of u-DWNT and c-DWNT. The dip in the RL curve indicates the appearances of absorption or reflection of the microwave where RL shows the interaction between conducting particles in both conducting material and electromagnetic material, and are calculated using formula, RL = 20 log S_{11}*. The microwave absorbance can be predicted from RL where the larger the negative values, the better the microwave absorption properties of a material.

As refer to the RL graph in Figure 4.33, PAni/HA/TiO_2/DWNT nanocomposites with u-DWNT exhibit the broad RL peak with poor absorption (RL = -5.8 – (-4.2) dB) in frequency range of 3-4 GHz. By comparison, PAni/HA/TiO_2/DWNT nanocomposites with c-DWNT possess the narrow and sharp RL peak with high absorption (RL = -18.3 – (-6.6) dB) at frequency range of 3-6 GHz. Commonly, polymer displays a broad absorption peak due to its various conductivities range along the PAni chain. However, the traditional microwave absorption material such as metal possesses the sharp RL peak due to its constant conductivity value. Besides, high conductivity, dielectric permittivity and magnetic permeability of a material will contribute to good microwave absorption and high EMI shielding efficiency (Su & Kuramoto, 2000).

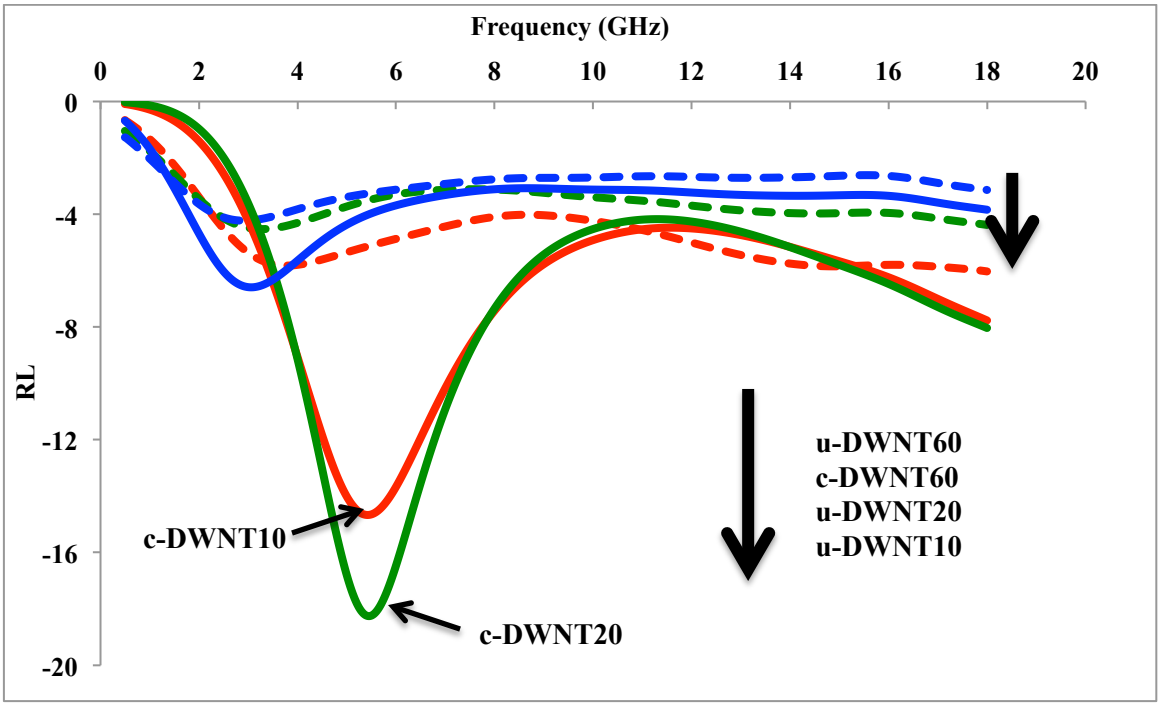

Figure 4.33. RL for both PAni/HA/TiO_2/DWNT nanocomposites with different contents (10%, 20% and 60%) of u-DWNT and c-DWNT.

As refer to Figure 4.33, RL of PAni nanocomposites increase linearly with increasing of DWNT content. Among all the PAni nanocomposites, PAni nanocomposites with 20 % of DWNT (u-DWNT and c-DWNT) possess highest RL that indicate the strongest microwave absorption. It is because most of the DWNT has been enwrapped by the PAni layer to form nanorods/nanotubes if compared to those with 10 % ad 40 % of DWNT. From the FESEM images (Figure 4.28 (ii)), PAni/HA/TiO_2/DWNT nanocomposites with 20 % of c-DWNT show larger amount of c-DWNT that has been covered by PAni layers to form the nanorods/nanotubes if compared to those with u-DWNT. PAni/HA/TiO_2/DWNT nanocomposites with c-DWNT that covered by PAni layers show high heterogeneity (large amount of nanorods/nanotubes) (Table 4.3) will enhance the dielectric permittivity and contribute more disordered motion of charge carriers along backbone of PAni chain (Chandrasekhar & Naishadham, 1999). Therefore, it will significantly contribute to a better microwave absorbing property of PAni nanocomposites.

Table 4.3. Comparison among σ, Ms and heterogeneity (ε') for PAni/HA/TiO_2/DWNT nanocomposites with u-DWNT and c-DWNT.

	u-DWNT	c-DWNT
σ	↑	↓
Ms	↓	↑ ↑
ε'	↓	↑ ↑ ↑

Figure 4.34 and 4.35 indicate the real (μ_r') and imaginary (μ_r'') part of magnetic permeability for PAni/HA/TiO_2/DWNT nanocomposites with different contents of u-DWNT and c-DWNT. In this research study, PAni/HA/TiO_2/DWNT nanocomposites with c-DWNT show higher RL (-18.3 – (-6.6) dB) if compared to those with u-DWNT (RL = -5.8 – (-4.2) dB). This phenomenon can be explained using the real (μ_r') and imaginary (μ_r'') of complex magnetic permeability.

Among the three main factors (electrical conductivity, dielectric permittivity and magnetic permeability) (Table 4.3) that indicate strong absorption, μ_r' and μ_r'' of complex magnetic permeability play a significant role that will significantly affect the RL result of PAni nanocomposites. Among all the PAni nanocomposites, PAni nanocomposites with c-DWNT possesses the higher RL value with strongest absorption because it exhibits high value of μ_r' and μ_r'' that induce the eddy current along PAni backbone. Thus, it eventually enhances the interaction between PAni and c-DWNT and show good absorption.

Besides, high heterogeneity of PAni/HA/TiO_2/DWNT nanocomposites with c-DWNT will consist large amount of nanorods/nanotubes that significantly induce the space charge polarization along PAni backbone. Finally, PAni/HA/TiO_2/DWNT nanocomposites with c-DWNT indicates the strongest microwave absorption if compared to those with u-DWNT which possesses lower heterogeneity, μ_r' and μ_r''.

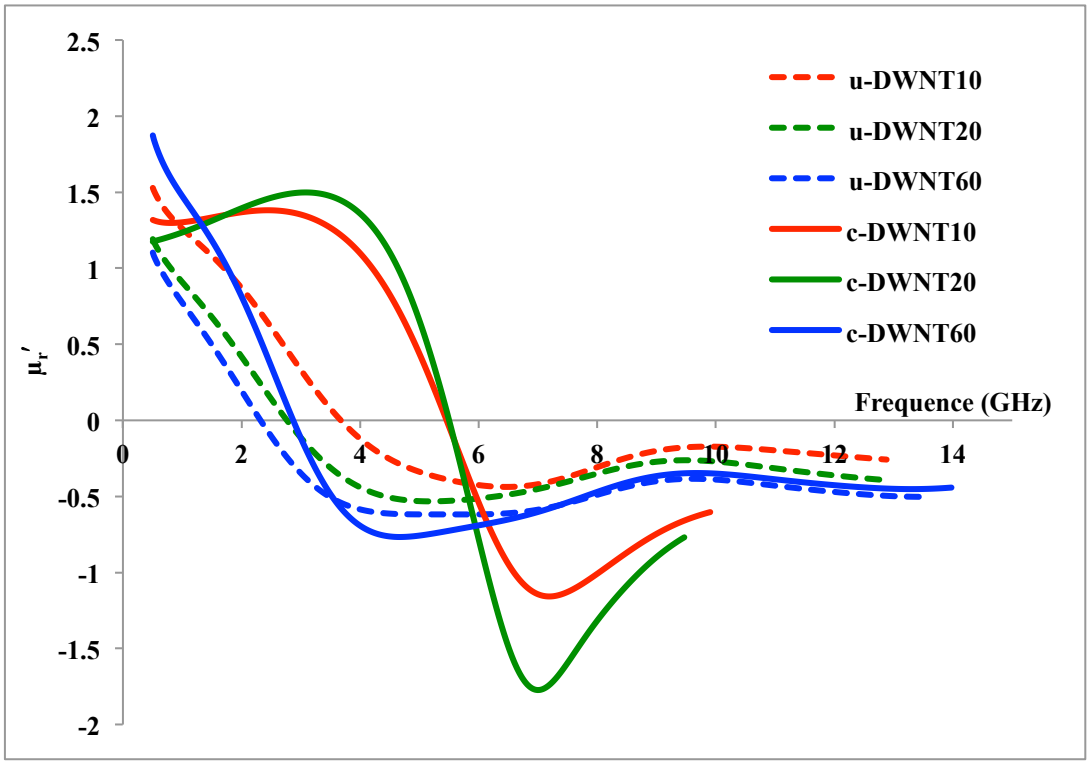

Figure 4.34. Real (μ_r') part of magnetic permeability for PAni/HA/TiO_2/DWNT nanocomposites with different contents of u-DWNT and c-DWNT.

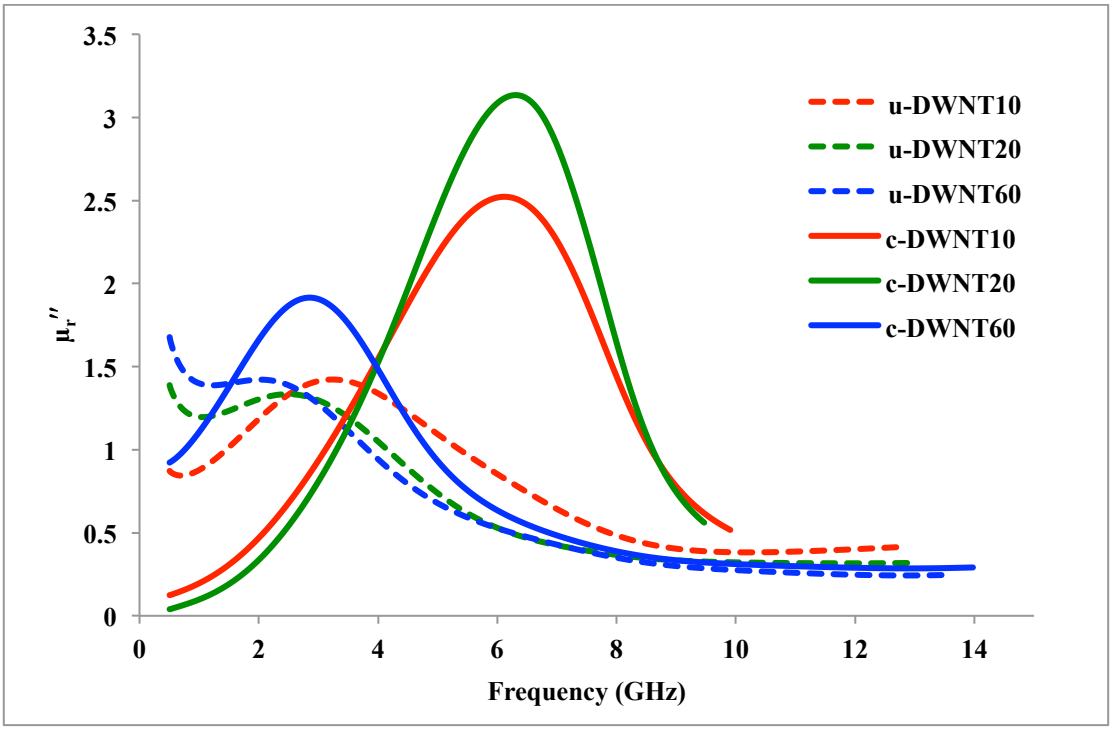

Figure 4.35. Imaginary (μ_r'') part of magnetic permeability for PAni/HA/TiO_2/DWNT nanocomposites with different contents of u-DWNT and c-DWNT.

In general, both RL and tan δ show in Figure 4.33 and 4.36, respectively possess similar trend in which RL with highest negative value will exhibit the highest tan δ that indicate the strong absorption. Hence, PAni/HA/TiO_2/DWNT nanocomposites with c-DWNT show the higher RL value of (RL = -18.3 – (-6.6) dB) with high tan δ (0.47 – 0.56) is a lossy material that indicate a better microwave absorption if compared to those with u-DWNT (RL = -5.8 – (-4.2) dB, tan δ = 0.32 – 0.56) (Makeiff & Huber, 2006).

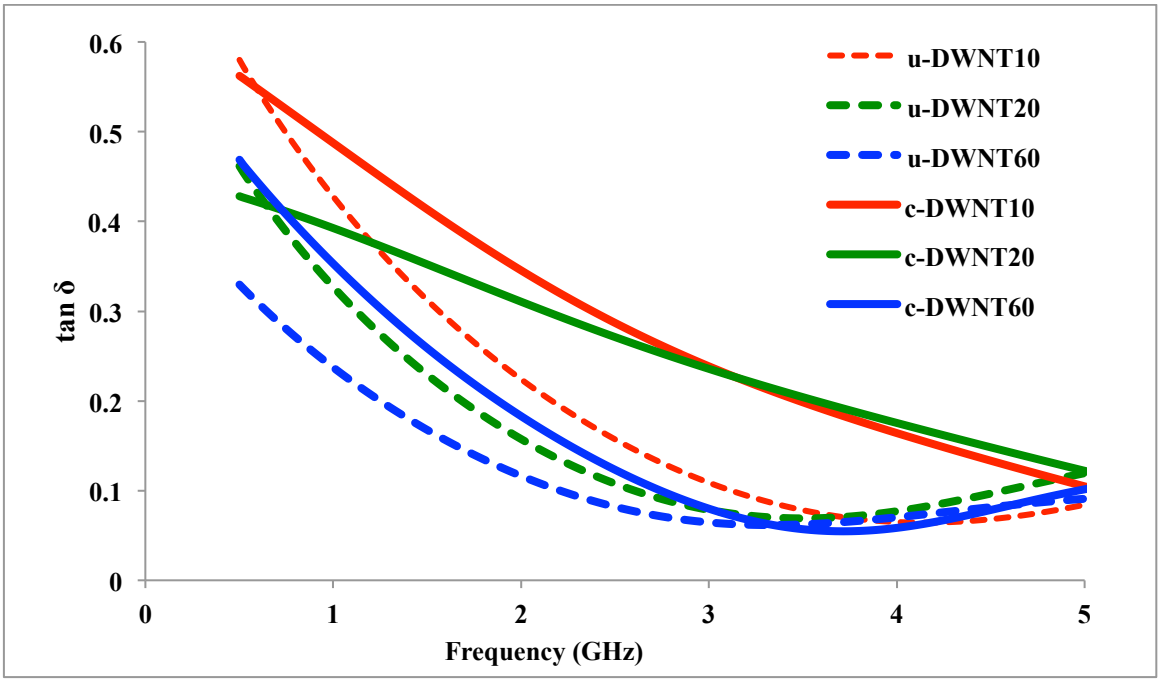

Figure 4.36 Loss tangent for both PAni/HA/TiO_2/DWNT nanocomposites with different contents (10 %, 20 % and 60 %) of u-DWNT and c-DWNT.

4.4 PAni/HA/TiO_2/GNP nanocomposites

4.4.1 FTIR analysis

Figure 4.37 shows the FTIR spectra of pristine PAni and PAni/HA/TiO_2/GNP nanocomposites with different contents of GNP. For the FTIR spectra of pristine PAni, it possesses the vibrational peak at 1593 cm^{-1} which is corresponding to the quinoid rings stretching while 1509 cm^{-1} is attributed to the benzenoid rings. Two vibrational peaks at 1313 and 1289 cm^{-1} are indicated to the C-N stretching of PAni while the peak at 1188 cm^{-1} is assigned to quinoid ring of doped-PAni (Yang & Wan, 2002).

All the PAni nanocomposites show the similar vibrational peak as pristine PAni. However, the PAni characteristic peaks become subtle and the intensity decrease when the ratios of GNP increasing from 10 % to 40 %. When introduce the GNP into the reaction system, Ani was penetrated and polymerization was carried out on the surface of GNP which will restrict the vibrations of PAni and thus significantly reduce the intensity of PAni (Nagaraja et al., 2012). No new peaks have been observed for GNP owing to pristine GNP was featureless in FTIR spectrum.

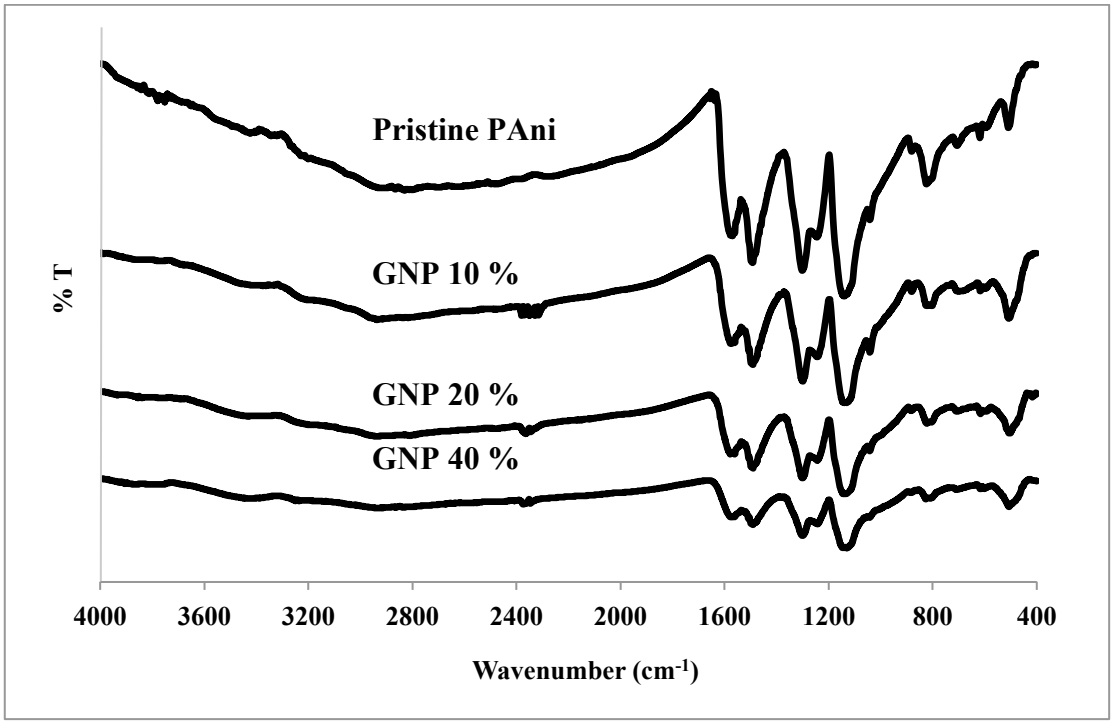

Figure 4.37. FTIR spectra of pristine PAni and PAni/HA/TiO_2/GNP nanocomposites with different contents of GNP.

4.4.2 UV-vis analysis

UV-vis spectrum in Figure 4.38 shows the electronic transition within the pristine PAni and PAni/HA/TiO_2/GNP nanocomposites with different contents of GNP. Pristine PAni exhibits three absorption bands in the UV-vis spectra where the peak at 380 nm is due to the π- π* electronic transition and the second absorption band at 470 nm is corresponding to the bipolaron of PAni. The third absorption band at 870 nm is assigned to the electronic transition of the π-localized polaron band (Lixia Zhang et al., 2006).

PAni/HA/TiO_2/GNP nanocomposites exhibit the same trend as pristine PAni but the bands intensity decreasing when the contents of GNP increase. As observed in the UV-vis spectrum of PAni/HA/TiO_2/GNP nanocomposites, the benzenoid peak (380 nm) decreased simultaneously with increasing of GNP content because GNP will

significantly increase the interaction energy and decrease the band gap between the PAni and GNP (Chakraborty, Gupta, Rana, & Meikap, 2012).

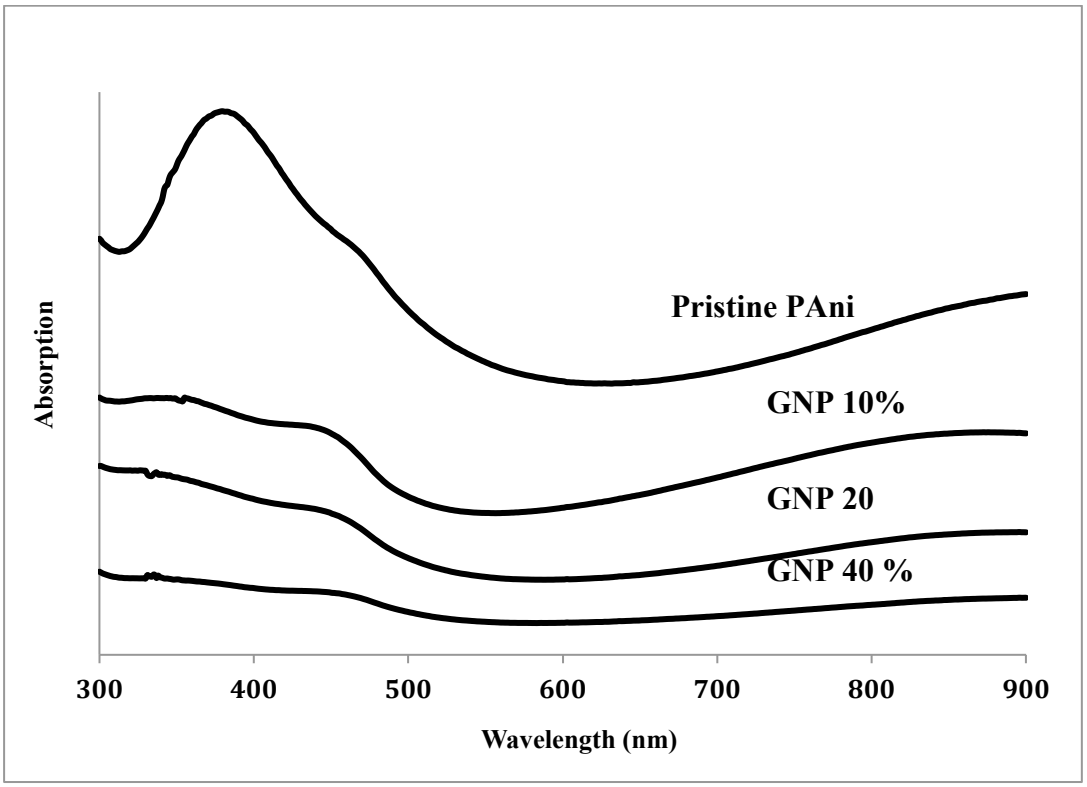

Figure 4.38. UV-vis spectra of pristine PAni and PAni/HA/TiO_2/GNP nanocomposites with different contents of GNP.

4.4.3 XRD analysis

Figure 4.39 shows the XRD spectra of PAni/HA/TiO_2/GNP nanocomposites with different contents of GNP. The crystallinity peaks at 25.2^{o}and 26.4^o belongs to doped-PAni and GNP, respectively. The intensity of GNP peak increased with increasing of GNP content for PAni/HA/TiO_2/GNP nanocomposites (Liu et al., 2013). The band at 25.2^o is attributed to the periodicity parallel and perpendicular of the polymer chain direction of PAni. Moreover, all the PAni/HA/TiO_2/GNP nanocomposites with different contents of GNP show the existence of TiO_2 peaks at 2θ = 36.8^o, 46.9^o, 52.9^o, 53.9^o and 61.6^o (Lijuan Zhang et al., 2005). Hence, it is clearly

determined that PAni is successfully doped by TiO_2 and GNP, which will act as a dielectric and magnetic fillers, respectively. As conclusion, it can be confirmed that there was no chemical interaction between the pristine PAni and GNP because there was no new peak has found in the FTIR, UV-vis and XRD spectra of PAni/HA/TiO_2/GNP nanocomposites.

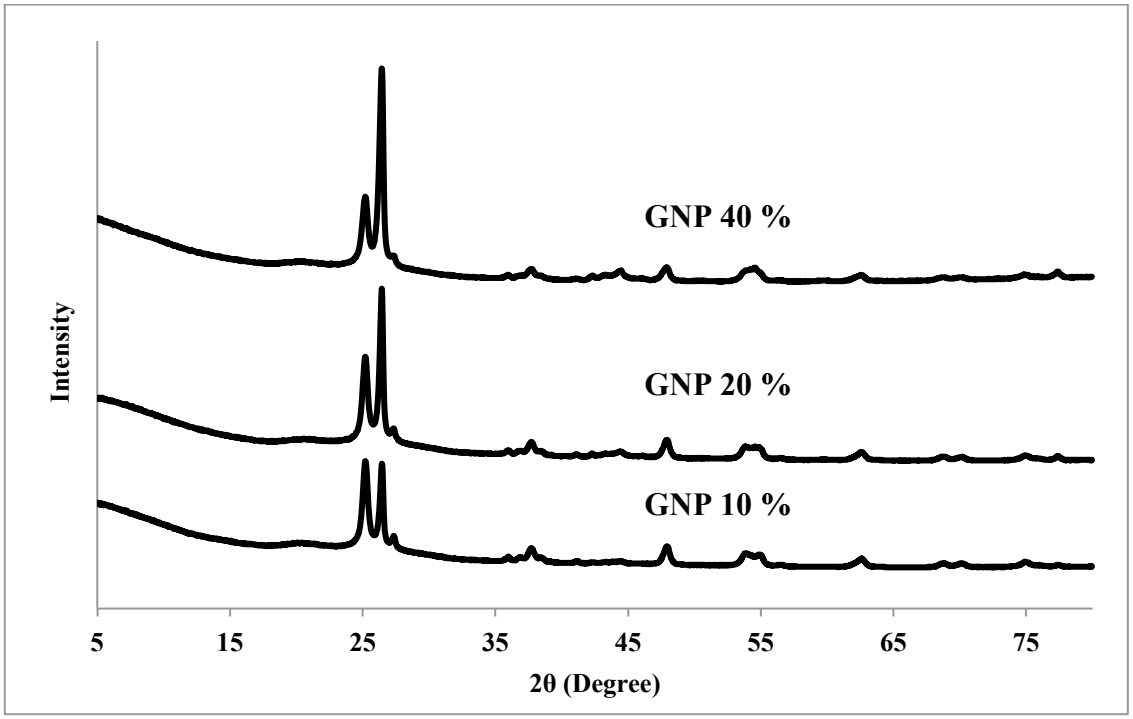

Figure 4.39. XRD diffractograms of PAni/HA/TiO_2/GNP nanocomposites with different contents of GNP.

4.4.4 TGA analysis

Figure 4.40 shows the TGA thermograms of PAni/HA/TiO_2/GNP nanocomposite with different contents of GNP (10 %, 20 % and 40 %). There are three stages of weight loss in the PAni/HA/TiO_2/GNP nanocomposites. In general, all PAni/HA/TiO_2/GNP nanocomposites experience small weight loss in temperature range of 50 - 100 ^{o}C due to the water molecules desorption from the PAni/HA/TiO_2/GNP nanocomposites while the decomposition of HA and PAni chain breakdown starts at

300 ^{o}C for all the PAni/HA/TiO_2/GNP nanocomposites. For PAni/HA/TiO_2/GNP nanocomposites with different GNP content, the decomposition temperature of HA and PAni increased gradually with increasing GNP contents (10 % to 40 %) from 670 ^{o}C to 710 ^{o}C (Lin, Hsu, & Wu, 2013).

Overall, the thermal stability of PAni/HA/TiO_2/GNP nanocomposites with different contents of GNP increased with the increasing GNP content in the nanocomposites. This is because GNP is a magnetic material, which possesses very high thermal stability and good barrier properties. Besides, GNP will absorb most of the heat applied to the PAni/HA/TiO_2/GNP nanocomposites compare to HA and PAni. So, the amount of heat needed to decompose the HA and PAni also increases significantly with increasing of GNP content (Gedler, Antunes, Realinho, & Velasco, 2012).

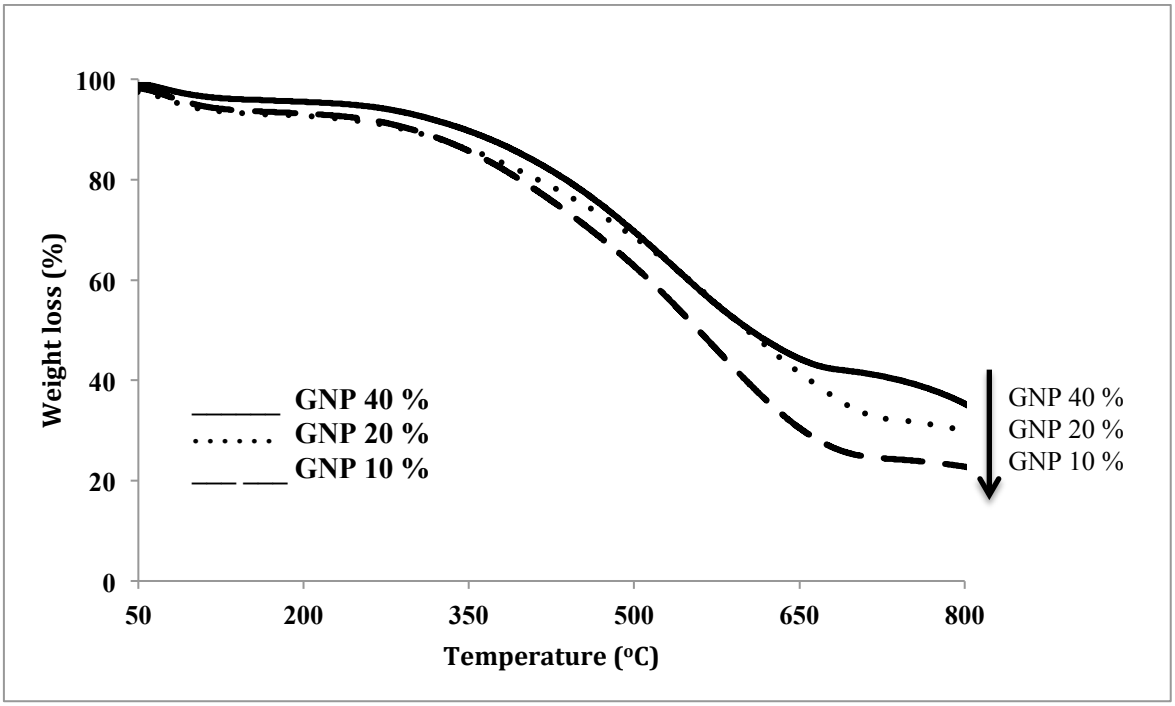

Figure 4.40. TGA thermograms of PAni/HA/TiO_2/GNP nanocomposites with different contents of GNP.

4.4.5 Morphology studies

FESEM images in Figure 4.41 shows the images of pristine GNP and PAni/HA/TiO_2/GNP nanocomposites with different contents of GNP at magnification of 30,000 ×. PAni/HA/TiO_2 formed bulk nanoparticles (X) in the nanocomposite based on the FESEM images as shown in Figure 4.41 while GNP will act as a template (Y) for polymerization of PAni. In general, Ani will grow through elongation by forming micelles with the present of HA. Since the synthesis under undisturbed condition, the big GNP template will act as barrier that blocked the polymerization through elongation. Thus, polymerization of the micelles was continued through accretion to form the PAni in the bulk form instead of the nanorods/nanotubes form and the bulk nanoparticles was penetrated on the surface of the GNP (Phang, Tadokoro, et al., 2008).

Moreover, from the morphology studies, it can be concluded that the PAni/HA/TiO_2/GNP nanocomposites consist of PAni/HA/TiO_2 bulk nanoparticles, individual TiO_2 nanoparticles (Z) and individual GNP which were physically mixed (Singh et al., 2013). The explanation here is strongly supported by the FTIR and UV-vis spectra from Figure 4.37 and Figure 4.38. Besides, it can be observed that increasing the contents of GNP will create more individual GNP that dispersed around the reaction system while the amount of PAni/HA/TiO_2 bulk nanoparticles and individual TiO_2 nanoparticles remain the same.

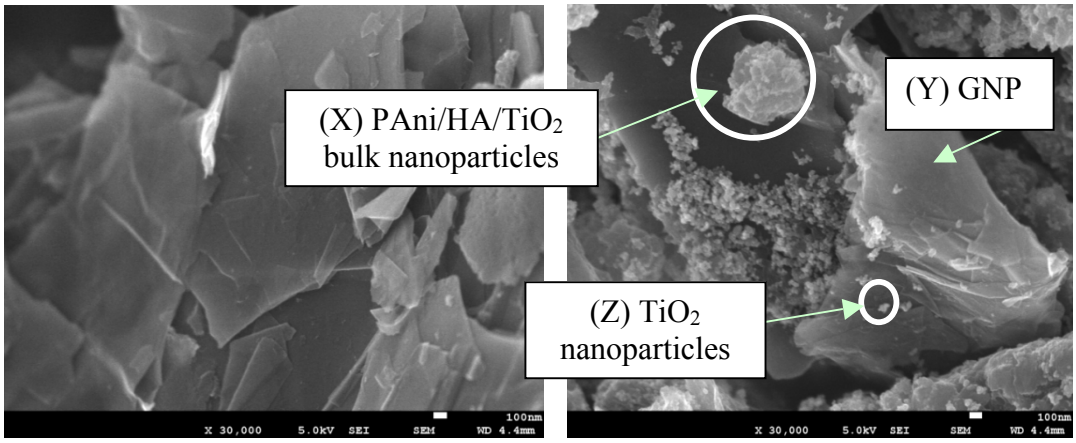

(a) Pristine GNP (b) PAni/HA/TiO_2/GNP (10 %)

(c) PAni/HA/TiO_2/GNP (20 %) (d) PAni/HA/TiO_2/GNP (40 %)

Figure 4.41. FESEM images of pristine GNP and PAni/HA/TiO_2/GNP nanocomposites with different contents of GNP (Magnification: 30,000 ×).

4.4.6 Conductivity studies

Figure 4.42 shows the electrical conductivities for PAni/HA/TiO_2/GNP nanocomposites with different contents of GNP. The conductivities of PAni/HA/TiO_2/GNP nanocomposites increased with increment contents of GNP. This is because the conductivity of pristine PAni is very low (10^{-2} S/cm) if compared to pristine GNP (10^{7} S/cm) (Koh, Sambasevam, Yahya, & Phang, 2013). Thus, addition of the GNP into the reaction system will significantly increase the electrical conductivities of PAni nanocomposites from 10 % (3.56 x 10^{-1} S/cm) to 40 % (2.56 S/cm). Since graphene nanoplatelets is an excellent electron donor, while Ani is a good electron

donor, therefore it will create a better charge transfer along the interface of PAni and graphene nanoplatelets (Singh et al., 2013). Hence, the electrical conductivities of PAni/HA/TiO_2/GNP nanocomposites (3.56 x 10^{-1} – 2.56 S/cm) are much more higher if compared to pristine PAni (2.37 x 10^{-2} S/cm).

From the FESEM images as shown in Figure 4.41 (d), it can be strongly proved that PAni nanocomposites with highest contents of GNP will cause more free individual GNP outside the PAni/HA/TiO_2/GNP nanocomposites. Thus, higher contents of GNP (large surface area) will create more conductive pathways within the PAni/HA/TiO_2/GNP nanocomposites structure through direct interfacial interaction between PAni and GNP. This causes the higher current to be generated in the external circuit through the dissociation of exciton at the interfaces of PAni and GNP and significantly lead to an improvement in electrical conductivities (Luan et al., 2013).

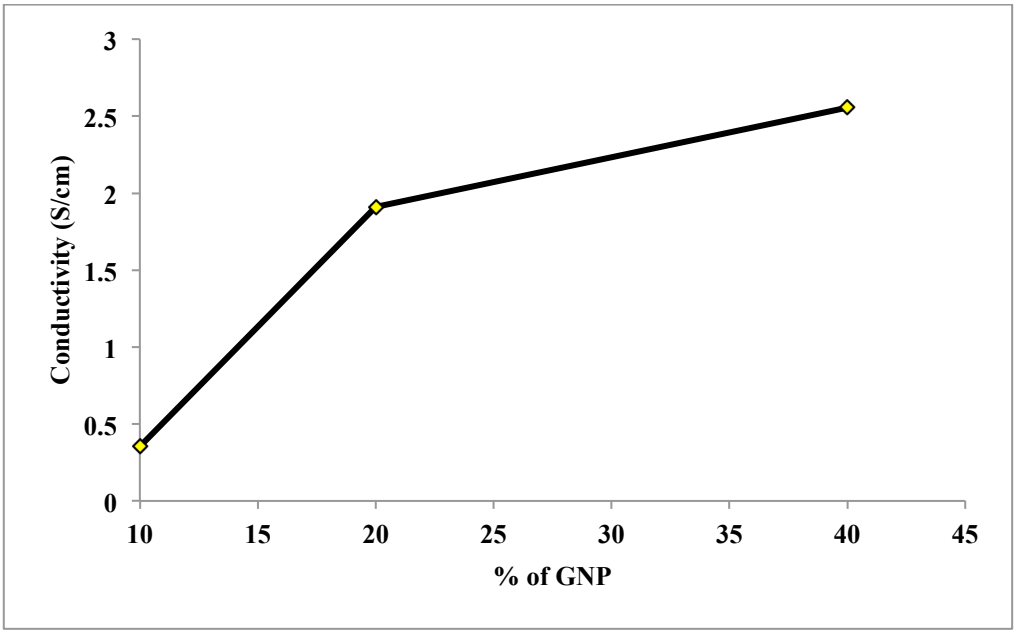

Figure 4.42. Electrical conductivities of PAni/HA/TiO_2/GNP nanocomposites with different contents of GNP.

4.4.7 Magnetization studies

The Ms, Mr and Hc are determined by the magnetization curves and all the PAni/HA/TiO_2/GNP nanocomposites exhibit a similar hysteric loops under applied magnetic field of -10 kOe to 10 kOe as mentioned in previous part (Figure 4.8). As shown in Figure 4.43, Ms of PAni/HA/TiO_2/GNP nanocomposites significantly increased from 10 % (1.17×10^{-2} emu/g) to 20 % (1.79×10^{-2} emu/g) of GNP but the Ms decreased at 40 % (9.24×10^{-3} emu/g) of GNP in the PAni/HA/TiO_2/GNP nanocomposites. PAni/HA/TiO_2/GNP nanocomposites with 20 % of GNP possess the highest Ms (1.79×10^{-2} emu/g) among the PAni/HA/TiO_2/GNP nanocomposites. This can be explained through the aid of percolation law.

The percolation law indicates that when the amount of conductive filler (GNP) increased in the PAni/HA/TiO_2/GNP nanocomposites, the conductivity also increases respectively. However, when the amount exceeds the percolation limit, the conductivity will increase in manifold. Thus it will significantly reduce the magnetization property of the PAni/HA/TiO_2/GNP nanocomposites at higher loading of GNP considerably (Huo et al., 2009; Song et al., 2014). Furthermore, PAni/HA/TiO_2/GNP nanocomposites with 40 % of GNP exhibit the lowest Ms value due to the restriction mobility by high contents of GNP along PAni backbone and thus lead to a poorer magnetization (Phang & Kuramoto, 2010).

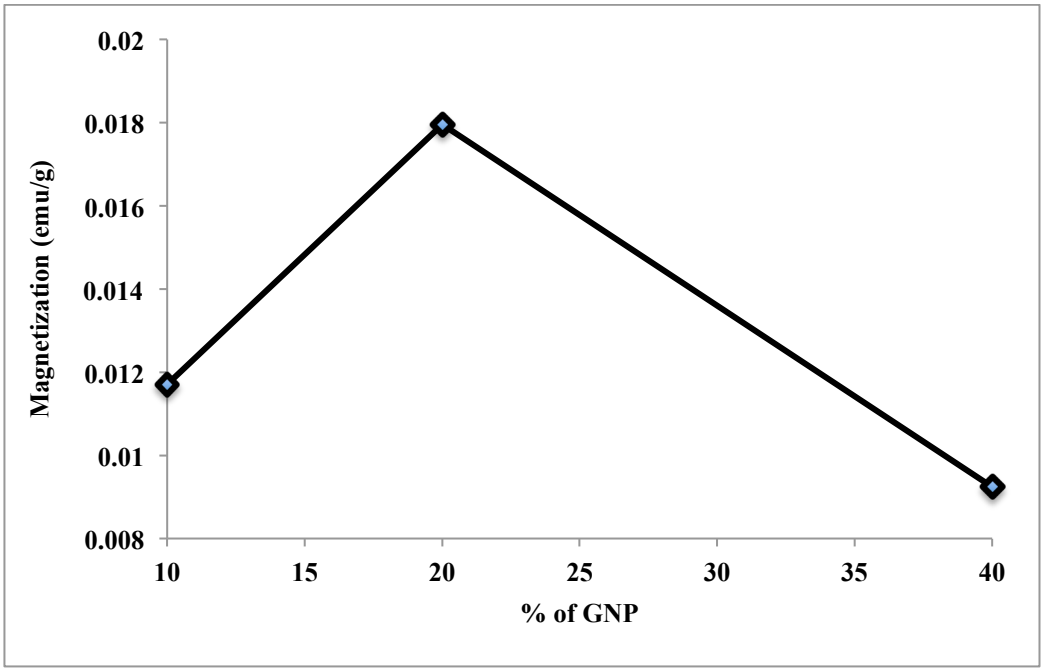

Figure 4.43. Ms value of PAni/HA/TiO_2/GNP nanocomposites with different contents of GNP.

4.4.8 Microwave absorption studies

Figure 4.44 shows the RL for PAni/HA/TiO_2/GNP nanocomposites with different contents of GNP. The dip in the RL curve indicates the appearances of absorption or reflection of the microwave and were calculated using formula, RL = 20 log S_{11}*. The microwave absorbance can be predicted from RL, where larger negative values are related to better microwave absorption properties of a material (Phang et al., 2004).

Refer to the RL graph in Figure 4.44, PAni/HA/TiO_2/GNP nanocomposites with 40 % of GNP possess a sharp RL peak with good absorption (RL = -6.6 dB) at 3 GHz while the PAni/HA/TiO_2/GNP nanocomposites with 10 % and 20 % of GNP show a broad RL peak with poor absorption (RL = -4.0 dB to -2.7 dB) in frequency range of 2 – 3 GHz. In general, polymer displays a broad absorption peak due to its various conductivities range along the polymer chain but the traditional microwave absorption

material such as metal possesses the sharp RL peak due to its constant conductivity value.

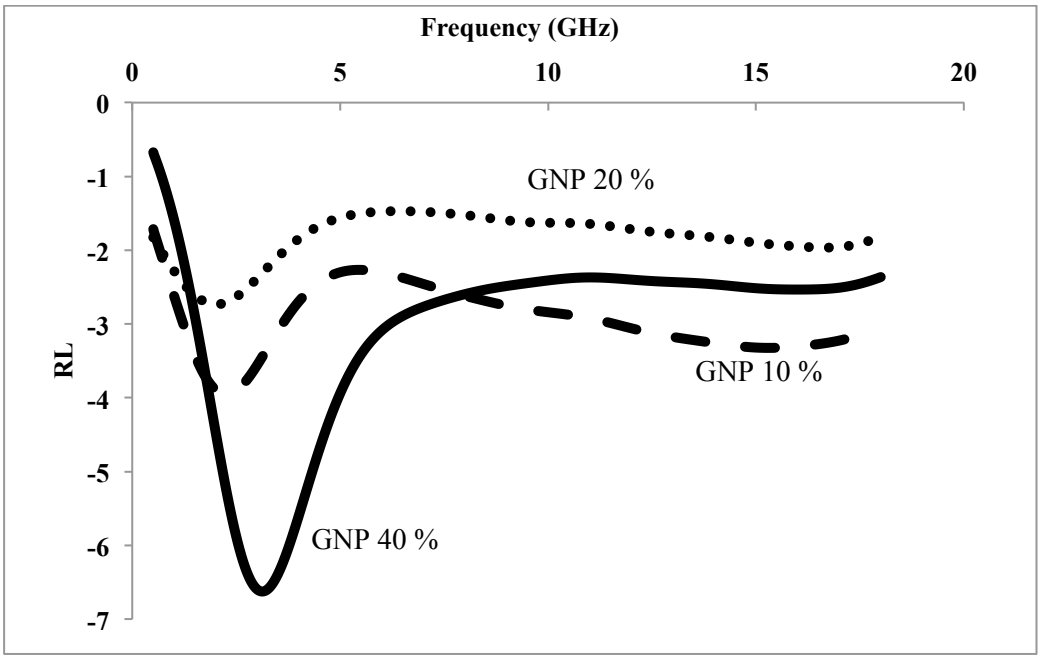

Figure 4.44. RL of PAni/HA/TiO_2/GNP nanocomposites with different contents of GNP.

Among the PAni/HA/TiO_2/GNP nanocomposites with different contents of GNP, PAni/HA/TiO_2/GNP nanocomposites with 40 % of exhibit the highest RL (RL = -6.6 dB), in which parallel with the highest conductivity (2.56 S/cm) and moderate Ms (0.009 emu/g) (Table 4.4). Thus, it can eventually show that the microwave absorption of PAni/HA/TiO_2/GNP nanocomposites significantly improved with the increasing of contents of GNP due to the increase in conductivity and moderate magnetization that induce more disordered motion of charge carriers along the PAni chain. On the other hand, PAni/HA/TiO_2/GNP nanocomposites with GNP contents do not show any difference in the heterogeneity due to the PAni/HA/TiO_2/GNP nanocomposites does not possess any nanorods/nanotubes. Hence, μ_r' and μ_r'' of complex magnetic permeability play a significant role that will result the RL result of PAni nanocomposites.

Table 4.4. Comparison among σ, Ms and heterogeneity (ε') for PAni/HA/TiO_2/GNP nanocomposites with different contents of GNP.

	GNP 10 %	GNP 20 %	GNP 40 %
σ	↑	↑↑	↑↑↑
Ms	↑	↑↑↑	↑↑
ε'	N/A	N/A	N/A

Real (μ_r') and imaginary (μ_r'') part of magnetic permeability for PAni/HA/TiO_2/GNP nanocomposites with different contents of GNP is shown in Figure 4.45 and 4.46. The data obtained clearly indicates that μ_r' and μ_r'' of complex magnetic permeability exhibit the same trend as RL in Figure 4.44 follow the sequence of 40 % > 10 % > 20 % (GNP). Based on Figure 4.41 and 4.42, μ_r' and μ_r'' of PAni/HA/TiO_2/GNP nanocomposites with 40 % of GNP show a higher value of -0.62 and 1.66 at 5 and 3 GHz respectively will eventually facilitate a higher eddy current and enhance the interaction between PAni and GNP. Hence, PAni/HA/TiO_2/GNP nanocomposites with 40 % of GNP show a strong microwave absorption if compared to those with 10 % and 20 % of GNP.

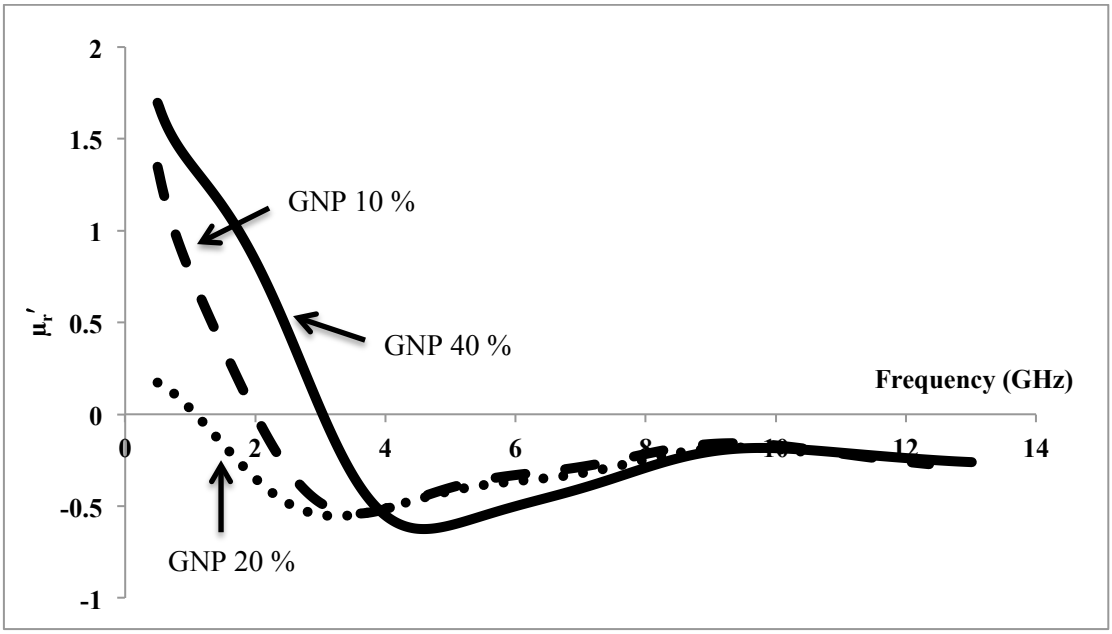

Figure 4.45. Real (μ_r') part of magnetic permeability for PAni/HA/TiO_2/GNP nanocomposites with different contents of GNP.

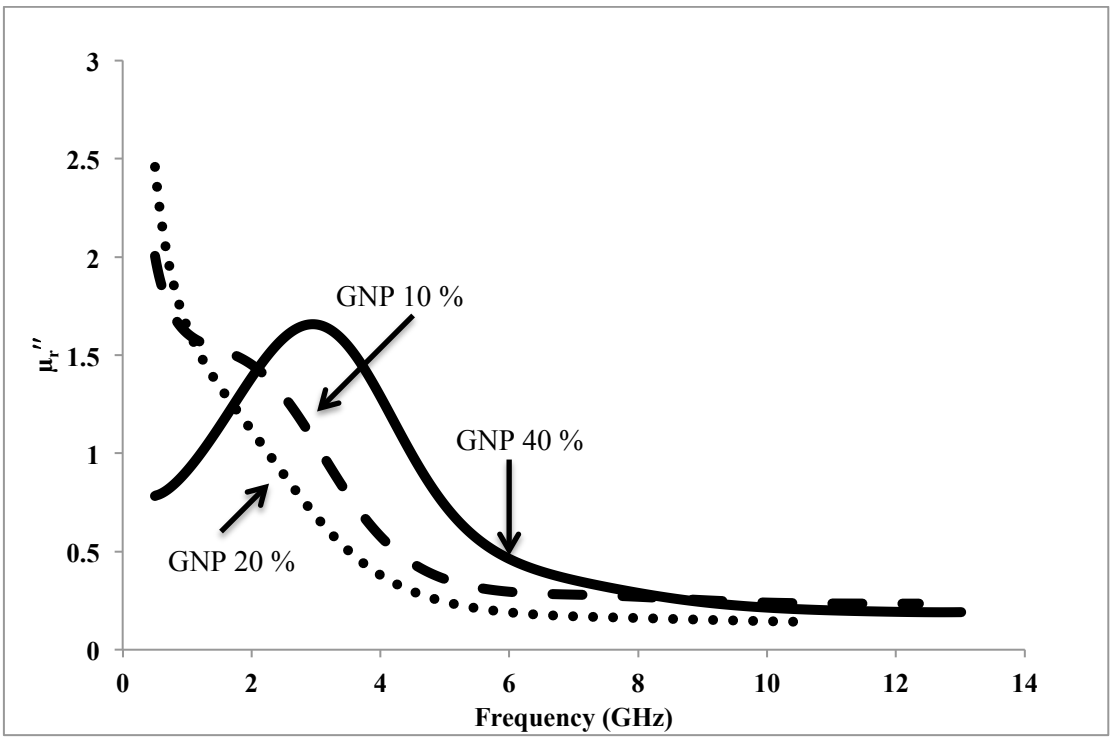

Figure 4.46. Imaginary (μ_r'') part of magnetic permeability for PAni/HA/TiO_2/GNP nanocomposites with different contents of GNP.

From the graph of loss tangent in Figure 4.47, PAni/HA/TiO_2/GNP nanocomposites with 40 % of GNP show higher tan δ that can be considered, as loosy material in which will induce the microwave absorbance properties. From the pervious study, it has been proposed that tan δ is directly proportional to the RL. Thus, it can be concluded that higher tan δ that obtained from the PAni/HA/TiO_2/GNP nanocomposites with 40 % of GNP will lead to a better RL as proved by the strong absorption peak as shown in Figure 4.44.

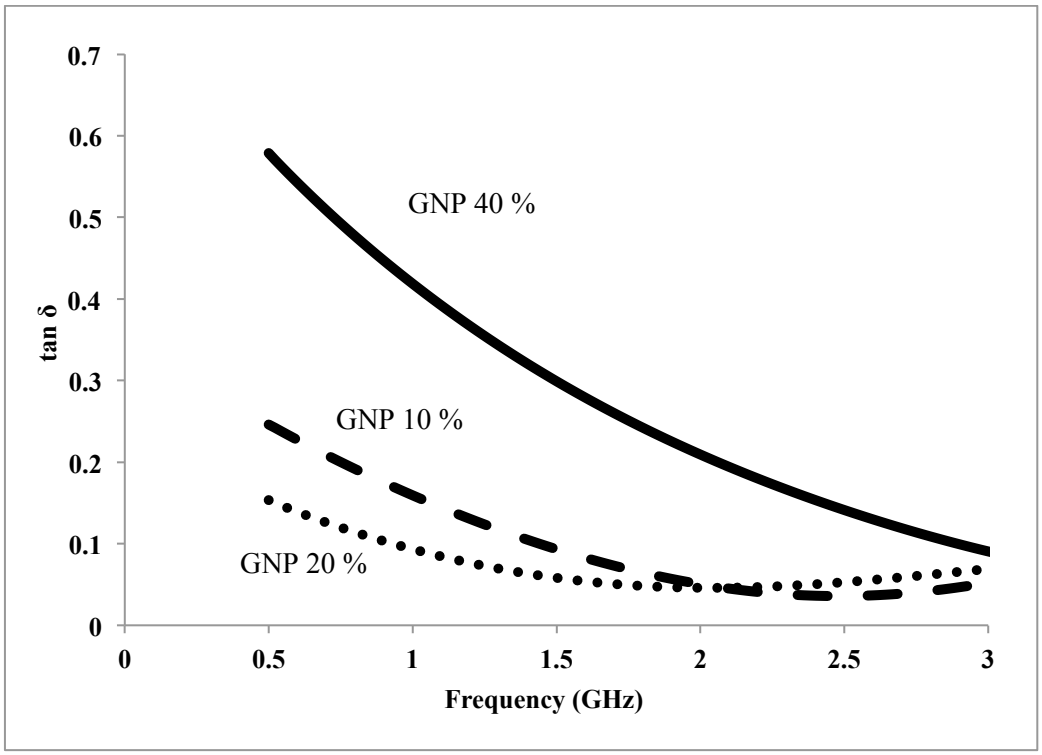

Figure 4.47. Loss tangent for PAni/HA/TiO_2/GNP nanocomposites with different contents of GNP.

4.5 Summary of microwave absorption for different types of PAni nanocomposites

Table 4.5 shows the summary of microwave absorption study for different types of PAni nanocomposites. Among all the PAni/HA/TiO_2/Fe_3O_4 nanocomposites (with and without chemical treatment), PAni/HA/TiO_2/Fe_3O_4 nanocomposites (40 % of Fe_3O_4) with chemical treatment possesses high conductivity, high heterogeneity (larger amount of nanorods/nanotubes), and moderate magnetization, which will induce the eddy current and thus indicate high microwave absorption (RL = -48.9 dB). While for the PAni/HA/TiO_2/MWNT nanocomposites with different diameter and length of MWNT, PAni/HA/TiO_2/MWNT nanocomposites with MWNT (D = 10-20 nm, l = 5-15 μm) shows the highest absorption due to the higher values of μ_r' and μ_r'' value, high heterogeneity and moderate electrical conductivity (1.11 x 10^{-2} S/cm) that lead to a more disordered motion of charge carrier along the PAni chain. Thus, it exhibits the highest RL value (-58 dB) among all the PAni nanocomposites.

For the PAni/HA/TiO_2/DWNT nanocomposites with different contents (10%, 20% and 60%) of u-DWNT and c-DWNT, PAni/HA/TiO_2/DWNT nanocomposites with 20 % of c-DWNT shows that larger amount of c-DWNT has been covered by PAni layers to form the nanorods/nanotubes and thus increase the heterogeneity that contribute to a better microwave absorption (RL = -18.3 dB). As for the PAni/HA/TiO_2/GNP nanocomposites, PAni/HA/TiO_2/GNP nanocomposites with 40 % of GNP exhibits a better absorption (RL = -6.44 dB) if compared to 10 % and 20 % of GNP because 40 % of GNP show the highest electrical conductivity and it will significantly improve the anisotropy of PAni nanocomposites.

Among all the PAni nanocomposites obtained in this study, PAni/HA/TiO_2/MWNT nanocomposites with smaller diameter and longer length of MWNT (D = 10-20 nm, l = 5-15 μm) with moderate heterogeneity (induce space charge polarization), highest μ_r' and μ_r'' value (enhance the interaction between PAni and MWNT) possesses the highest RL (-58 dB). On the other hand, PAni/HA/TiO_2/GNP nanocomposites with 40 % of GNP possess the lowest RL (-6.6 dB) because it does not show any heterogeneity (GNP in nanoplatelets form) and due to their poor μ_r' and μ_r'' value, and the absent of nanorods/nanotubes.

Table 4.5. Summary for different types of PAni nanocomposites for microwave absorption study.

No.	Sample name	Supporting data			tan δ	RL (dB)
		Heterogeneity	σ (S/cm)	Ms (emu/g) / #μ_r' & μ_r''		
1)	PAni/HA		2.37×10^{-2}	N/A	0.46	-17.0
	PAni/HA/TiO_2/Fe10 (with)		4.77×10^{-2}	6.03	0.66	-35.6
	PAni/HA/TiO_2/Fe10 (without)		1.23×10^{-2}	8.87	0.36	-11.0
	PAni/HA/TiO_2/Fe20 (with)		4.42×10^{-2}	10.10	0.38	-36.2
	PAni/HA/TiO_2/Fe20 (without)		3.51×10^{-3}	16.69	0.38	-13.8
	PAni/HA/TiO_2/Fe40 (with)	* 	3.58×10^{-2}	*** 16.90**	0.54	-48.9
	PAni/HA/TiO_2/Fe40 (without)		8.48×10^{-4}	28.48	0.45	-13.0
2)	PAni/HA/TiO_2/MWNT (D=60-100nm, l=1-2 μm)		6.53×10^{-3}	#-2.7 & 3.66	0.37	-20.6
	PAni/HA/TiO_2/MWNT (D=60-100nm, l=5-15 μm)		1.51×10^{-2}	#-1.57 & 2.73	0.39	-18.9
	PAni/HA/TiO_2/MWNT (D=10-20nm, l=5-15 μm)	* 	1.11×10^{-2}	**#-10.42 & 8.14 ***	0.40	-58.0
3)	PAni/HA/TiO_2/DWNT10 (u-DWNT)		1.23×10^{-1}	#-0.44 & 1.42	0.58	-5.8
	PAni/HA/TiO_2/DWNT20 (u-DWNT)		4.28×10^{-1}	#-0.53 & 1.33	0.46	-4.5
	PAni/HA/TiO_2/DWNT60 (u-DWNT)		1.13	#-0.62 & 1.42	0.33	-4.2
	PAni/HA/TiO_2/DWNT10 (c-DWNT)		3.43×10^{-2}	#-1.16 & 2.52	0.56	-14.7
	PAni/HA/TiO_2/DWNT20 (c-DWNT)	* 	4.43×10^{-2}	**#-1.77 & 3.13 ***	0.43	-18.3
	PAni/HA/TiO_2/DWNT60 (c-DWNT)		4.48×10^{-1}	#-0.77 & 1.92	0.47	-6.6
4)	PAni/HA/TiO_2/GNP10	N/A	3.56×10^{-1}	#-0.54 & 1.50	0.25	-4.0
	PAni/HA/TiO_2/GNP20	N/A	1.91	#-0.55 & 1.34	0.15	-2.7
	PAni/HA/TiO_2/GNP40	N/A	***2.56**	**#-0.62 & 1.66 ***	0.58	-6.6

#Special condition: μ' and μ" play significant role that affect RL instead of Ms.
*Main factors that contribute to high absorption.

CHAPTER 5

Conclusion

In this research study, several types of PAni nanocomposites with dielectric material (TiO_2) and different types of magnetic materials (Fe_3O_4, MWNT, DWNT and GNP) are successfully synthesized by template free method. Chemical structure of the PAni nanocomposites was not disturbed by addition of dielectric and magnetic materials because it shows almost identical peaks for all FTIR, UV-vis, and XRD spectra. From the FESEM images obtained, this strongly proves that PAni nanocomposites will induce the formation of nanorods/nanotubes and thus significantly enhanced the conductivity, tan δ and heterogeneity of the resulted polymer as confirmed by the suggested mechanism. Among all the PAni nanocomposites, PAni/HA/TiO_2/GNP nanocomposites with different contents of GNP do not show any heterogeneity due to the absence of nanorods/nanotubes.

In general, high electrical conductivity, complex dielectric permittivity and magnetic permeability are the three main properties to achieve high microwave absorption of a material. Among all the PAni nanocomposites in this study, PAni/HA/TiO_2/MWNT nanocomposites with MWNT (D = 10-20 nm, l = 5-15 μm) possesses the highest RL (-58 dB) at 7 GHz due to the moderate electrical conductivity, high heterogeneity, high μ_r' and μ_r'' value, which is suitable to use in computer. Oppositely, PAni/HA/TiO_2/GNP nanocomposites with 40 % of GNP possess the lowest RL (-6.6 dB) at 3 GHz because it possesses lowest μ_r' and μ_r'' value, in which adequate to apply in mobile phone application. In this study, it can eventually prove that high aspect ratio with unique electrical properties of carbonaceous material will significantly enhance the microwave shielding performance.

As for the future work, different types of dielectric ($SiTiO_3$) and magnetic (fullerene) materials can be added in order to enhance the dielectric and magnetic property of the nanocomposites. Moreover, different synthesis parameter such as subzero synthesis temperature (-5 ^{o}C, -10 ^{o}C or -20 ^{o}C) for PAni synthesis could be an attractive idea in the near future in order to achieve higher absorption for a particular applications such as electronic devices, telecommunications, mobile phones, radar applications and etc.

REFERENCES

Abbas, S. M., Chatterjee, R.,Dixit, A. K., Kumar, A. V. R. & Goel, T. C. (2007). Electromagnetic and microwave absorption properties of (Co^{2+} - Si^{4+}) substituted Ba-Hexaferrites and its polymer composites. *Journal of Applied Physics, 101*(7), 074105.

Abdul Hamid, Siti Atkah, Abdullah, Mustaffa Hj., Ahmad, Sahrim Hj., Mansor, Abdul Aziz, & Yusoff, Ahmad Nazlim. (2002). Effects of Natural Rubber on Microwave Absorption Characteristics of Some Li-Ni-Zn Ferrite-Thermoplastic Natural Rubber Composites. *Japanese Journal of Applied Physics, 41*(9), 5815-5820.

Akman, O., Durmus, Z., Kavas, H., Aktas, B., Kurtan, U., Baykal, A., & Sözeri, H. (2013). Effect of conducting polymer layer on microwave absorption properties of BaFe12O19.TiO_2 composite. *physica status solidi (a), 210*(2), 395-402.

Al-Ibrahim, Maher, Ambacher, Oliver, Sensfuss, Steffi, & Gobsch, Gerhard. (2005). Effects of solvent and annealing on the improved performance of solar cells based on poly(3-hexylthiophene): Fullerene. *Applied Physics Letters, 86*(20), 201120.

Basuli, Utpal, Chattopadhyay, Santanu, Nah, Changwoon, & Chaki, Tapan Kumar. (2012). Electrical properties and electromagnetic interference shielding effectiveness of multiwalled carbon nanotubes-reinforced EMA nanocomposites. *Polymer Composites, 33*(6), 897-903.

Bhadra, Sambhu, Khastgir, Dipak, Singha, Nikhil K., & Lee, Joong Hee. (2009). Progress in preparation, processing and applications of polyaniline. *Progress in Polymer Science, 34*(8), 783-810.

Bhadra, Sambhu, Singha, Nikhil K., & Khastgir, Dipak. (2009). Dielectric properties and EMI shielding efficiency of polyaniline and ethylene 1-octene based semi-conducting composites. *Current Applied Physics, 9*(2), 396-403.

Bhatia, Ravi, Prasad, V., & Menon, Reghu. (2010). Characterization, electrical percolation and magnetization studies of polystyrene/multiwall carbon nanotube composite films. *Materials Science and Engineering: B, 175*(3), 189-194.

Burgei, Wesley, Pechan, Michael J., & Jaeger, Herbert. (2003). A simple vibrating sample magnetometer for use in a materials physics course. *American Journal of Physics, 71*(8), 825-828.

Chakraborty, Goutam, Gupta, Kajal, Rana, Dipak, & Meikap, Ajit Kumar. (2012). Effect of multiwalled carbon nanotubes on electrical conductivity and magnetoconductivity of polyaniline. *Advances in Natural Sciences: Nanoscience and Nanotechnology, 3*(3), 035015.

Chandrasekhar, P., & Naishadham, K. (1999). Broadband microwave absorption and shielding properties of a poly(aniline). *Synthetic Metals, 105*(2), 115-120.

Chapal, K. D., Pallab, B., & Swinderjeet, S. K. (2012). Graphene and MWCNT: Potential Candidate for Microwave Absorbing Materials. *Journal of Materials Science Research, 1*(2), 126-132.

Chen, Aihua, Wang, Haiqiao, Zhao, Bin, & Li, Xiaoyu. (2003). The preparation of polypyrrole–Fe_3O_4 nanocomposites by the use of common ion effect. *Synthetic Metals, 139*(2), 411-415.

Cochet, Murielle, Maser, Wolfgang K., Benito, Ana M., Callejas, M. Alicia, Martinez, M. Teresa, Benoit, Jean-Michel, . . . Chauvet, Olivier. (2001). Synthesis of a new polyaniline/nanotube composite: "" polymerisation and charge transfer through site-selective interaction. *Chemical Communications*(16), 1450-1451.

Costa, L. C., Valente, M., Sá, M. A., & Henry, F. (2006). Electrical and magnetic properties of Polystyrene doped with Iron nanoparticles. *Polymer Bulletin, 57*(6), 881-887.

Czekelius, Constantin, Hafer, Jillian, Tonzetich, Zachary J., Schrock, Richard R., Christensen, Ronald L., & Müller, Peter. (2006). Synthesis of Oligoenes that Contain up to 15 Double Bonds from 1,6-Heptadiynes. *Journal of the American Chemical Society, 128*(51), 16664-16675.

Deivanayaki, S., Ponnuswamy, V., Ashokan, S., Jayamurugan, P., & Mariappan, R. (2013). Synthesis and characterization of TiO_2-doped Polyaniline nanocomposites by chemical oxidation method. *Materials Science in Semiconductor Processing, 16*(2), 554-559.

Deng, Jianguo, Peng, Yuxing, He, Chuanlan, Long, Xingping, Li, Pei, & Chan, Albert S. C. (2003). Magnetic and conducting Fe_3O_4–polypyrrole nanoparticles with core-shell structure. *Polymer International, 52*(7), 1182-1187.

Dubnikova, Irina, Kuvardina, Evgeniya, Krasheninnikov, Vadim, Lomakin, Sergey, Tchmutin, Igor, & Kuznetsov, Sergey. (2010). The effect of multiwalled carbon nanotube dimensions on the morphology, mechanical, and electrical properties of melt mixed polypropylene-based composites. *Journal of Applied Polymer Science, 117*(1), 259-272.

Endo, M., Takeuchi, K., Hiraoka, T., Furuta, T., Kasai, T., Sun, X., Dresselhaus, M. S. (1997). Stacking nature of graphene layers in carbon nanotubes and nanofibres. *Journal of Physics and Chemistry of Solids, 58*(11), 1707-1712.

Faez, R., Martin, I. M., De Paoli, M. A., & Rezende, M. C. (2001). Microwave properties of EPDM/PAni-DBSA blends. *Synthetic Metals, 119*(1–3), 435-436.

Fehse, Karsten, Schwartz, Gregor, Walzer, Karsten, & Leo, Karl. (2007). Combination of a polyaniline anode and doped charge transport layers for high-efficiency organic light emitting diodes. *Journal of Applied Physics, 101*(12), -.

Feng, W., Bai, X. D., Lian, Y. Q., Liang, J., Wang, X. G., & Yoshino, K. (2003). Well-aligned polyaniline/carbon-nanotube composite films grown by in-situ aniline polymerization. *Carbon, 41*(8), 1551-1557.

Gedler, G., Antunes, M., Realinho, V., & Velasco, J. I. (2012). Thermal stability of polycarbonate-graphene nanocomposite foams. *Polymer Degradation and Stability, 97*(8), 1297-1304.

Håkansson, Eva, Amiet, Andrew, Nahavandi, Saeid, & Kaynak, Akif. (2007). Electromagnetic interference shielding and radiation absorption in thin polypyrrole films. *European Polymer Journal, 43*(1), 205-213.

Heeger, Alan J. (2001). Semiconducting and Metallic Polymers: The Fourth Generation of Polymeric Materials (Nobel Lecture). *Angewandte Chemie International Edition, 40*(14), 2591-2611.

Hekmatara, H., Seifi, M., & Forooraghi, K. (2013). Microwave absorption property of aligned MWCNT/Fe_3O_4. *Journal of Magnetism and Magnetic Materials, 346*(0), 186-191.

Hsieh, Tar-Hwa, Ho, Ko-Shan, Huang, Ching-Hung, Wang, Yen-Zen, & Chen, Zhi-Long. (2006). Electromagnetic properties of polyaniline/maghemite nanocomposites: I. The effect of re-doping time on the electromagnetic properties. *Synthetic Metals, 156*(21–24), 1355-1361.

Huo, Jia, Wang, Li, & Yu, Haojie. (2009). Polymeric nanocomposites for electromagnetic wave absorption. *Journal of Materials Science, 44*(15), 3917-3927.

Hwang, Seok-Ho, Jeong, Kyung-Sun, & Jung, Jae-Chang. (1999). Thermal and mechanical properties of amorphous copolyester (PETG)/LCP blends. *European Polymer Journal, 35*(8), 1439-1443.

Iijima, Sumio. (1991). Helical microtubules of graphitic carbon. *Nature, 354*(6348), 56-58.

Jeevananda, T., Siddaramaiah, Kim, Nam Hoon, Heo, Seok-Bong, & Lee, Joong Hee. (2008). Synthesis and characterization of polyaniline-multiwalled carbon nanotube nanocomposites in the presence of sodium dodecyl sulfate. *Polymers for Advanced Technologies, 19*(12), 1754-1762.

Jiang, Jing, Li, Liangchao, & Zhu, Mingli. (2008). Polyaniline/magnetic ferrite nanocomposites obtained by in situ polymerization. *Reactive and Functional Polymers, 68*(1), 57-62.

Junfeng, Wen, Yadong, Jiang, Yajie, Yang, Junsheng, Yu, & Jianhua, Xu. (2011). Self-Assembled of Conducting Polymeric Nanoparticles and its Application for OLED Hole Injection Layer. *Energy Procedia, 12*(0), 609-614.

Kim, M. S., Kim, H. K., Byun, S. W., Jeong, S. H., Hong, Y. K., Joo, J. S., . . . Lee, J. Y. (2002). PET fabric/polypyrrole composite with high electrical conductivity for EMI shielding. *Synthetic Metals, 126*(2–3), 233-239.

Kim, Y. H., Foster, C., Chiang, J., & Heeger, A. J. (1989). Localized charged excitations in polyaniline: Infrared photoexcitation and protonation studies. *Synthetic Metals, 29*(1), 285-290.

Koh, Yen-Nee, Sambasevam, Kavirajaa Pandian, Yahya, Rosiyah, & Phang, Sook-Wai. (2013). Improvement of microwave absorption for PAni/HA/TiO_2/Fe_3O_4 nanocomposite after chemical treatment. *Polymer Composites, 34*(7), 1186-1194.

Koul, S., Chandra, R., & Dhawan, S. K. (2000). Conducting polyaniline composite for ESD and EMI at 101 GHz. *Polymer, 41*(26), 9305-9310.

Kulkarni, Milind V., & Viswanath, Annamraju Kasi. (2004). Comparative studies of chemically synthesized polyaniline and poly(o-toluidine) doped with p-toluene sulphonic acid. *European Polymer Journal, 40*(2), 379-384.

Kumar, Abhishek, Agarwala, Vijaya, & Singh, Dharmendra. (2013). Microwave absorbing behavior of metal dispersed TiO_2 nanocomposites. *Advanced Powder Technology*(0).

Li, F., Cheng, H. M., Bai, S., Su, G., & Dresselhaus, M. S. (2000). Tensile strength of single-walled carbon nanotubes directly measured from their macroscopic ropes. *Applied Physics Letters, 77*(20), 3161-3163.

Li, Yongbo, Chen, Gen, Li, Qihou, Qiu, Guanzhou, & Liu, Xiaohe. (2011). Facile synthesis, magnetic and microwave absorption properties of Fe_3O_4/polypyrrole core/shell nanocomposite. *Journal of Alloys and Compounds, 509*(10), 4104-4107.

Li, Zhongrui, Kandel, Hom R., Dervishi, Enkeleda, Saini, Viney, Biris, Alexandru S., Biris, Alexandru R., & Lupu, Dan. (2007). Does the wall number of carbon nanotubes matter as conductive transparent material? *Applied Physics Letters, 91*(5), -.

Lin, Yu-Chun, Hsu, Feng-Hao, & Wu, Tzong-Ming. (2013). Enhanced conductivity and thermal stability of conductive polyaniline/graphene composite synthesized by in situ chemical oxidation polymerization with sodium dodecyl sulfate. *Synthetic Metals, 184*(0), 29-34.

Liu, Panbo, Huang, Ying, Wang, Lei, & Zhang, Wei. (2013). Preparation and excellent microwave absorption property of three component nanocomposites: Polyaniline-reduced graphene oxide-Co3O4 nanoparticles. *Synthetic Metals, 177*(0), 89-93.

Luan, Van Hoang, Tien, Huynh Ngoc, Hoa, Le Thuy, Hien, Nguyen Thi Minh, Oh, Eun-Suok, Chung, JinSuk, . . . Hur, Seung Hyun. (2013). Synthesis of a highly conductive and large surface area graphene oxide hydrogel and its use in a supercapacitor. *Journal of Materials Chemistry A, 1*(2), 208-211.

Makeiff, Darren A., & Huber, Trisha. (2006). Microwave absorption by polyaniline–carbon nanotube composites. *Synthetic Metals, 156*(7–8), 497-505.

Martin, Charles R. (1996). Membrane-Based Synthesis of Nanomaterials. *Chemistry of Materials, 8*(8), 1739-1746.

Mathew, K. T., Praveen Kumar, A. V., & John, Honey. (2006, 14-18 Aug. 2006). *Polyaniline and polypyrrole with PVC content for effective EMI shielding.* Paper presented at the Electromagnetic Compatibility, 2006. EMC 2006. 2006 IEEE International Symposium on.

Mirmohseni, Abdolreza, & Oladegaragoze, Ali. (2000). Anti-corrosive properties of polyaniline coating on iron. *Synthetic Metals, 114*(2), 105-108.

Mo, Te-Cheng, Wang, Hong-Wen, Chen, San-Yan, & Yeh, Yun-Chieh. (2008). Synthesis and dielectric properties of polyaniline/titanium dioxide nanocomposites. *Ceramics International, 34*(7), 1767-1771.

Nagaraja, M., Mahesh, H. M., Manjanna, J., Rajanna, K., Kurian, M. Z., & Lokesh, S. V. (2012). Effect of Multiwall Carbon Nanotubes on Electrical and Structural Properties of Polyaniline. *Journal of Electronic Materials, 41*(7), 1882-1885.

Olmedo, L., Hourquebie, P., & Jousse, F. (1995). Microwave properties of conductive polymers. *Synthetic Metals, 69*(1–3), 205-208.

Olmedo, L.; Hourquebie, P. & Jousse, F. (1997). *In Handbook of Organic Conductive Molecules and Polymers* (H. S., Ed. ed. Vol. 3): John Wiley & Sons Ltd: Chichester.

Osawa, Zenjiro, & Kuwabara, Satoshi. (1992). Thermal stability of the shielding effectiveness of composites to electromagnetic interference. Effects of matrix polymers and surface treatment of fillers. *Polymer Degradation and Stability, 35*(1), 33-43.

Painter, P.C., & Coleman, M.M. (1997). *Fundamentals of Polymer Science: An Introductory Text*: Technomic Publishing Company.

Peacock, A.J., & Calhoun, A.R. (2006). *Polymer Chemistry: Properties and Applications*: Hanser Gardner Publications.

Phang, Sook Wai, Daik, Rusli, & Abdullah, M. H. (2004). Microwave properties of poly(4,4′-diphenylene diphenylvinylene). *Polymer Testing, 23*(3), 275-279.

Phang, Sook Wai, Hino, Tetsuo, & Kumamoto, Noriyuki. (2008). Development and investigation of polyaniline micro/nanocomposites that possess moderate conductivity, dielectric and magnetic properties. *Polym. J, 40*(1), 25-32.

Phang, Sook Wai, & Kuramoto, Noriyuki. (2010). Microwave absorption property of polyaniline nanocomposites containing TiO_2 and Fe_3O_4 nanoparticles after FeCl36H2O treatment. *Polymer Composites, 31*(3), 516-523.

Phang, Sook Wai, Tadokoro, Masato, Watanabe, Jiro, & Kuramoto, Noriyuki. (2008). Microwave absorption behaviors of polyaniline nanocomposites containing TiO_2 nanoparticles. *Current Applied Physics, 8*(3–4), 391-394.

Phang, Sook Wai, Tadokoro, Masato, Watanabe, Jiro, & Kuramoto, Noriyuki. (2009). Effect of Fe_3O_4 and TiO_2 addition on the microwave absorption property of polyaniline micro/nanocomposites. *Polymers for Advanced Technologies, 20*(6), 550-557.

Quillard, S., Louarn, G., Lefrant, S., & Macdiarmid, A. G. (1994). Vibrational analysis of polyaniline: A comparative study of leucoemeraldine, emeraldine, and pernigraniline bases. *Physical Review B, 50*(17), 12496-12508.

Ramya, R., Sivasubramanian, R., & Sangaranarayanan, M. V. (2013). Conducting polymers-based electrochemical supercapacitors—Progress and prospects. *Electrochimica Acta, 101*(0), 109-129.

Rao, C. N. R., Biswas, Kanishka, Subrahmanyam, K. S., & Govindaraj, A. (2009). Graphene, the new nanocarbon. *Journal of Materials Chemistry, 19*(17), 2457-2469.

Saini, Parveen, Choudhary, Veena, Singh, B. P., Mathur, R. B., & Dhawan, S. K. (2009). Polyaniline–MWCNT nanocomposites for microwave absorption and EMI shielding. *Materials Chemistry and Physics, 113*(2–3), 919-926.

Schulz, R. B., Plantz, V. C., & Brush, D. R. (1988). Shielding theory and practice. *Electromagnetic Compatibility, IEEE Transactions on, 30*(3), 187-201.

Shakoor, Abdul, & Rizvi, Tasneem Zahra. (2010). Synthesis and characterization of polypyrrole dodecylbenzenesulfonate-titanium dioxide nanocomposites. *Journal of Applied Polymer Science, 117*(2), 970-973.

Shalini, K., Subbanna, G. N., Chandrasekaran, S., & Shivashankar, S. A. (2003). Thin films of iron oxide by low pressure MOCVD using a novel precursor: tris(t-butyl-3-oxo-butanoato)iron(III). *Thin Solid Films, 424*(1), 56-60.

Sharma, Bhupendra K., Khare, Neeraj, Sharma, Rajbeer, Dhawan, S. K., Vankar, V. D., & Gupta, H. C. (2009). Dielectric behavior of polyaniline–CNTs composite in microwave region. *Composites Science and Technology, 69*(11–12), 1932-1935.

Shimano, James Y., & MacDiarmid, Alan G. (2001). Polyaniline, a dynamic block copolymer: key to attaining its intrinsic conductivity? *Synthetic Metals, 123*(2), 251-262.

Singh, Kuldeep, Ohlan, Anil, Pham, Viet Hung, R, Balasubramaniyan, Varshney, Swati, Jang, Jinhee, . . . Chung, Jin Suk. (2013). Nanostructured graphene/Fe_3O_4 incorporated polyaniline as a high performance shield against electromagnetic pollution. *Nanoscale, 5*(6), 2411-2420.

Song, Wei-Li, Cao, Mao-Sheng, Lu, Ming-Ming, Bi, Song, Wang, Chan-Yuan, Liu, Jia, . . . Fan, Li-Zhen. (2014). Flexible graphene/polymer composite films in sandwich structures for effective electromagnetic interference shielding. *Carbon, 66*(0), 67-76.

Star, Alexander, Stoddart, J. Fraser, Steuerman, David, Diehl, Mike, Boukai, Akram, Wong, Eric W., . . . Heath, James R. (2001). Preparation and Properties of Polymer-Wrapped Single-Walled Carbon Nanotubes. *Angewandte Chemie International Edition, 40*(9), 1721-1725.

Su, Shi-Jian, & Kuramoto, Noriyuki. (2000). Processable polyaniline–titanium dioxide nanocomposites: effect of titanium dioxide on the conductivity. *Synthetic Metals, 114*(2), 147-153.

Sun, Yi, Wilson, Stephen R., & Schuster, David I. (2001). High Dissolution and Strong Light Emission of Carbon Nanotubes in Aromatic Amine Solvents. *Journal of the American Chemical Society, 123*(22), 5348-5349.

Sun, Yong-kang, Ma, Ming, Zhang, Yu, & Gu, Ning. (2004). Synthesis of nanometer-size maghemite particles from magnetite. *Colloids and Surfaces A: Physicochemical and Engineering Aspects, 245*(1–3), 15-19.

Süsskind, Charles. (1988). Heinrich Hertz and the discovery of electromagnetic-wave propagation. *Endeavour, 12*(2), 84-85.

Tishkova, Victoria, Raynal, Pierre-Ivan, Puech, Pascal, Lonjon, Antoine, Fournier, Marion Le, Demont, Philippe, . . . Bacsa, Wolfgang. (2011). Electrical conductivity and Raman imaging of double wall carbon nanotubes in a polymer matrix. *Composites Science and Technology, 71*(10), 1326-1330.

Trchová, Miroslava, Šeděnková, Ivana, Tobolková, Eva, & Stejskal, Jaroslav. (2004). FTIR spectroscopic and conductivity study of the thermal degradation of polyaniline films. *Polymer Degradation and Stability, 86*(1), 179-185.

Wallace, P. R. (1947). The Band Theory of Graphite. *Physical Review, 71*(9), 622-634.

Wan, Meixiang, Liu, Jing, Qiu, Hongjin, Li, Junchao, & Li, Shuzhen. (2001). Template-free synthesized microtubules of conducting polymers. *Synthetic Metals, 119*(1–3), 71-72.

Wan, Meixiang, Wei, Zhiiang, Zhang, Zhiming, Zhang, Lijuan, Huang, Kun, & Yang, Yongsheng. (2003). Studies on Nanostructures of Conducting Polymers via Self-assembly Method. *Synthetic Metals, 135–136*(0), 175-176.

Wang, Baomin, Guo, Zhiqiang, Han, Yu, & Zhang, Tingting. (2013). Electromagnetic wave absorbing properties of multi-walled carbon nanotube/cement composites. *Construction and Building Materials, 46*(0), 98-103.

Wu, Tzong-Ming, & Lin, Yen-Wen. (2006). Doped polyaniline/multi-walled carbon nanotube composites: Preparation, characterization and properties. *Polymer, 47*(10), 3576-3582.

Xia, Lin, Wei, Zhixiang, & Wan, Meixiang. (2010). Conducting polymer nanostructures and their application in biosensors. *Journal of Colloid and Interface Science, 341*(1), 1-11.

Yang, Yongsheng, & Wan, Meixiang. (2002). Chiral nanotubes of polyaniline synthesized by a template-free method. *Journal of Materials Chemistry, 12*(4), 897-901.

Yoon, H., Chang, M., & Jang, J. (2007). Formation of 1D Poly(3,4-ethylenedioxythiophene) Nanomaterials in Reverse Microemulsions and Their Application to Chemical Sensors. *Advanced Functional Materials, 17*(3), 431-436.

Zhang, Lijuan, Wan, Meixiang, & Wei, Yen. (2005). Polyaniline/TiO_2 microspheres prepared by a template-free method. *Synthetic Metals, 151*(1), 1-5.

Zhang, Lixia, Zhang, Lijuan, Wan, Meixiang, & Wei, Yen. (2006). Polyaniline micro/nanofibers doped with saturation fatty acids. *Synthetic Metals, 156*(5–6), 454-458.

Zhang, Yi-Jing, Lin, Yen-Wen, Chang, Chia-Chih, & Wu, Tzong-Ming. (2011). Conducting and magnetic behaviors of polyaniline coated multi-walled carbon nanotube composites containing monodispersed magnetite nanoparticles. *Synthetic Metals, 161*(11–12), 937-942.

Zhang, Z., & Wan, M. (2002). Composite films of nanostructured polyaniline with poly(vinyl alcohol). *Synthetic Metals, 128*(1), 83-89.

Zhao, Dong-Lin, Li, Xia, & Shen, Zeng-Min. (2008). Electromagnetic and microwave absorbing properties of multi-walled carbon nanotubes filled with Ag nanowires. *Materials Science and Engineering: B, 150*(2), 105-110.

APPENDICES

(A) UV-vis spectra

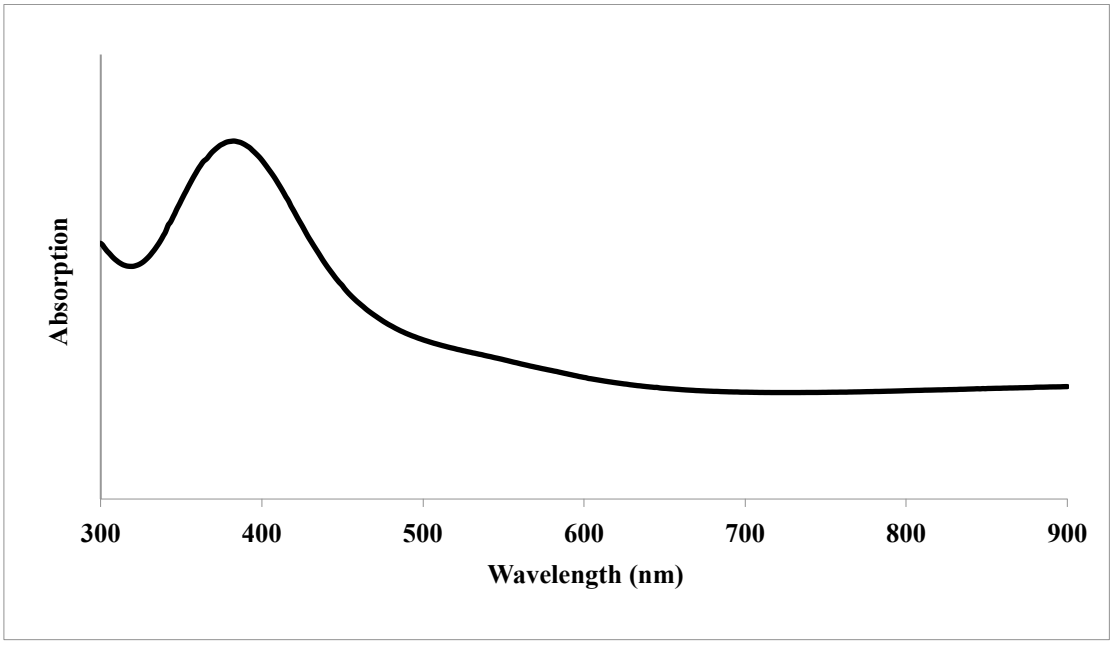

Appendix A1: UV-vis spectrum of PAni/HA/TiO_2/Fe_3O_4 nanocomposites (without chemical treatment) with 10 % of TiO_2 and 20 % of Fe_3O_4.

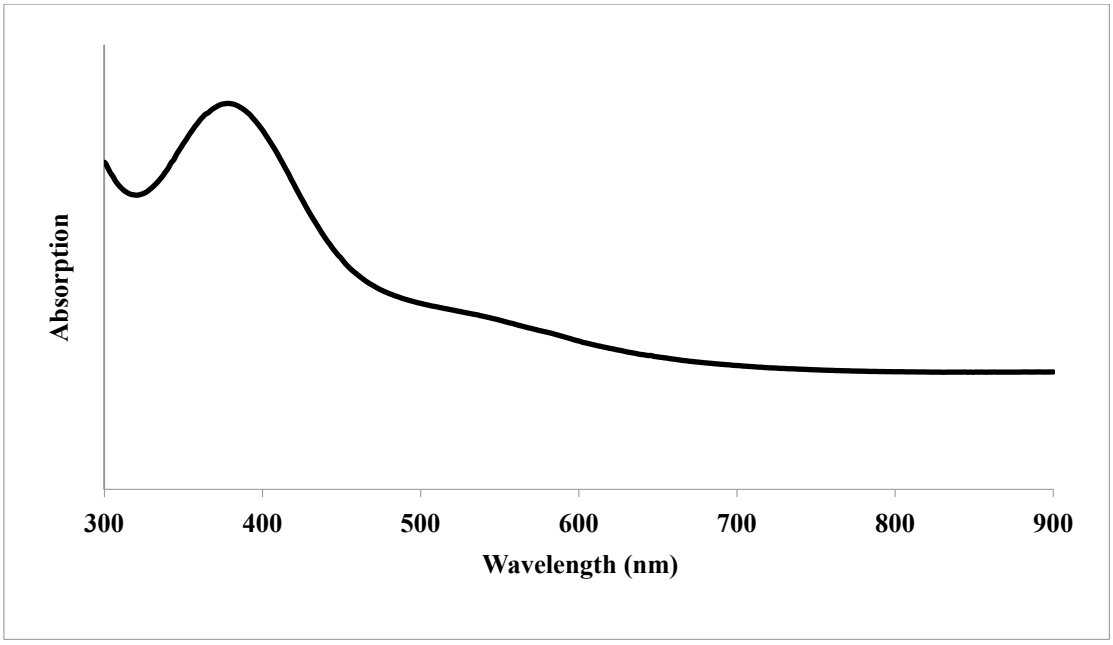

Appendix A2: UV-vis spectrum of PAni/HA/TiO_2/Fe_3O_4 nanocomposites (without chemical treatment) with 10 % of TiO_2 and 40 % of Fe_3O_4.

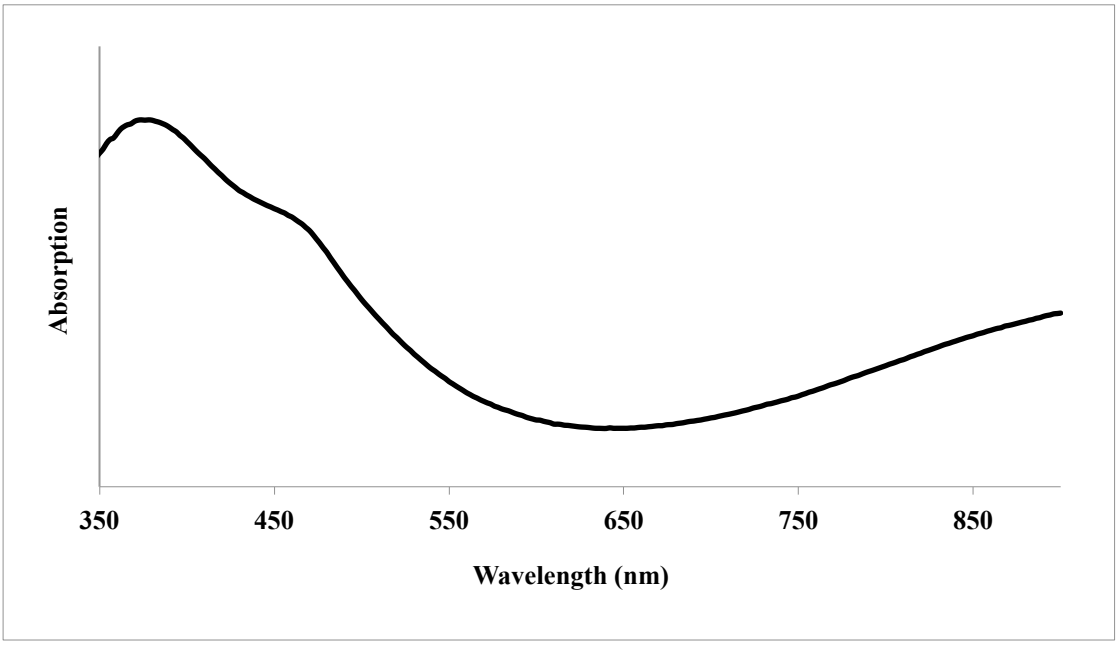

Appendix A3: UV-vis spectrum of PAni/HA/TiO_2/MWNT nanocomposites with MWNT (D = 60-100 nm, l = 5-15 μm).

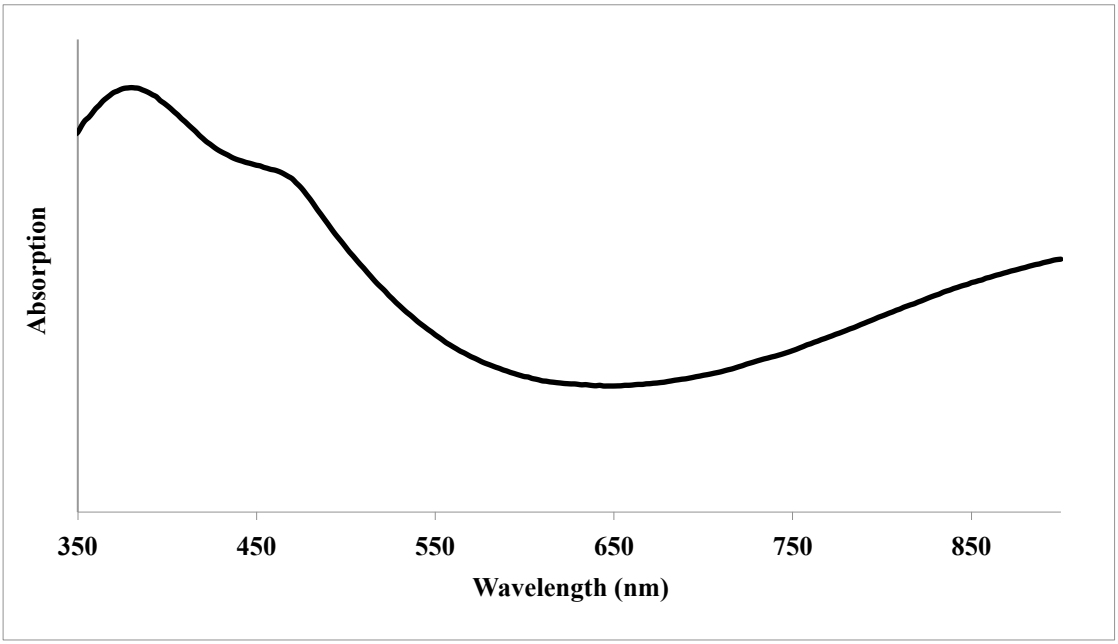

Appendix A4: UV-vis spectrum of PAni/HA/TiO_2/MWNT nanocomposites with MWNT (D = 10-20 nm, l = 5-15 μm).

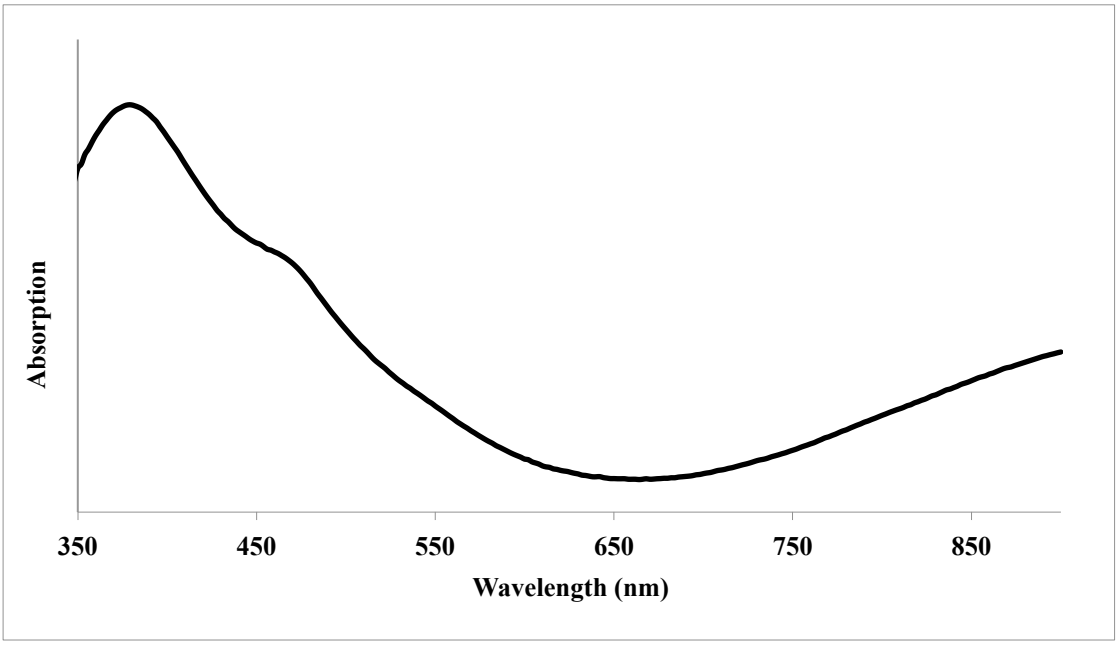

Appendix A5: UV-vis spectrum of PAni/HA/TiO_2/DWNT nanocomposites with 20 % of c-DWNT.

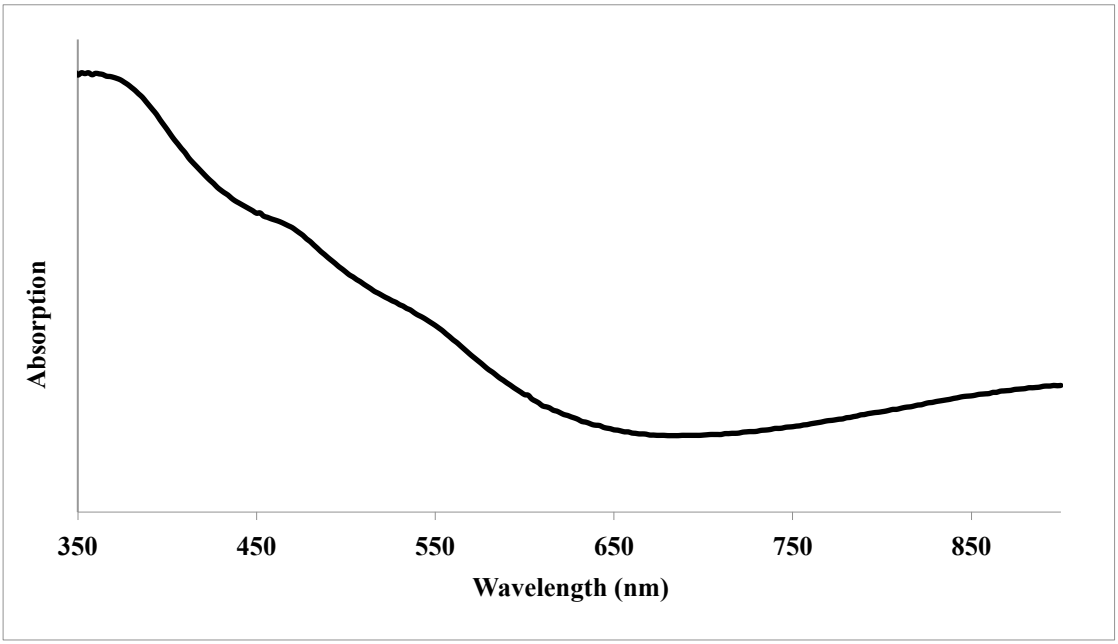

Appendix A6: UV-vis spectrum of PAni/HA/TiO_2/DWNT nanocomposites with 60 % of c-DWNT.

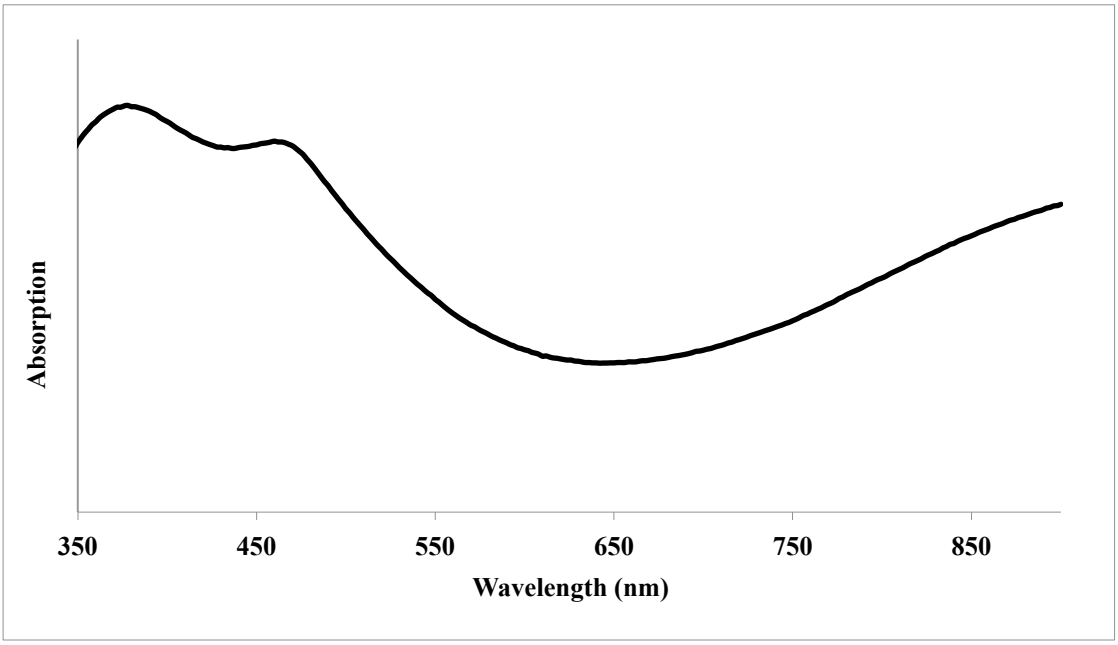

Appendix A7: UV-vis spectrum of PAni/HA/TiO_2/DWNT nanocomposites with 10 % of u-DWNT.

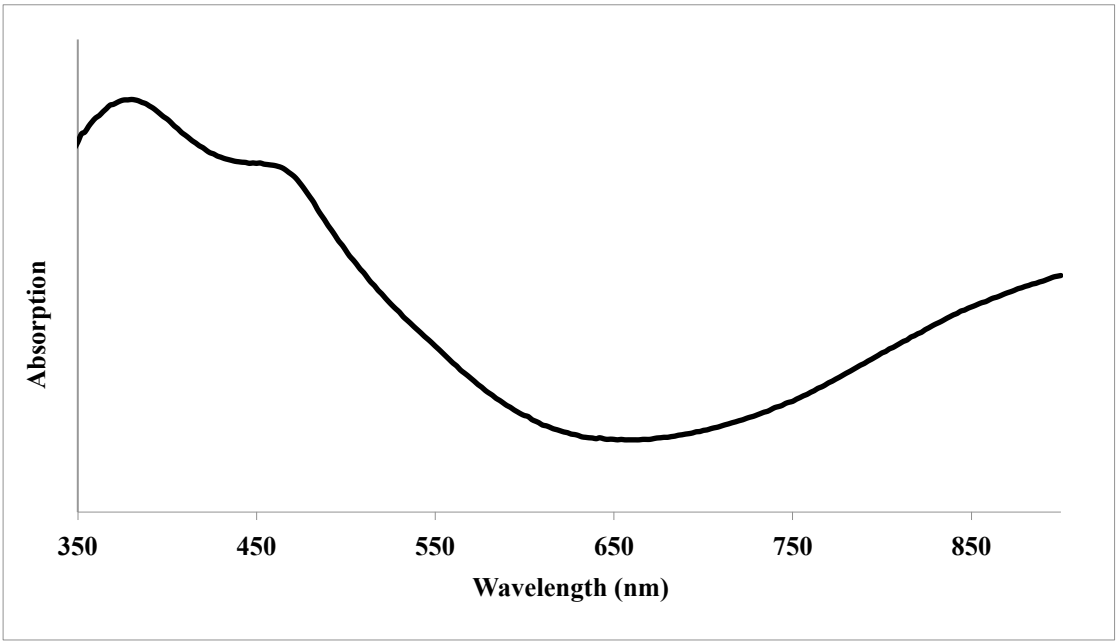

Appendix A8: UV-vis spectrum of PAni/HA/TiO_2/DWNT nanocomposites with 20 % of u-DWNT.

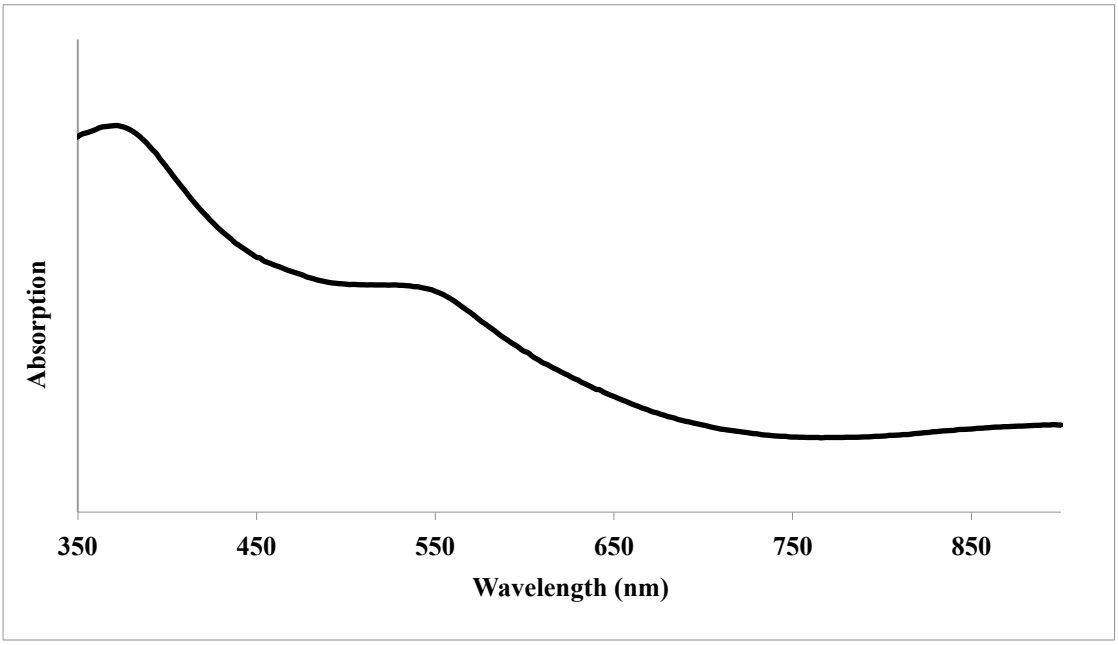

Appendix A9: UV-vis spectrum of PAni/HA/TiO_2/DWNT nanocomposites with 60 % of u-DWNT.

(B) XRD diffractogram

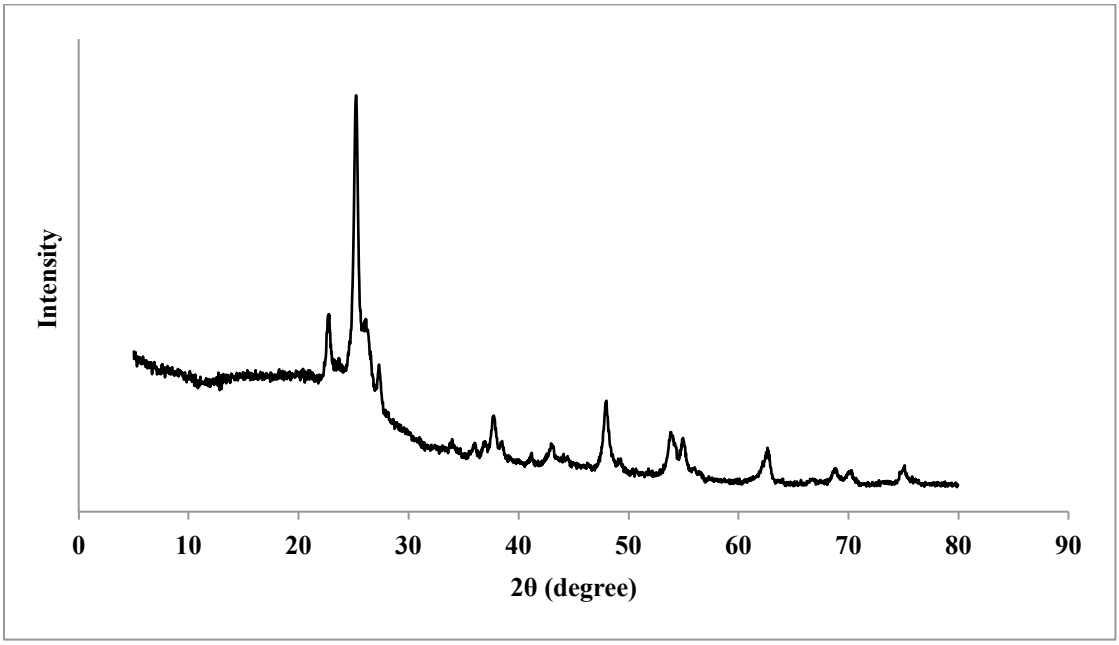

Appendix B1: X-ray diffraction patterns of PAni/HA/TiO_2/MWNT nanocomposites with MWNT (D = 60-100 nm, l = 5-15 μm).

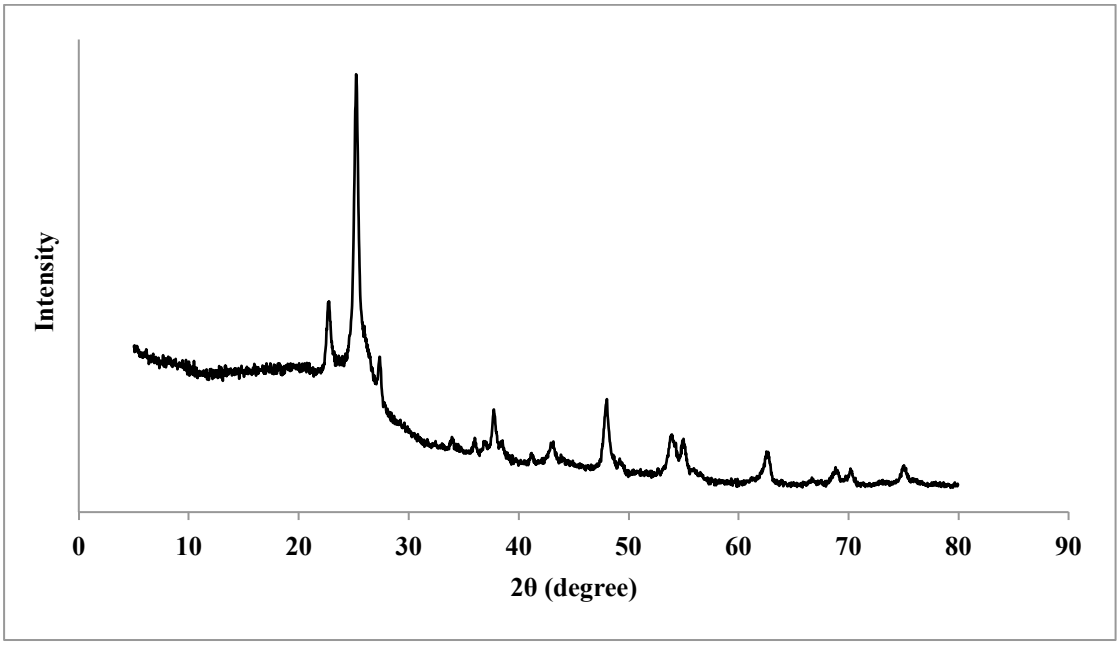

Appendix B2: X-ray diffraction patterns of PAni/HA/TiO_2/MWNT nanocomposites with MWNT (D = 10-20 nm, l = 5-15 μm).

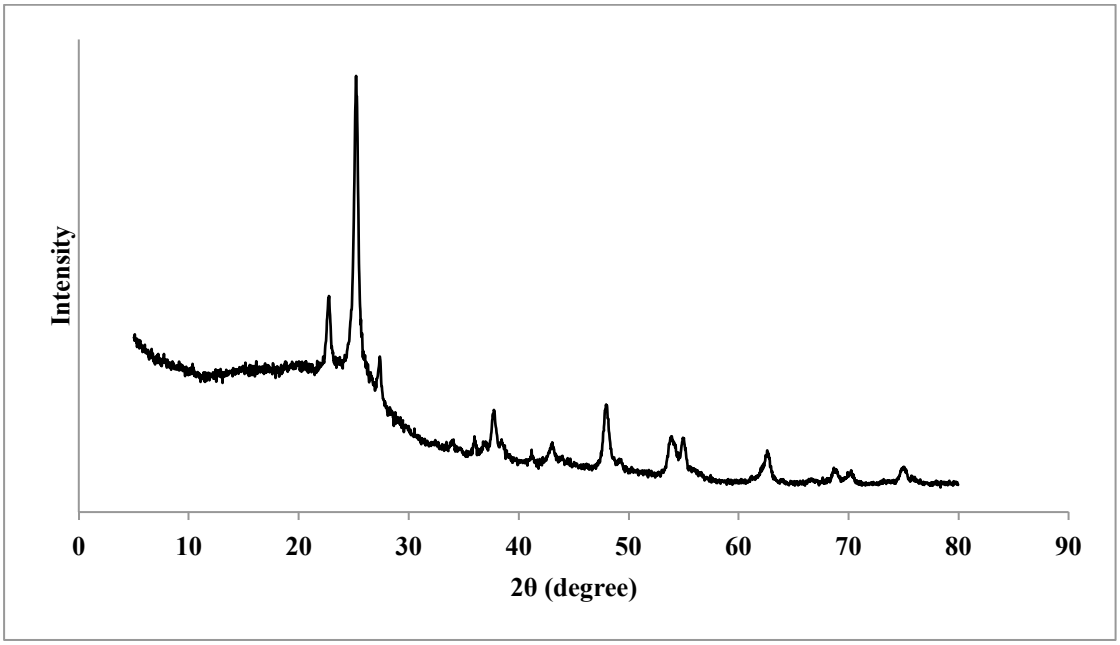

Appendix B3: X-ray diffraction patterns of PAni/HA/TiO_2/DWNT nanocomposites with 10 % of u-DWNT.

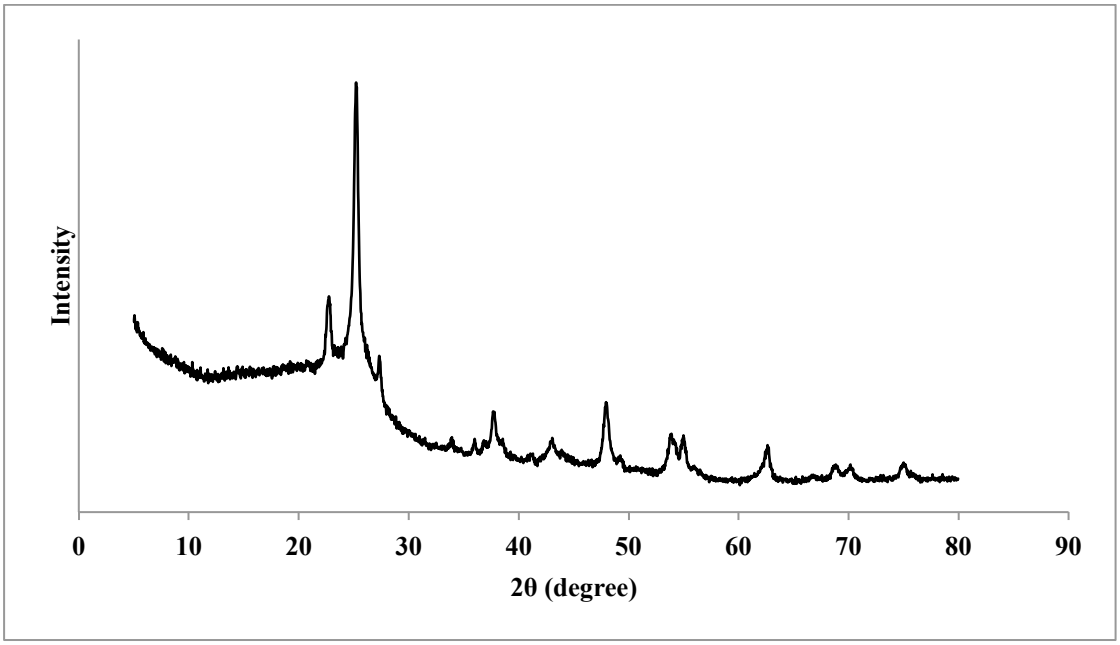

Appendix B4: X-ray diffraction patterns of PAni/HA/TiO_2/DWNT nanocomposites with 20 % of u-DWNT.

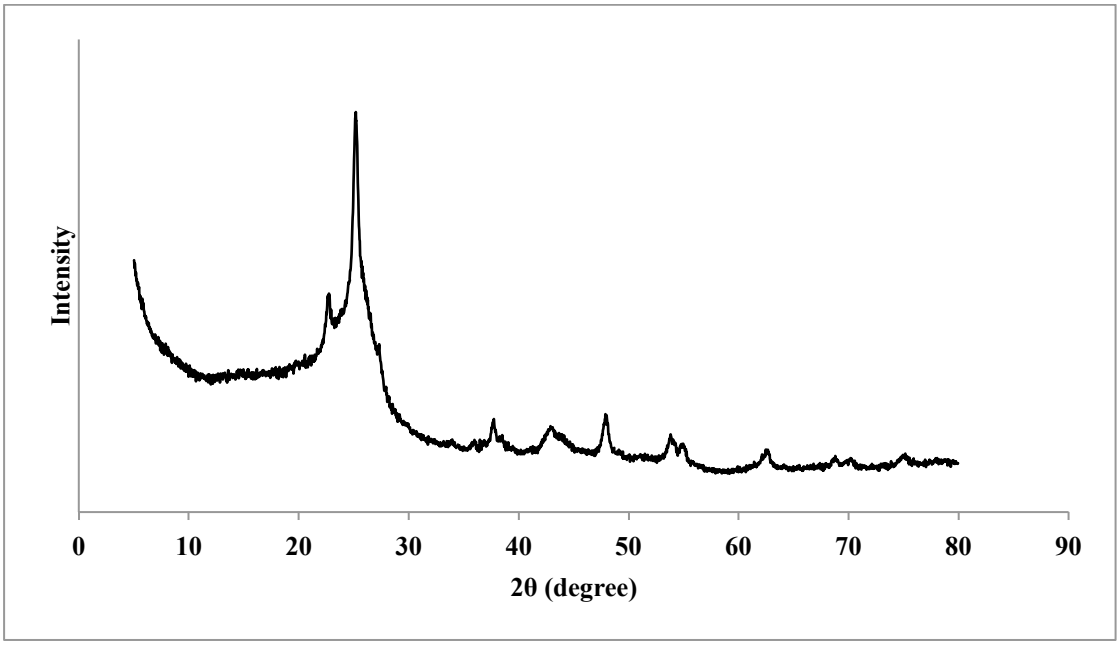

Appendix B5: X-ray diffraction patterns of PAni/HA/TiO_2/DWNT nanocomposites with 60 % of u-DWNT.

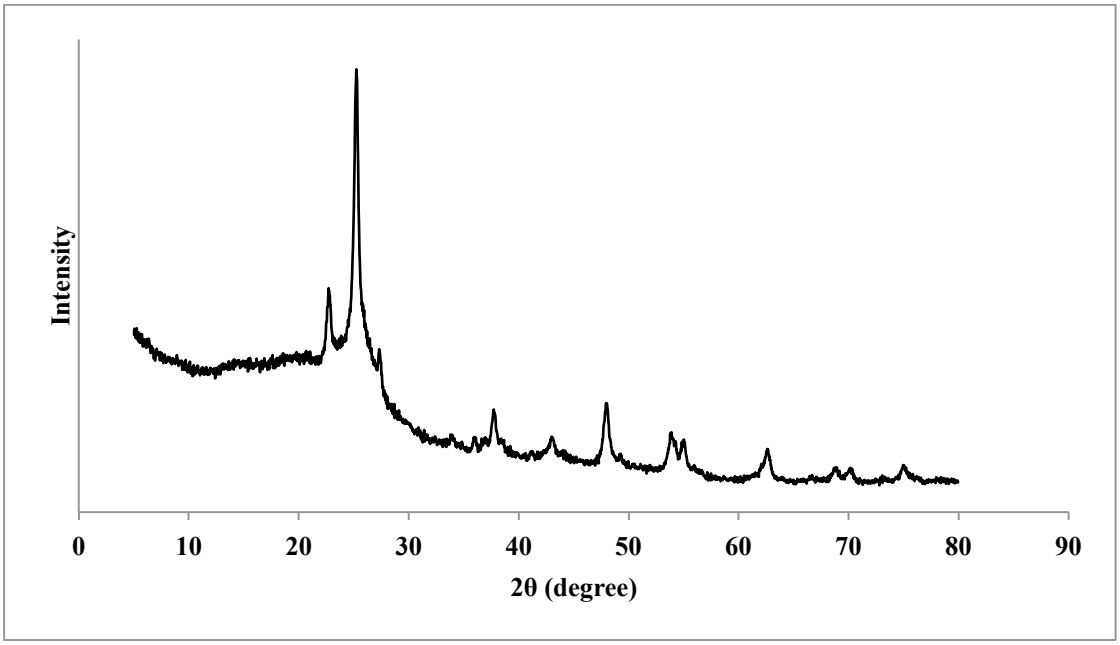

Appendix B6: X-ray diffraction patterns of PAni/HA/TiO_2/DWNT nanocomposites with 20 % of c-DWNT.

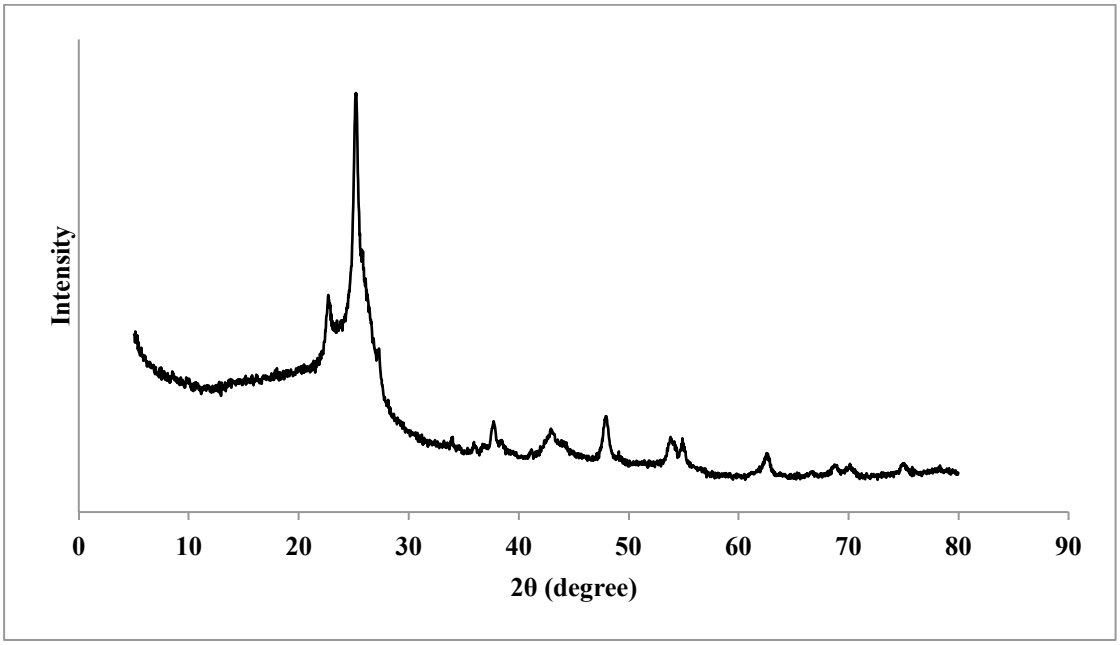

Appendix B7: X-ray diffraction patterns of PAni/HA/TiO_2/DWNT nanocomposites with 60 % of c-DWNT.

(C) FESEM images

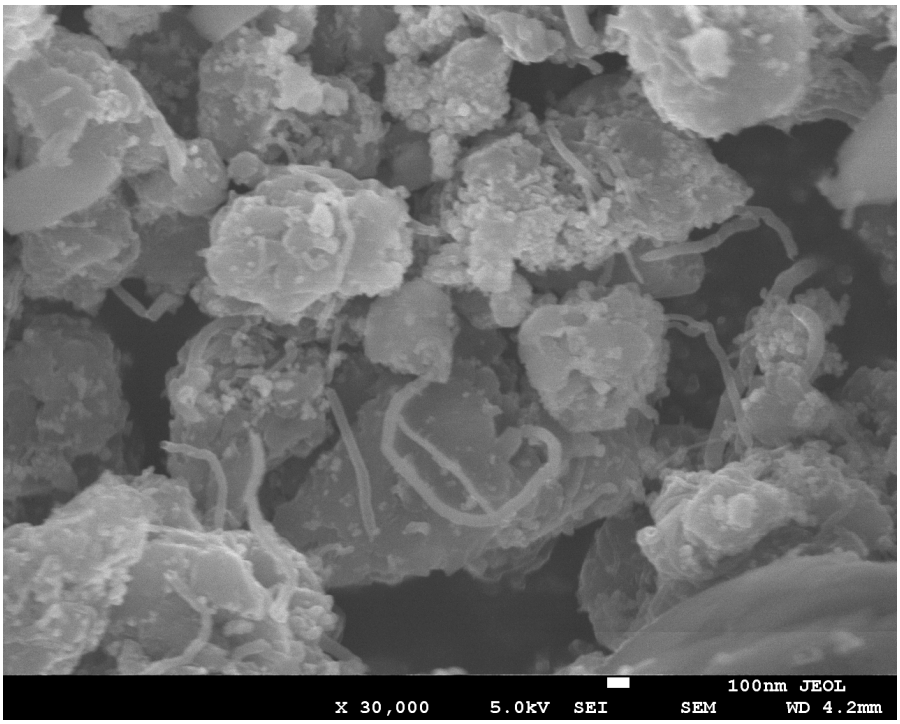

(C1) (a) PAni/HA/TiO_2/MWNT (D = 60-100 nm, l = 1-2 μm).

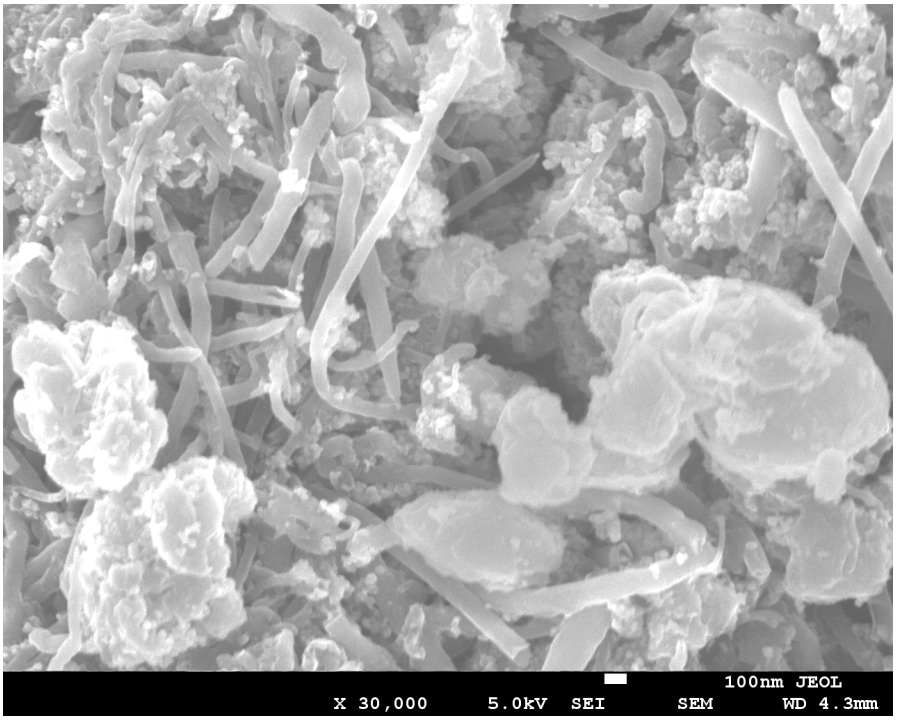

(C1) (b) PAni/HA/TiO_2/MWNT (D = 60-100 nm, l = 5-15 μm).

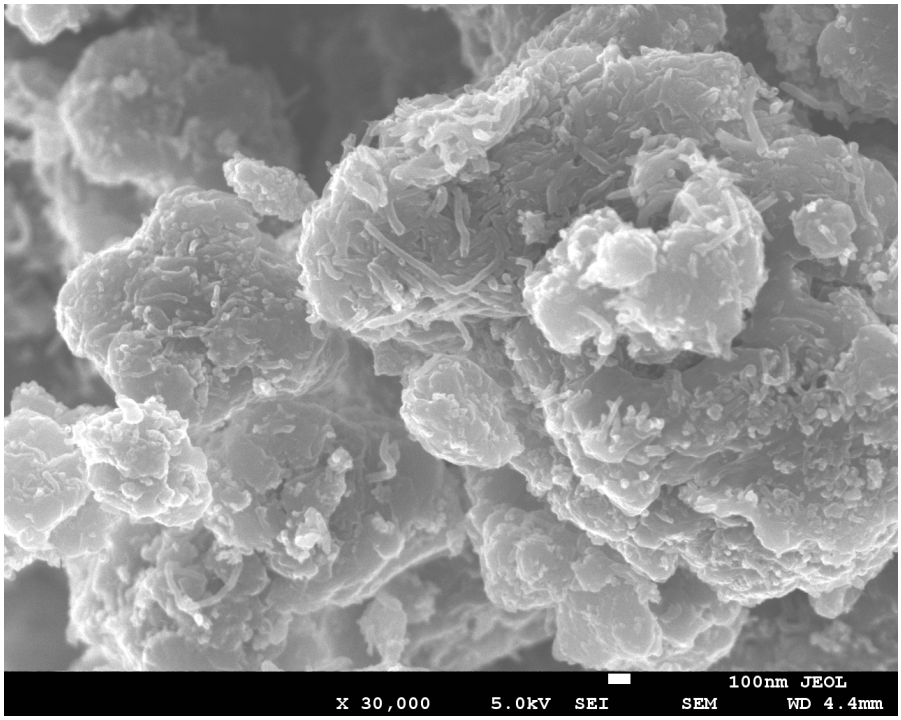

(C1) (c) PAni/HA/TiO_2/MWNT (D = 10-20 nm, l = 5-15 μm).

Appendix C1: FESEM images for PAni/HA/TiO_2/MWNT with different diameter and length of MWNT. (Magnification: 30, 000 ×)

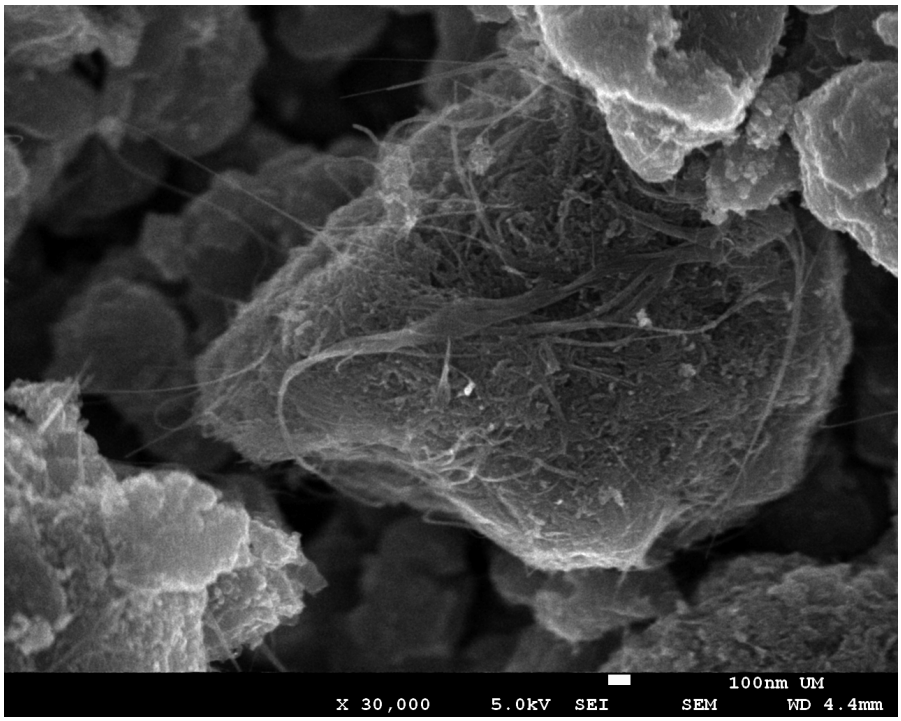

(C2) (a) PAni/HA/TiO_2/DWNT with 10 % of u-DWNT.

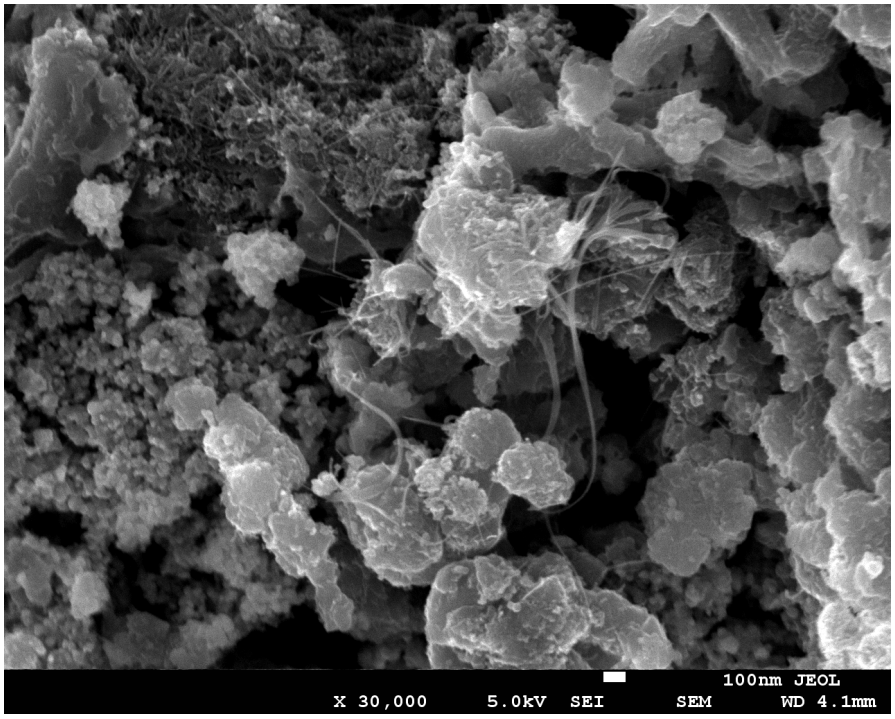

(C2) (b) PAni/HA/TiO_2/DWNT with 20 % of u-DWNT.

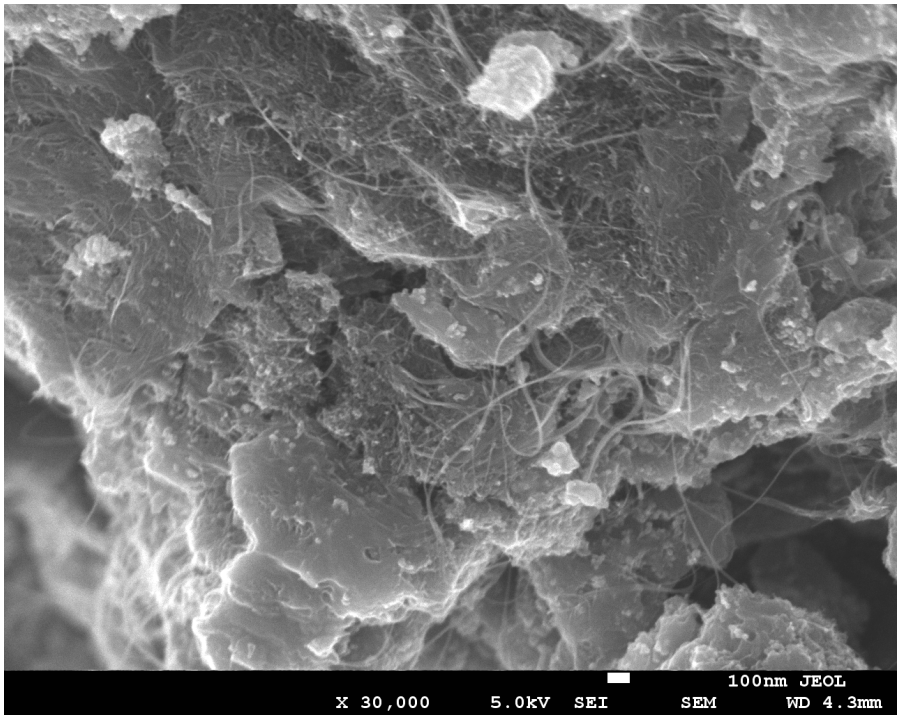

(C2) (c) PAni/HA/TiO_2/DWNT with 60 % of u-DWNT.

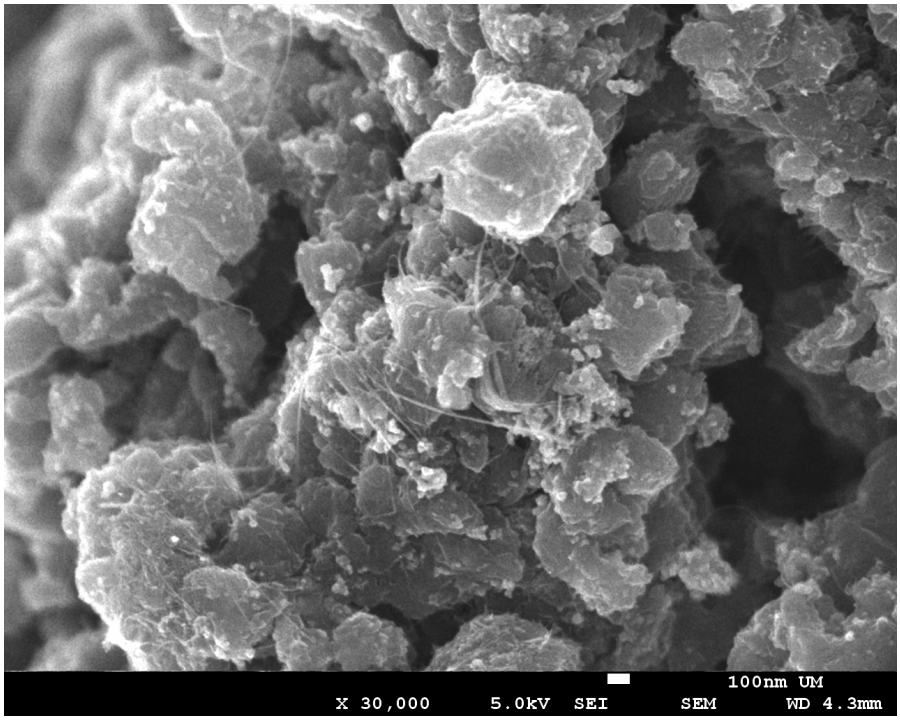

(C2) (d) PAni/HA/TiO_2/DWNT with 10 % of c-DWNT.

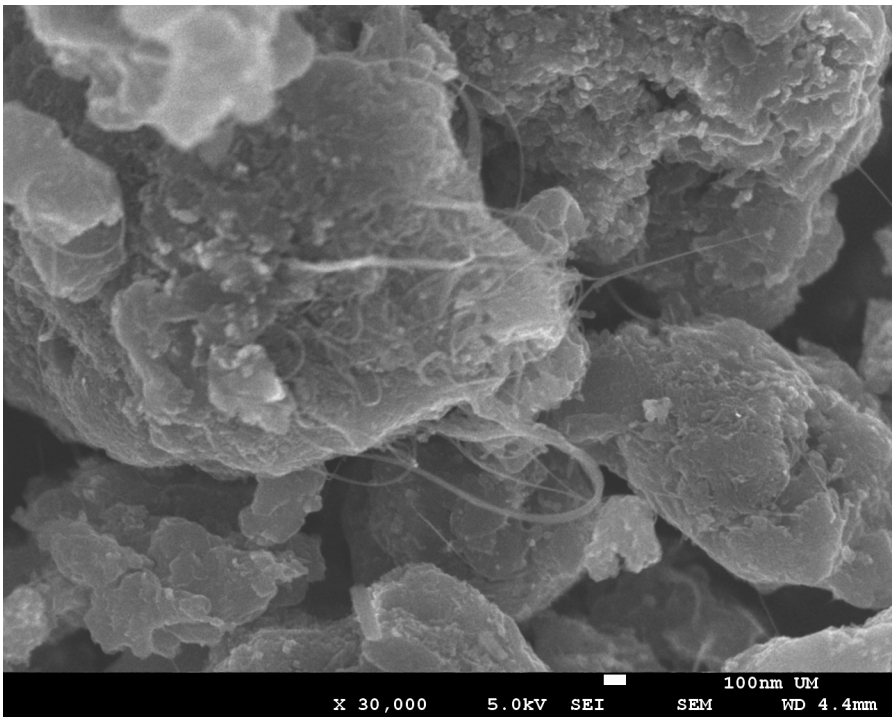

(C2) (e) PAni/HA/TiO_2/DWNT with 20 % of c-DWNT.

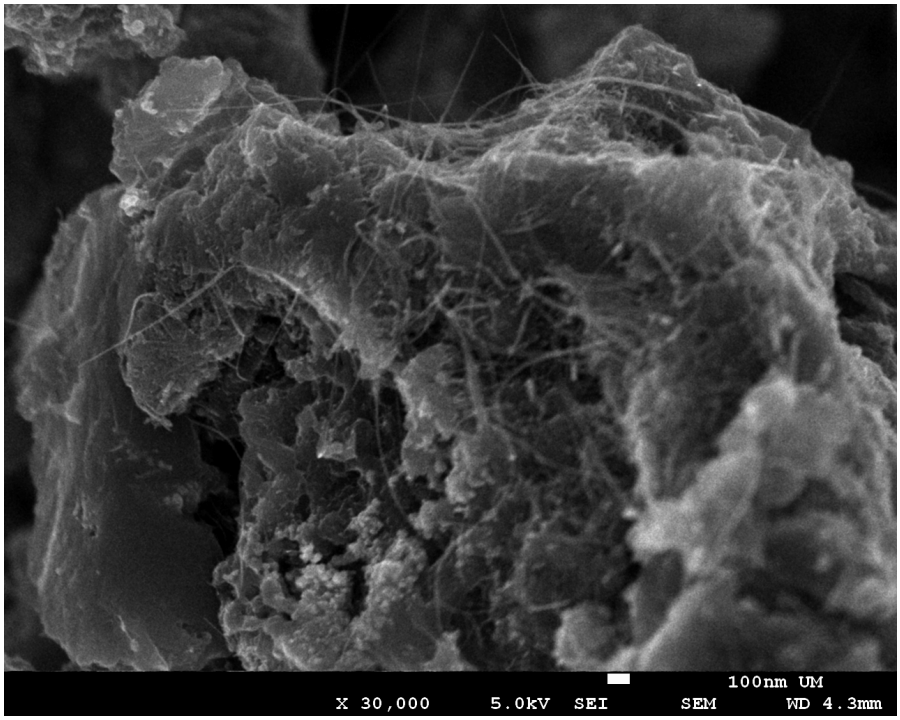

(C2) (f) PAni/HA/TiO_2/DWNT with 60 % of c-DWNT.

Appendix C2: FESEM images for PAni/HA/TiO_2/DWNT with different contents of u-DWNT and c-DWNT. (Magnification: 30, 000 ×)

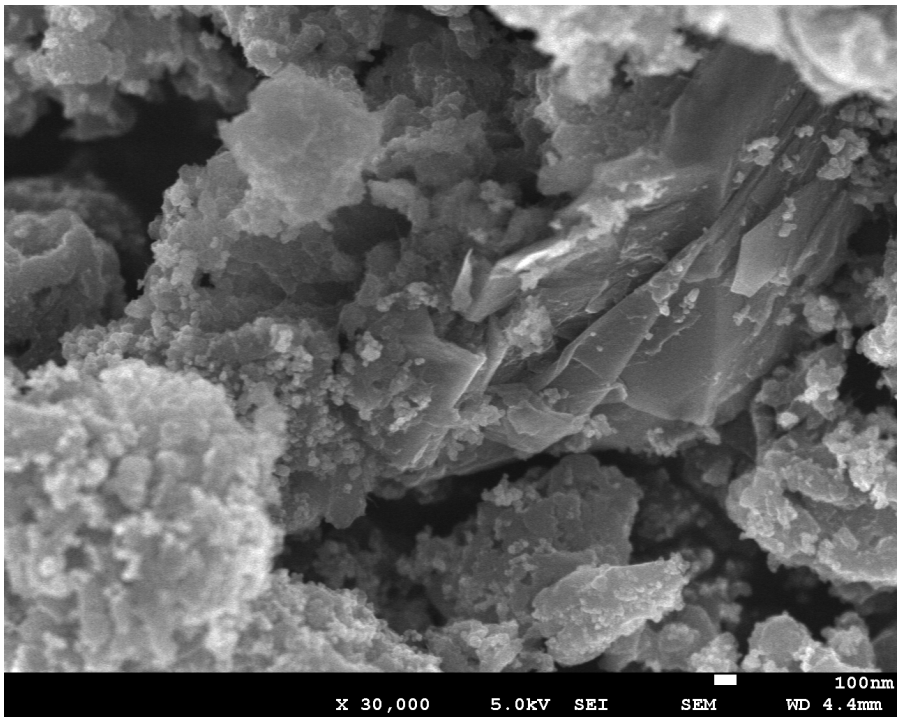

(C3) (a) PAni/HA/TiO_2/GNP with 10 % of GNP.

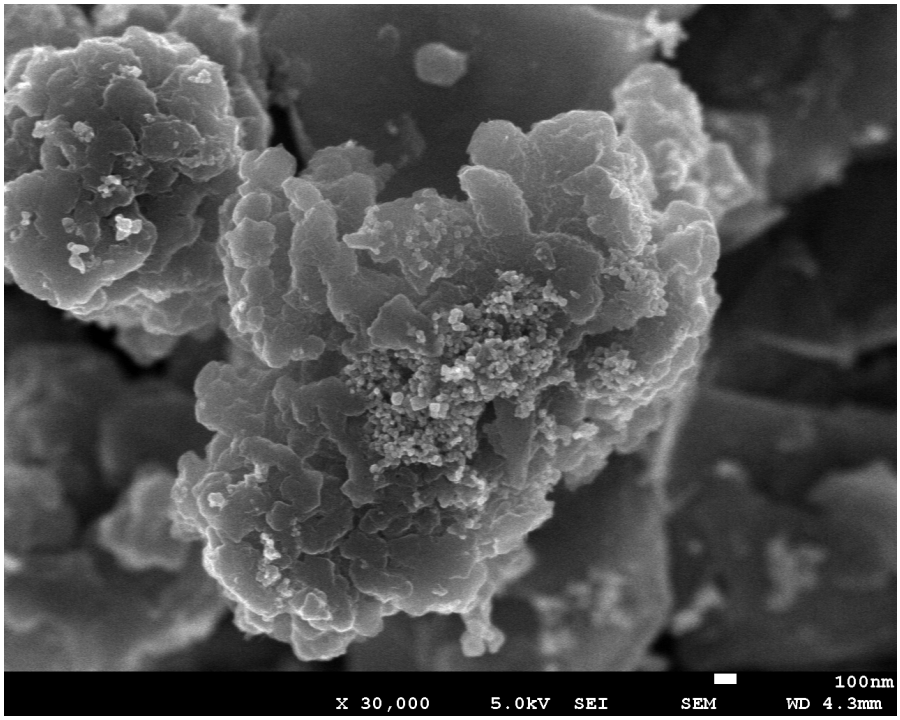

(C3) (b) PAni/HA/TiO_2/GNP with 20 % of GNP.

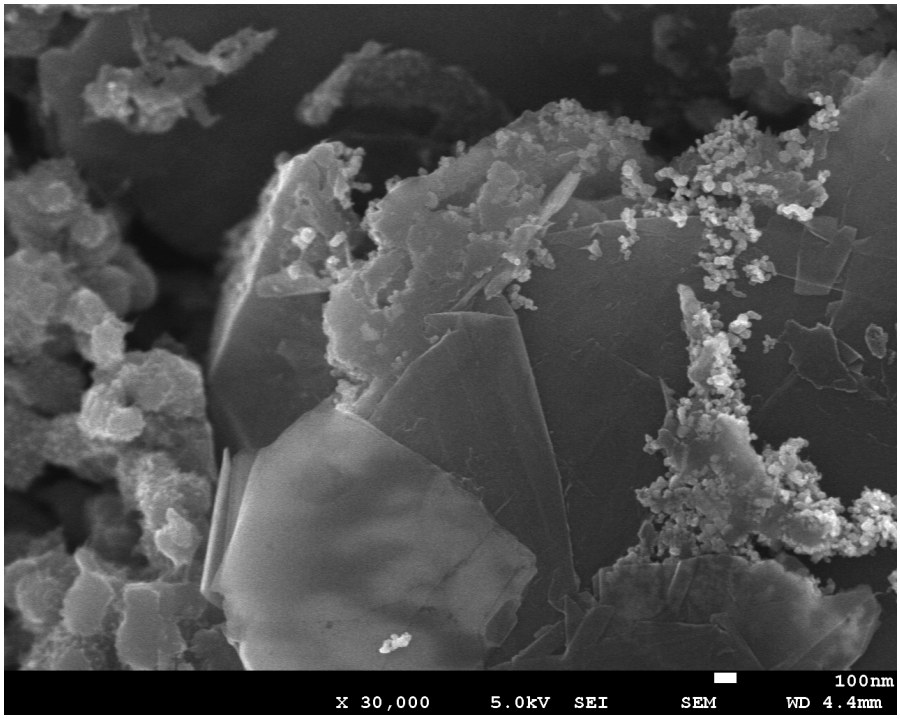

(C3) (c) PAni/HA/TiO_2/GNP with 40 % of GNP.

Appendix C3: FESEM images for PAni/HA/TiO_2/GNP with different contents of GNP. (Magnification: 30, 000 ×)

(D) Magnetic permeability study (μ_r' and μ_r'')

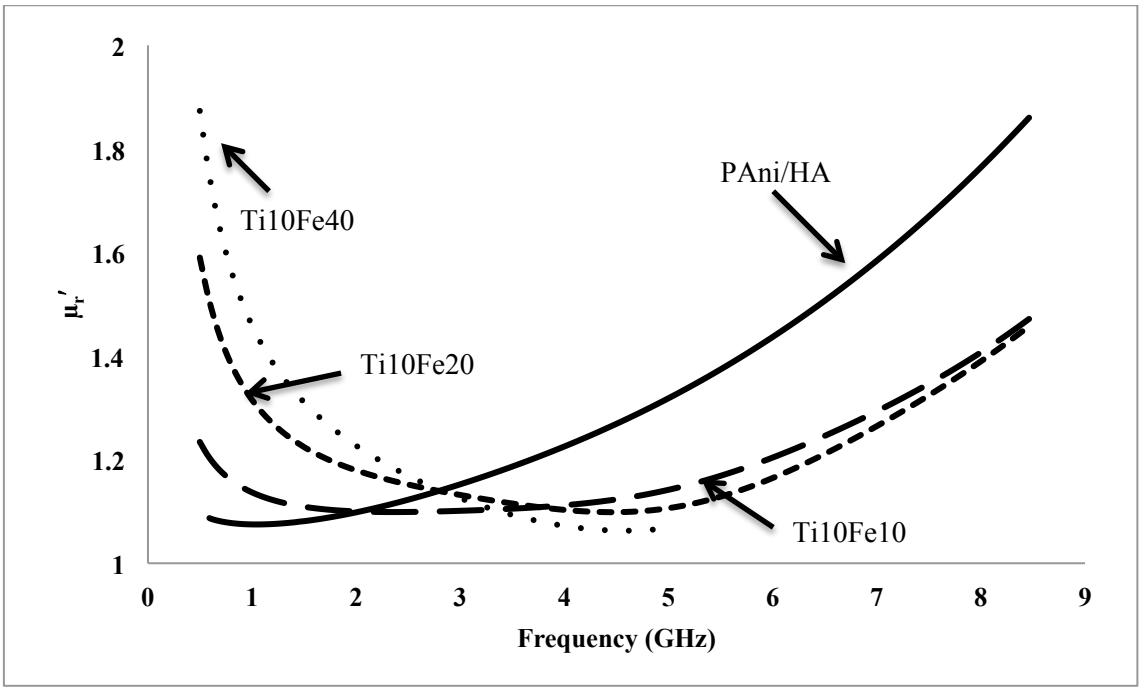

Appendix D1: Real (μ_r') part of magnetic permeability for PAni/HA/TiO_2/Fe_3O_4 nanocomposites (without chemical treatment) with different contents of Fe_3O_4.

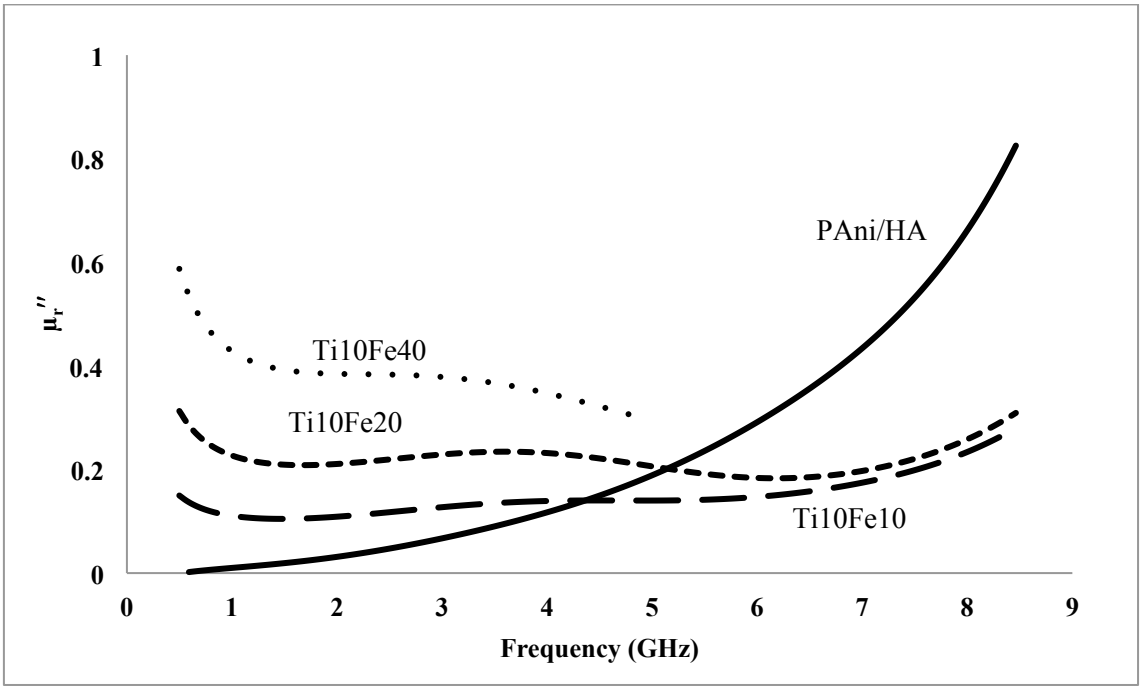

Appendix D2: Imaginary (μ_r'') part of magnetic permeability for PAni/HA/TiO_2/Fe_3O_4 nanocomposites (without chemical treatment) with different contents of Fe_3O_4.

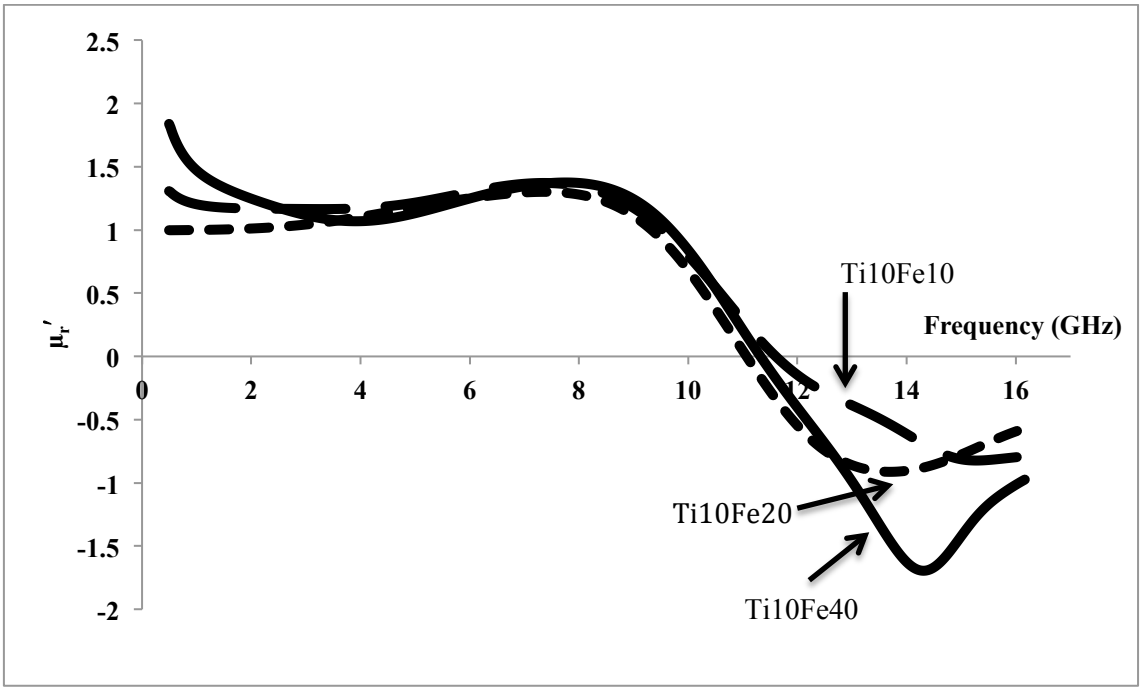

Appendix D3: Real (μ_r') part of magnetic permeability for PAni/HA/TiO_2/Fe_3O_4 nanocomposites (with chemical treatment) with different contents of Fe_3O_4.

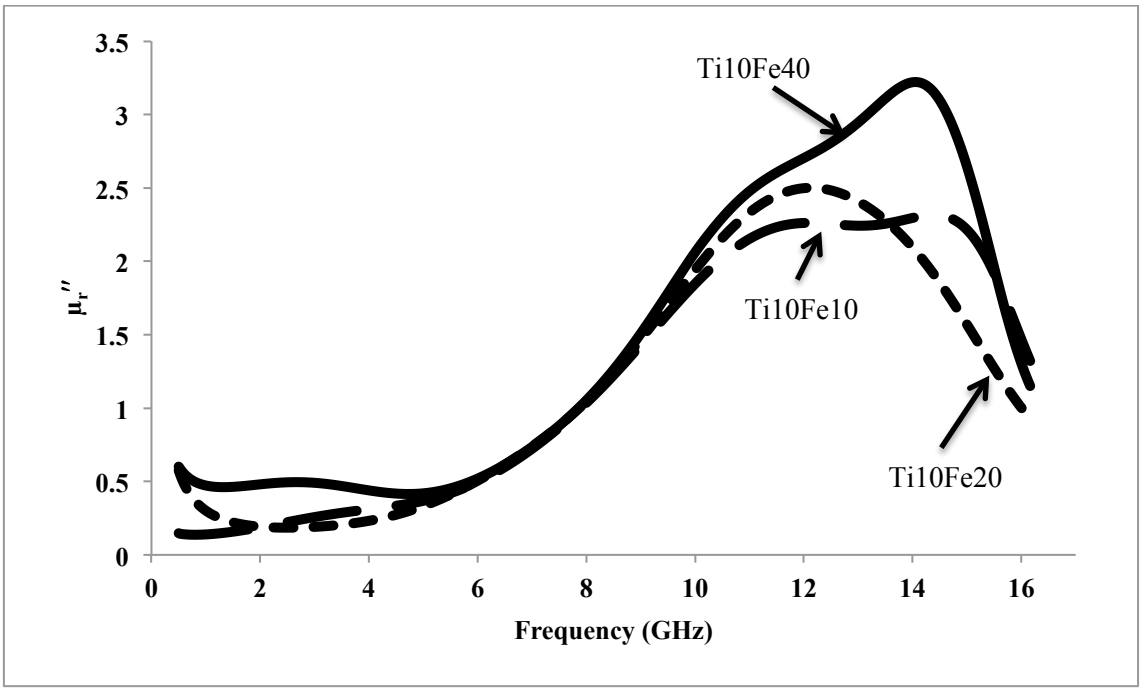

Appendix D4: Imaginary (μ_r'') part of magnetic permeability for PAni/HA/TiO_2/Fe_3O_4 nanocomposites (with chemical treatment) with different contents of Fe_3O_4.